

# **POLITECNICO DI TORINO**

Master of Science in Mechanical Engineering

## **Mechanical properties of non-woven composite material**



**Politecnico  
di Torino**

### **Supervisors:**

**Prof. Raffaele Ciardiello  
Prof. Davide Salvatore Paolino  
Ing. Andrea Iadarola**

### **Candidate:**

**M. Sufyan Nasir**

**OCTOBER 2023**



# Index

<b>Index of figures</b> .....	<b>5</b>
<b>Index of tables</b> .....	<b>7</b>
<b>Abstract</b> .....	<b>8</b>
<b>Chapter 1: Introduction</b> .....	<b>9</b>
<b>Chapter 2: Materials and methods</b> .....	<b>17</b>
<b>2.1: Materials</b> .....	<b>17</b>
2.1.1: Epoxy resin and hardener .....	17
2.1.2: Non-woven carbon fiber mats .....	18
2.1.3: Water jet.....	19
2.1.4: Oven.....	20
2.1.5: Three-point bending test machine .....	21
2.1.6: Tensile test machine.....	22
2.1.7: Digital image correlation DIC .....	24
<b>2.2: Procedures</b> .....	<b>25</b>
2.2.1: Vacuum Assisted Resin Infusion (VARI).....	25
2.2.2: Curing.....	29
<b>2.3: Specimens production</b> .....	<b>29</b>
2.3.1: Bending test specimens .....	31
2.3.2: Tensile test specimens.....	32
2.3.3: Compression test specimens .....	33
2.3.4: Shear test specimens.....	36
<b>2.4: Mechanical tests</b> .....	<b>37</b>
2.4.1: Three-point bending test.....	37
2.4.2: Tensile test .....	39
2.4.3: Compression test .....	40
2.4.4: Shear test.....	41
<b>Chapter 3: Results and discussion</b> .....	<b>44</b>
<b>3.1: Bending test</b> .....	<b>44</b>
3.1.1: 0° degree.....	44
3.1.2: 30° degree.....	45
3.1.3: 60° degree.....	46
3.1.4: 90° degree.....	47
3.1.5: Comparison of bending stress at different orientations .....	49
3.1.6: Comparison of bending modulus at different orientations .....	50
3.1.7: Comparison of bending strain at different orientations .....	51
<b>3.2: Tensile tests</b> .....	<b>53</b>
3.2.1: 0° degree.....	53
3.2.2: 30° degree.....	54
3.2.3: 60° degree.....	55
3.2.4: 90° degree.....	56
3.2.5: Comparison of tensile stress at different orientations .....	58

3.2.6: Comparison of tensile strain at different orientations .....	59
3.2.7: Comparison of tensile modulus at different orientations .....	60
<b>3.3- Compression tests .....</b>	<b>62</b>
3.3.1: 0° degree .....	62
3.3.2: 30° degree .....	63
3.3.3: 60° degree .....	64
3.3.4: 90° degree .....	65
3.3.5: Comparison of compression stress at different orientations .....	67
3.3.6: Comparison of compression strain at different orientations .....	68
3.3.7: Comparison of compression modulus at different orientations .....	69
<b>3.4: Shear tests .....</b>	<b>71</b>
3.4.1: 0° degree .....	71
3.4.2: 30° degree .....	72
3.4.3: 60° degree .....	73
3.4.4: 90° degree .....	74
3.4.5: Comparison of shear stress at different Orientations .....	77
3.4.6: Comparison of shear strain at different Orientations .....	78
3.4.7: Comparison of shear modulus at different Orientations .....	79
<b>3.5: Optical analysis .....</b>	<b>81</b>
3.5.1: Microscopic study of bending specimens .....	81
3.5.2: Microscopic study of tensile specimens .....	85
3.5.3: Microscopic study of compression specimens .....	90
3.5.4: Microscopic study of shear specimens .....	94
<b>Chapter 4: Conclusion .....</b>	<b>100</b>
<b>Acknowledgment .....</b>	<b>102</b>
<b>References .....</b>	<b>103</b>

## *Index of figures*

Figure 1: Comparison of mechanical properties of carbon fibers and steel materials[5] .....	9
Figure 2: Sustainable fibers[19].....	11
Figure 3: Comparison of molding process of woven fibers and non-woven fibers[3] .....	13
Figure 4: Structure of woven, knitted, non-woven fabric[26] .....	13
Figure 5: Vacuum Assisted Infusion Resin process[32].....	15
Figure 6: Basic principle of DIC[33].....	16
Figure 7: IN2 epoxy infusion resin[34] .....	17
Figure 8: AT30 epoxy hardener[35].....	18
Figure 9: Non-woven carbon fiber mats .....	18
Figure 10: Water jet cutting machine. ....	19
Figure 11: Precision Composites Curing Oven[36] .....	20
Figure 12: Specifications of OV301[36].....	21
Figure 13: Specifications of three-point bending test machine[37].....	21
Figure 14: Instron 8801.....	22
Figure 15: Non-woven carbon fiber with flow mesh and sealed plastic bag connected with pump just before the infusion of resin. ....	26
Figure 16: Resin flow.....	28
Figure 17: Strain gauges bonded to compression specimens.....	34
Figure 18: Specimen undergoing bending during three-point bending test.....	37
Figure 19: Tensile test configuration .....	39
Figure 20: Compression test configuration.....	40
Figure 21: Instron 8801 along with DIC system during shear testing .....	41
Figure 22: Shear testing configuration.....	42
Figure 23: Stress-strain curves for 0° specimens.....	44
Figure 24: Stress-strain curves for 30° specimens.....	45
Figure 25: Stress-strain curves for 60° specimens.....	46
Figure 26: Stress-strain curves for 90° specimens.....	47
Figure 27: Specimens after bending test.....	48
Figure 28: Bar chart showing bending stress at different orientations. ....	49
Figure 29: Bar chart showing bending modulus at different orientations. ....	50
Figure 30: Bar chart showing bending strain at different orientations. ....	51
Figure 31: Stress vs strain at 0° degree.....	53
Figure 32: Stress vs strain at 30° degree.....	54
Figure 33: Stress vs strain at 60° degree.....	55
Figure 34: Stress vs strain at 90° degree.....	56
Figure 35: Specimens after tensile test .....	57
Figure 36: Bar chart showing tensile stress at different orientations.....	58
Figure 37: Bar chart showing tensile strain at different orientations.....	59
Figure 38: Bar chart showing tensile modulus at different orientations.....	60
Figure 39: Stress vs strain at 0° degree.....	62
Figure 40: Stress vs strain at 30° degree.....	63
Figure 41: Stress vs strain at 60° degree.....	64
Figure 42: Stress vs strain at 90° degree.....	65

Figure 43: Specimens after compression test.....	66
Figure 44: Bar chart showing compression stress at different orientations. ....	67
Figure 45: Bar chart showing compression strain at different orientations. ....	68
Figure 46: Bar chart showing compression modulus at different orientations. ....	69
Figure 47: Stress vs strain at 0° degree.....	71
Figure 48: Stress vs strain at 30° degree.....	72
Figure 49: Stress vs strain at 60° degree.....	73
Figure 50: Stress vs strain at 90° degree.....	74
Figure 51: Specimens after shear test.....	76
Figure 52: Bar chart showing shear stress at different orientations.....	77
Figure 53: Bar chart showing shear strain at different orientations.....	78
Figure 54: Bar chart showing shear modulus at different orientations.....	79
Figure 55: Microscopic image of 0° fractured specimen.....	81
Figure 56: Microscopic image of 30° fractured specimen.....	82
Figure 57: Microscopic image of 60° fractured specimen.....	83
Figure 58: Microscopic image of 90° fractured specimen.....	84
Figure 59: Microscopic image of 0° fractured specimen.....	85
Figure 60: Microscopic image of 0° fractured specimen near the grip.....	86
Figure 61: Microscopic image of 30° fractured specimens.....	87
Figure 62: Microscopic image of 60° fractured specimens.....	88
Figure 63: Microscopic image of 90° fractured specimen.....	89
Figure 64: Microscopic image of 90° fractured specimen.....	89
Figure 65: Microscopic image of 0° fractured specimens.....	90
Figure 66: Microscopic image of 30° fractured specimens.....	91
Figure 67: Microscopic image of 60° fractured specimen.....	92
Figure 68: Microscopic image of 90° fractured specimen.....	93
Figure 69: Microscopic image of 0° fractured specimens.....	94
Figure 70: 0° Specimen fractured by shear testing.....	95
Figure 71: Microscopic image of 30° fractured specimens.....	95
Figure 72: 30° Specimen fractured by shear testing.....	96
Figure 73: Microscopic image of 60° fractured specimens.....	97
Figure 74: 60° Specimen fractured by shear testing.....	98
Figure 75: Microscopic image of 90° fractured specimens.....	98
Figure 76: 90° Specimen fractured by shear testing.....	99

## *Index of tables*

Table 1: Total number of specimens used in testing. ....	30
Table 2: Dimensions of bending specimens.....	31
Table 3: Dimensions of tensile specimens .....	32
Table 4: Dimensions of compression specimens .....	33
Table 5: Specifications of strain gauges used for compression tests. ....	35
Table 6: Dimensions of shear specimens .....	36
Table 7: Mean force, mean stress, mean strain, and mean modulus at different orientations .....	52
Table 8: Mean stress, mean strain, and mean modulus at different orientations .....	61
Table 9: Mean stress, mean strain, and mean modulus at different orientations .....	70
Table 10: Mean stress, mean strain, and mean modulus at different orientations .....	80

# Abstract

In recent years, the interest in recycled and sustainable materials in engineering applications has grown due to the need to reduce environmental impact and industrial scrap wastes, especially in composite material applications. Among the reinforcements that can be used in composite production, non-woven random mat carbon fibers are one of the most interesting solutions, since they allow the use of the scraps coming from the production of carbon fibers using a very easy and low energy consuming method. In this study, the mechanical properties of non-woven carbon fiber/epoxy matrix composites have been investigated by means bending, compression, tensile, and shear tests.

Composite laminates were manufactured using the vacuum infusion process. Specimens were cut at four different angles ( $0^\circ$ ,  $30^\circ$ ,  $60^\circ$ ,  $90^\circ$ ) with respect to the resin flow direction using a water jet cutting system. For tensile and shear tests, Digital Image Correlation (DIC) was used to map the strain on the surface of the specimen during the test, whereas, for compression and bending test, the strain was measured by means of strain gauges. The elastic modulus and the ultimate tensile stress of the considered specimens were computed and compared, considering different orientations. Finally, in order to analyze the orientation of the fibers inside the epoxy matrix, an optical analysis of the fracture surfaces was conducted using a digital microscope.

Experimental results showed that for bending and tensile tests, the maximum stress and the maximum modulus were obtained for the specimens oriented at  $90^\circ$  while the maximum strain was obtained for the specimens along the longitudinal direction. By contrast, for compression and shear tests, the maximum stress and maximum modulus were obtained for the specimens oriented at  $60^\circ$  and  $90^\circ$ , respectively. Therefore, experimental results verify that the mechanical properties of non-woven carbon composites are affected at different angles with respect to the resin flow direction.

# Chapter 1: Introduction

Composite materials have revolutionized many industries, from the aerospace and automotive industry to the construction industry; composites have emerged as the basis of technological innovation. Due to their extraordinary strength-to-weight ratio and adaptability, they have become the first choice for applications that demand superior mechanical performance. Since last few decades carbon fiber composites are extensively in use, an emerging trend in composites has sparked interest in non-woven carbon composites.

In recent years, carbon composites have set new trends in the industry. Carbon composites have become very important for industrial sectors especially for the automotive and aerospace ones[1]. In the automotive industry, carbon composites are used in structural components such as chassis, drive shafts, suspension systems[2]. Recently, BMW introduced carbon fiber car bodies[3], and research has shown that using carbon fiber drastically reduces the weight of cars. There is almost a 30-35% reduction in the weight of vehicles adopting carbon fiber composites [3]. The carbon fiber industry has increased over the years to meet the demands of other sectors. It is used in offshore structures, pressure vessels, turbine blades, medical applications, and sports goods[4].

Nowadays, carbon composites represent a good solution to substitute steels in structural applications given the better mechanical properties lightweight, and good corrosion resistance properties. Figure 1 below shows that the strength and modulus of carbon fibers are greater than Steel.

Material type		Density $\rho$ ( $\text{kg/m}^3$ )	Tensile Strength $\sigma_{II}$ (GPa)	Elastic Modulus $E$ (GPa)	Breaking Length $\sigma_{II}/(\rho g)$ (km)
Carbon fiber	Standard	1760	3.53	230	205
	High strength	1820	7.06	294	396
	High modulus	1870	3.45	441	188
Steel	S355	7850	0.50	210	6
	Wire	7850	1.77	210	23

Figure 1: Comparison of mechanical properties of carbon fibers and steel materials[5]

It should also be noted that not all composites surpass metals in strength. Only specific composites with advanced fiber reinforcement have shown equal or more strength than steel and aluminum[6].

Composites are created by combining two or more materials typically a matrix and a reinforcement. The matrix provides cohesion and helps transfer the load. Matrix is a continuous phase that surrounds the support and helps in bonding and cohesion. Composites give designers flexibility during designing shapes. They can be molded into intricate shapes and components and help to achieve precise performance properties.

Epoxy resins act as a matrix and are combined with reinforcements to make composites. Epoxy resins have very efficient and excellent adhesion properties, and they can be used with various reinforcements, such as glass, carbon, and aramid fibers[7][8]. Because of its efficiency and strong bonding, it plays an important role in supporting the reinforcement and enhancing the composites' mechanical performance[9].

Studies have shown that modification of epoxy resins with rubber and then using anhydride for curing improves toughness[10]. However, some other studies[11] have shown that although using rubber in epoxy resin increases the toughness, but it reduces modulus and glass transition temperature ( $T_g$ ). They can be tailored to produce composites with high strength and low weight[12]. They can be personalized to make composites with good chemical and environmental resistance[5].

The ability of the composites to bear loads depends also on the orientation of the fibers. When the applied load is parallel to the fibers, they are capable of bearing higher loads[13]. Therefore, in general, conventional carbon composites show superior mechanical properties in the direction aligned with the fibers [14]. In some applications mechanical properties of non-woven composites depend on cross direction (CD) of fibers and machine direction (MD) of fibers. Non-woven fibers in cross direction (CD) have shown higher resistance to tensile load as compared to fibers in machine direction (MD)[15].

In recent times, companies have supported the idea of sustainability by making their production more and more sustainable so that the negative impact of production on the environment can be reduced. Since most thermoset resins are made from petrol-based compounds, they pose a significant threat to our environment as they cannot be adequately degraded at the end of life.

Sustainability is an issue while dealing with the composites. Because the components that combine to make composites are not biodegradable[16] .To mitigate this effect of composites on the environment, efforts have been made to reduce the environmental impact of composites on the environment, this includes using non-woven fibers, bio-based epoxy resins[17], and recycled carbon fibers (rCF) [3].

rCF are not waste but can be used for second applications to get valuable and sustainable raw materials. Adding value to already used carbon fibers and making them suitable to be used again plays a role in sustainability and circular economy [10]. Figure 2 shows sustainable fibers are made from wastes using less energy methods and at the end of life they are biodegradable, therefore, they pose minimum harm to the environment. From the sustainable point of view, some of the aspects of non-woven carbon fibers are discussed below[18]:



Figure 2: Sustainable fibers[19]

**Recycling:**

Carbon fibers from the end of life are used to make non-woven carbon fibers. Used waste is sorted and then recycled to make non-woven carbon fibers. Carbon fibers from edge trimmings and non-crimp fabric productions can be used for this purpose.

**Circular economy:**

Using rCF to make non-woven fibers creates no burden on natural resources. Virgin fibers are not used; instead, rCF are used for production. This will contribute to the circular economy[20], [21]. It is like a closed-loop system that involves collecting and recycling carbon fibers and then integrating them into the production cycle[20].

**Energy saving:**

It is an energy-saving process. The production of carbon fibers leads to the utilization of enormous amounts of energy. However, energy to produce a new thread is saved in this case. There are reduced processing steps in production, which ultimately leads to less energy usage[22]. Overall, simple manufacturing processes, lower processing temperatures, and fewer processing steps lead to energy-saving aspects of non-woven carbon fiber production[3].

**CO<sub>2</sub> footprints:**

By using less energy, it is evident that there will be an improvement in carbon footprints and, ultimately, a positive effect on the components' Life Cycle Assessment (LCA)[23], [24]. Using recycled raw materials, utilizing less energy, involving closed-loop production, and focusing on sustainable manufacturing leads to improving carbon dioxide footprints[24].

For sustainable manufacturing, use of carbon fiber non-woven composites (CFNWC) can be an interesting solution. Industry and academic experts have found CFNWC very interesting due to their lightweight and high specific strength. Fibers for producing (CFNWC) can be obtained from rCF, which is sustainable because no virgin resources are used in producing new fibers. The energy required to make non-woven carbon fabric from rCF is less intensive than that used to create woven carbon fabric from virgin carbon fiber[19]. Therefore, it has positive effect on the life cycle assessment (LCA) of the components[19][23].

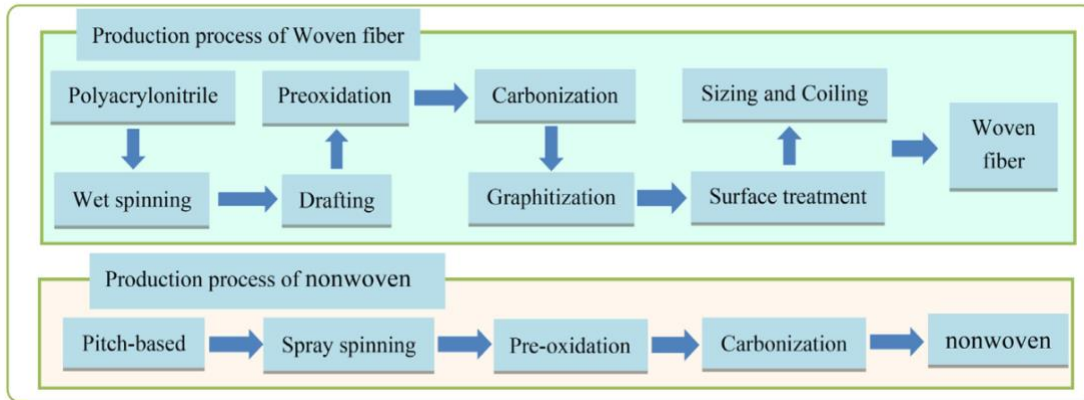


Figure 3: Comparison of molding process of woven fibers and non-woven fibers[3]

Figure 3 shows the comparison of steps used to make woven and non-woven fabric. Steps used to make non-woven carbon fibers are half as compared to the steps used to make woven fibers. Recently, many car manufacturers such as BMW, Ford, Volvo, and Chevrolet are using rCF composites based on body panels in their production, and many companies such as Volvo have started to use rCF composites in heavy-duty trucks[25]. rCF have many benefits that include building circular economy, as waste is reduced, and valuable natural resources are conserved.

Figure 4 shows the structure of woven, knitted, and non-woven fabric. In a non-woven fabric, there is a random arrangement of yarns without proper placement, and there is no weft or warp patterns as shown in Figure 4 (woven fabric). The strings are disposed randomly into a cohesive structure.

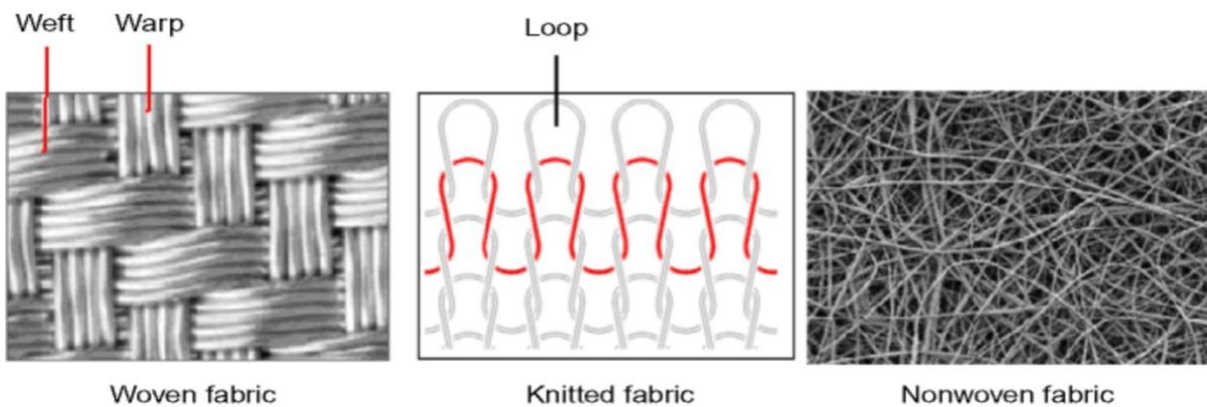


Figure 4: Structure of woven, knitted, non-woven fabric[26]

When the flexural modulus of composites having rCF is compared with the flexural modulus of composites having flax fibers, it is seen that the composite with rCF show superior strength and flexural modulus[27]. Moreover, the strength and modulus of composites are also affected by the manufacturing techniques[28]. When composites containing unidirectional non-woven carbon fibers and woven carbon fibers are manufactured by 3D printing, it is seen that composites containing unidirectional non-woven carbon fibers have superior strength compared to composites containing woven carbon fibers [29]. In some other studies researchers have found that using 3D non-woven carbon fibers composites, high ductility and strain hardening response can be achieved that is not common in traditional 2D composites[30].

Some other toughening methods are also studied to enhance mechanical properties of composites using non-woven fibers[8]. Fiber veils are used to enhance the mechanical properties of the composites. By using nonwoven aramid fiber veils delamination and deformation is restricted[31]. It is observed that by using aramid fiber veils in carbon composites compressive strength is greatly enhanced[31].

Different techniques are used to manufacture composites such as injection moulding, compression moulding, pultrusion, wet lay-up and vacuum assisted resin infusion [32] . The reinforcements can be glass fiber, flax fiber, carbon fiber depending on the applications. In this study, we used recycled non-woven carbon fiber mats instead of woven carbon fibers as reinforcement material. In order to manufacture the laminate Vacuum Assisted Resin Infusion (VARI) technique was adopted. In this technique, a vacuum is created, which helps to drive the resin into the mold. Once the wax is distributed evenly on the whole mold, the process is stopped, and then the laminate is left to dry for at least 24 hours. However, if the temperature of the surrounding environment is low, then the waiting time must be increased to ensure that the laminate has appropriately dried. Figure 5 illustrates the setup to manufacture composite laminates using VARI.

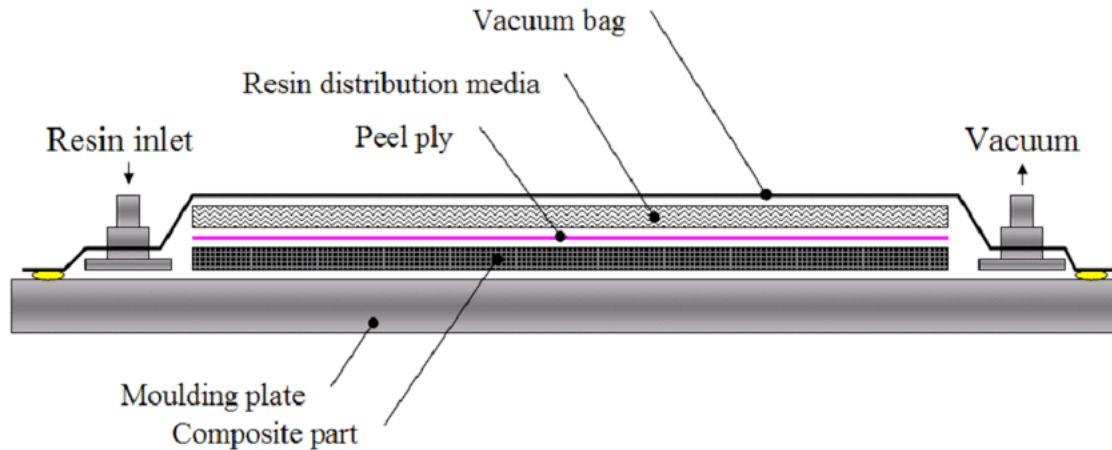


Figure 5: Vacuum Assisted Infusion Resin process[33]

After manufacturing of composite laminates, they were cured in an oven and then using water jet cutting system specimens were cut from the laminates according to the ASTM standards. Four mechanical tests namely Bending, Tensile, Compression, and Shear were applied on the specimens. In case of compression tests strain gauges were used to measure the strain. In case of tensile and shear specimens Digital Image Correlation (DIC) was used to map the strain on the surface of specimens.

The basic principle of DIC is that it tracks the changes in the same points, also called pixels, between two images. This is a non-contact measurement method, and it is most commonly used in engineering. It tracks the different patterns in images, and then, with the help of these patterns, it determines the deformation in the material. Figure 6 shows the mapping of reference subset in reference image to the corresponding subset on deformed image.

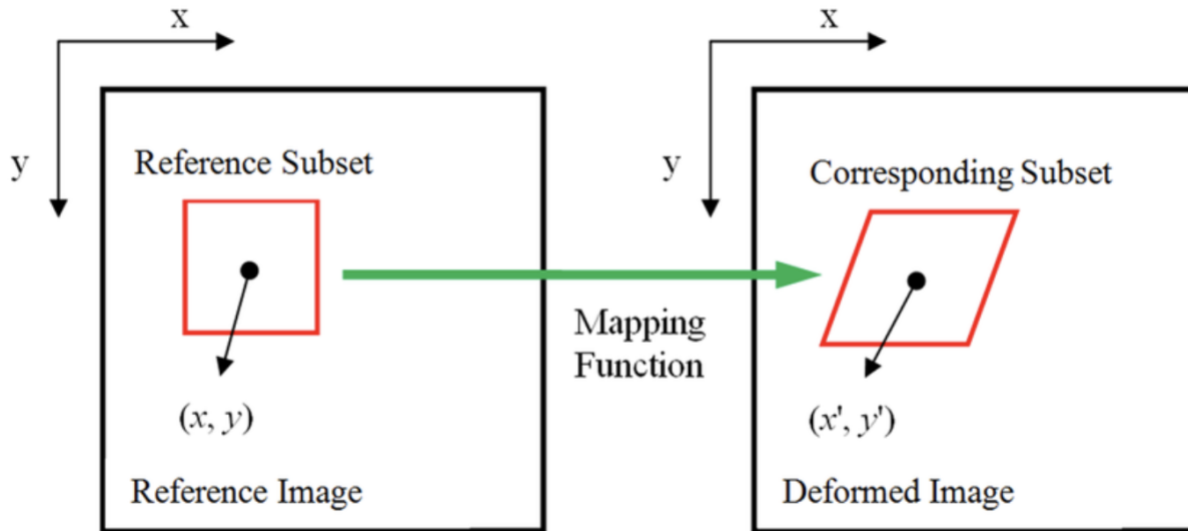


Figure 6: Basic principle of DIC[34]

The primary objective of this work was to examine the mechanical properties of non-woven carbon composites with a specific focus on their behavior at four distinct orientations:  $0^\circ$ ,  $30^\circ$ ,  $60^\circ$ , and  $90^\circ$ . The results from mechanical tests help us to study the strength and modulus of non-woven carbon composites at these different orientations. By studying the mechanical properties at different orientations, we gain insights into how these composites withstand different mechanical stresses.

Finally, we conducted the optical analysis of the fractured specimens. The aim of this analysis was to understand the fiber orientation in the region where fracture occurred. This allowed us to inspect the alignment and interconnection of fibers in the fracture zone. It helped to study the delamination, material defects and type of fracture that occurred in the specimens.

# Chapter 2: Materials and methods

## 2.1: Materials

### 2.1.1: Epoxy resin and hardener

In the present work, laminates of non-woven carbon fibers were manufactured using IN2 epoxy infusion resin Figure 7 and AT30 slow epoxy hardener Figure 8. Epoxy hardeners help to cure the resin, without hardener resin will always be near liquid state.



Figure 7: IN2 epoxy infusion resin[35]



*Figure 8: AT30 epoxy hardener[36]*

### **2.1.2: Non-woven carbon fiber mats**

Figure 9 shows random carbon fiber mats that are used as reinforcement material inside the composite. Fibers in these carbon mates are randomly oriented without any specific orientation.

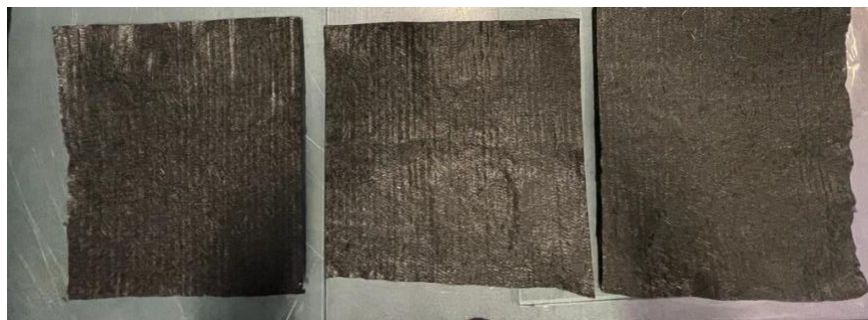


*Figure 9: Non-woven carbon fiber mats*

### 2.1.3: Water jet

After the drawings of specimens are completed in AutoCAD, it is then exported to WAM-WAZER. Wam is a software to generate a cutting file for Wazer (water jet cutting machine). In this software we give our desired inputs to generate a cutting file according to which Wazer cuts samples from the laminate. After generating the cutting file in WAM-WAZER software, the next step is cutting specimens.

Wazer water jet cutting machine works on the principle of water jet technology. Water through small orifice flows with very high pressure. Tremendous cutting power with which water streams hit the material helps in cutting. Abrasive materials are introduced in the water, which helps in enhancing the cutting ability. Various materials, such as metals, glass, plastics, and composites, can be cut using this machine.



*Figure 10: Water jet cutting machine.*

Figure 10 shows the water jet cutting machine that was used to cut the specimens. One of the most critical features of this machine is its compact size, and thus, it is suitable for the lab. This helps it to fit in small spaces and to occupy very little floor space. Waterjet that is used in cutting helps in precision cutting, and complex shapes and geometries can be cut. These features make it suitable for various artistic and industrial applications. It has an in-built user interface, ideal for professionals and new learners. Its comfort in use and ability to adapt to varying situations make it suitable for high-quality cuts. It is designed to be cost-effective, and thus, it is ideal for small-scale businesses, and educational institutions can also benefit from this cost-effective cutting machine.

#### 2.1.4: Oven



*Figure 11: Precision Composites Curing Oven[37]*

Figure 11 shows the oven OV301 that is used to cure the laminates. Most of the resins used in the composites show complete mechanical properties once they are adequately cured at high temperatures. Therefore, to achieve maximum glass transition temperature  $T_g$ , it is crucial to cure the laminates of composites at high temperature in the oven.

Specifications of OV301 are shown in the Figure 12:

Heating Power	1750	W	Vacuum Port Thread	1/4"	BSPP Female (G)	Gross Internal Volume	267	litres
Maximum Heating Rate	6	°C/min						
Maximum Cooling Rate	1	°C/min	Auxiliary Temperature Sensor Type	PT100 or PT1000	RTD 2-wire	Maximum Loading per Shelf	20	kg
Maximum Internal Temperature Variation	2	±°C	Auxiliary Temperature Sensor Socket	RTD Miniature Socket (White CU)		Working Internal Volume	235	Litres
Internal Dimensions	1070 x 440 x 500	W x D x H (mm)	Supply Voltage	220-240	VAC	Maximum Total Wattage	2300	W
			Electrical Supply Frequency	50 to 60	Hz			

Figure 12: Specifications of OV301[37]

## 2.1.5: Three-point bending test machine

Three-point bending tests were done using Zwick/Roell's z005 testing machine in lab. The equipment is specially designed for applying standardized tests on components.

### UTM (Zwick Roell- Z005)



#### Specifications

Maximum Test Load (kN)	5		
Max Crosshead Speed (mm/min)	3000		
Crosshead Travel Resolution (micro m)	0.0410		
Power Consumption, kVA	2		
Load Cells	Xforce P		
Load Cell Capacities	500 N and 5 kN		
Load Cell Mounting Stud Dia	20 mm		
Pneumatic Grip (Type 8297)	Fmax 2.5 kN and 5 kN		
Compression Platens	Dia (mm)	Fmax (kN)	Area Contact Pressure (N/mm <sup>2</sup> )
	Die-Cylinder	30	250
	Platen-Round	90	20
Temperature Range	50-250 Deg C		
Interface Software	testXpert -II		

Figure 13: Specifications of three-point bending test machine[38]

Specifications of three-point bending test machine can be seen in Figure 13, bending specimen is placed in the machine and it is bend due to the force applied by the machine during the experiment.

### 2.1.6: Tensile test machine

Tensile tests were performed using the Instron 8801 testing machine in the Lab. Instron 8801 is an advanced and versatile testing machine that is the flagship of Instron. Instron 8801 is the updated model of Instron 8800. Figure 14 below shows the setup of INSTRON 8801 along with DIC before the start of test.



*Figure 14: Instron 8801*

Some of the critical features of Instron 8801 are as follows:

**1- Flexibility:** Instron 8801 is flexible in a way that it can test a variety of materials such as rubbers, plastics, textiles, a variety of composites, biomaterials, etc. This flexibility makes Instron 8801 suitable to be used in a variety of applications related to industrial applications, quality control, and research purposes.

**2- Load capacity:** The load-carrying capacity of Instron 8801 makes it suitable for testing high-strength materials. Its load-carrying capacity varies from a few newtons to thousands of newtons. Therefore, it can be used to test low-strength to high-strength materials.

**3- Advanced software:** Instron 8801 uses very advanced and powerful Bluehill software that is user-friendly. It allows the user to monitor and visualize test data in real time.

**4- Precision and accuracy:** Instron 8801 has advanced load and displacement control systems that help acquire precise and accurate data. The integrity of the acquired data is maintained with the help of a strong frame of Instron 8801, which minimizes any unwanted vibrations.

**5- Customize test configurations:** Instron 8801 is suitable for doing customized tests. It can be used for compression, tensile, flexural, fatigue, tear, and peel tests.

**6- High-Temperature testing:** It's suitable to test materials at high temperatures. Therefore, it can be used in applications where materials experience extreme conditions.

**7- Industrial applications:** Instron 8801 is used in various industries, from automotive and aerospace to textile and plastic industries, where the performance of materials is considered critical.

## 2.1.7: Digital image correlation DIC

In Tensile testing, we used the DIC system along with Instron 8801. DIC measures the objects' displacement and strain when under forcing conditions. With the help of high-resolution cameras, several images are captured during the testing procedure. Specialized software is then used to correlate the pixel-level changes in these images. While using specimens during the test with DIC, they must be sprayed using the spray cans and creating random patterns in white and black. The process is very delicate as this pattern will be used to track the changes on the surface of the specimen using the postprocessing software.

When the process starts, a series of images are taken of the object under consideration. Two cameras are usually placed at a certain distance from the thing, and they capture these images. These cameras are high-resolution cameras, and they are specialized for this process. The images captured by cameras show different states such as the states before and after deformation. In each image, a subset is defined. Subset is a region of interest; it contains specific patterns that help to track displacements.

After that, different images are correlated, and patterns within the subsets are tracked. This is done to find the corresponding points between a reference image, usually an undeformed image, and a deformed image. This is done using image processing techniques. Usually, VIC-2D or 3D systems are employed for this purpose. These systems use specific optimization algorithms to provide displacement or strain data in all areas of interest[39] .

During the calculation of strain, distance, and angle changes between two points are considered. So, in the end, strain is calculated considering these two factors. Calibration must be done while using DIC. Therefore, calibration is performed using calibration grids. At the end of the process, when displacement and strain data are obtained, distribution plots and displacement plots can be drawn. These plots provide essential information about the deformation of the object and the area where maximum stress occurs.

## 2.2: Procedures

### 2.2.1: Vacuum Assisted Resin Infusion (VARI)

**1- Preparation of mold:** A mold is a tool that determines the final shape of our laminate. It is usually made of hard materials such as aluminum, carbon fiber, glass, etc. In our lab, we used a mold of glass, and it's a rectangular shape. Before the start of the process, it must be ensured that the surface of the mold is clean. Contaminants from the surface of the mold must be removed before the initiation of the process so that any residue from the previous process should not contaminate the process. If there is any residue left, then it will affect the adhesion between resin and mold. So, it must be prevented.

**2- Dry lay-up:** After cleaning the surface of the mold, we put the releasing agent onto the mold and left it to dry for 15 minutes. Releasing agents are essential because they help to remove the laminate at the end of the process. Without the releasing agent, the composite material will stick to the mold surface, and during the release, it will affect the surface of the composite. It must be placed evenly. Too much-releasing agents also sometime affect the quality of the composite. After drying it properly, we put non-woven carbon fiber cut into dimensions (350\*350) mm onto the mold and fixe it in the center using tape. After that, we placed a pre-ply on the non-woven carbon fiber. Dry lay-ups are usually of the same shape as mold. Figure 15 below shows the whole setup for vacuum infusion process just before the infusion of resin.

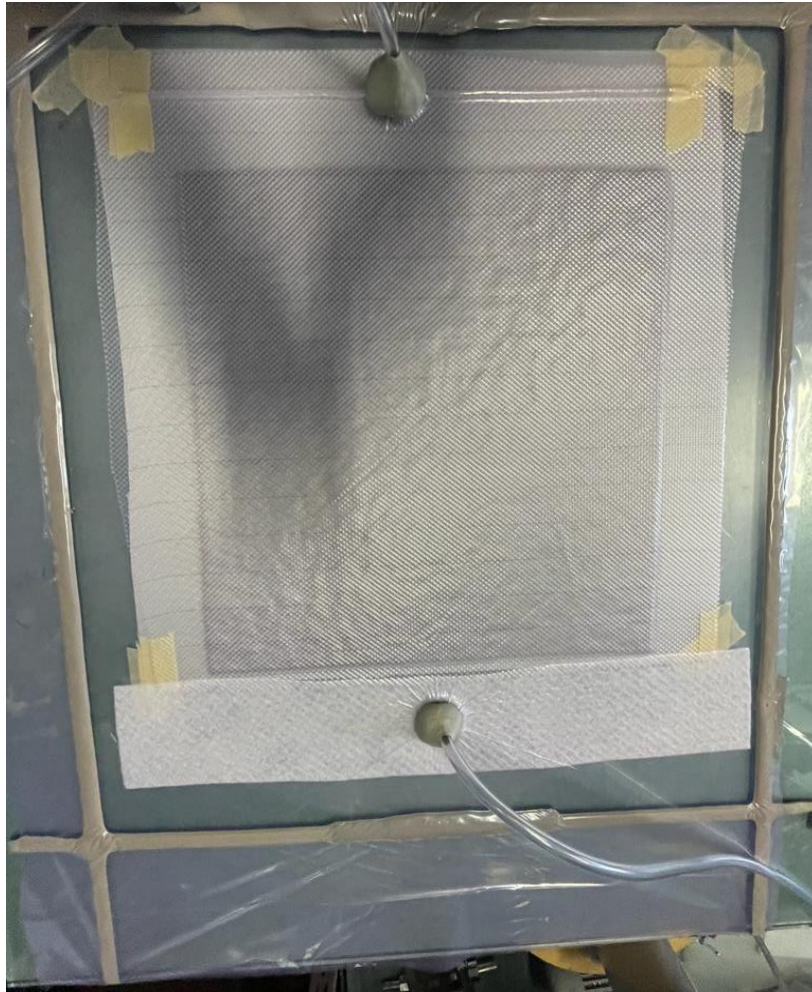


*Figure 15: Non-woven carbon fiber with flow mesh and sealed plastic bag connected with pump just before the infusion of resin.*

**3- Flow mesh:** We placed flow mesh over the pre-ply to distribute the resin evenly on the non-woven carbon fiber. Spiral tubing and breather are also used to assist the flow of infusion. Along with the flow, mesh bleeder and breather materials also play an essential role in the vacuum infusion process. Bleeder materials are also called peel ply. Their primary function is to absorb the excess resin. They act as a pool where excess resin is absorbed, preventing resin accumulation in a specific location. Due to their textured surface, they help to create channels, thus making sure that resin is evenly distributed throughout the lay-up. Moreover, breather materials are placed in the lay-up to help escape air and other volatiles while applying vacuum. They also help to spread the resin in the lay-up uniformly.

**4- Vacuum Bagging:** A flexible vacuum bag made of plastic is placed over the whole distribution, and it is sealed using silicon tapes on the edges of the mold. The load is then connected to the pump, which creates a vacuum in the bag, removing all the air inside. After making the vacuum inside the bag, we waited for 10 minutes as a precaution to check that the pressure on the pump needle should not change and that the vacuum was created perfectly. If there is even a slight change on the pump needle, then the vacuum bag is not sealed correctly, and there remains some passage for air to flow inside the bag. This should be stopped because if there is air inside the bag and we do the infusion of resin, our laminate will not hold the actual mechanical properties and will lead to the making of voids.

**5- Resin Infusion:** We used IN2 epoxy infusion resin mixed with AT30 slow epoxy hardener. It is in a liquid form with low viscosity and is introduced to the mold using inlet ports. As the vacuum is applied, the resin flows from the inlet port towards the outlet port, and it spreads over the whole dry lay-up, ensuring the complete impregnation of the reinforcement. During the process, there must be continuous monitoring of the process. The vacuum must be the same throughout the process and should not change. Any change in the vacuum level will lead to defects and leads to improper infusion process. Care must be taken in this aspect.

It can be seen in the Figure 16 that resin flows from one side and is in a halfway during the manufacturing of composite through vacuum infusion process.



*Figure 16: Resin flow*

**6- Demolding:** After the infusion of resin is complete the setup is left as it is. The pump is switched off. We leave the setup for almost 24 hours for curing to occur. Curing must be done depending on the type of resin used. Usually, manufacturers of a particular resin also give its curing time. Good monitoring and curing lead to the proper manufacturing of the laminates. After the curing has occurred properly, we remove the vacuum bag. After that part is de-molded from the mold, other extra materials, such as ply and flow mesh, are taken off the part.

### 2.2.2: Curing

After demolding, laminates were cured in an oven (OV301) Figure 11, under high temperature to cure it properly. In our case, we placed the laminate in the oven at 100 degrees Celsius for 2.5 hours. After curing, specimens can be cut from the laminates using a water jet cutting machine.

## 2.3: Specimens production

Specimens of different sizes were cut from the laminates. The dimensions of samples for the various mechanical test are different and depends on the dimensions available in the literature.

At first, specimens of each test (tensile, compression, shear, bending) were drawn in AutoCAD. Separate samples of each specific dimension were drawn, considering respective geometries. The drawings also helped us to understand how many laminates we need for our work. Therefore, in the end, it was clear that at least three laminates, each of (350\*350) mm, must be produced to get the required specimens for testing.

The Dimension of each specimen is as follows:

- 1- Tensile: (250\*25) mm
- 2- Compression: (150\*10) mm
- 3- Bending: (76\*19) mm
- 4- Shear: (80\*12.7) mm

Table 1 shows the number of specimens manufactured for each type of test and each orientation. Four mechanical tests, namely Tensile, Compression, Bending, and Shear, were done on four different angels such as 0°, 30°, 60°, 90°. For each test, twelve specimens were made, three specimens for each orientation.

Angle \ Test	Tensile	Compression	Bending	Shear
0°	3	3	3	3
30°	3	3	3	3
60°	3	3	3	3
90°	3	3	3	3
<b>Total</b>	12	12	12	12

*Table 1: Total number of specimens used in testing.*

### 2.3.1: Bending test specimens

Bending test samples were cut from composite laminate manufactured using non-woven carbon fiber according to **ASTM standard D790**. In total, 12 specimens were tested for four different angles (0°, 30°, 60°, 90°) angles—three specimens for one angle. Table 2 consists of data regarding the dimensions of all 12 samples.

<b>Samples for 0° degree</b>	<b>Dimensions (Width*Thickness) mm</b>
1-	11.94*2.26
2-	12.16*2.19
3-	12.13*2.12
<b>Samples for 30° degree</b>	<b>Dimensions (Width*Thickness) mm</b>
1-	12.19*1.99
2-	12.12*2.18
3-	12.15*2.17
<b>Samples for 60° degree</b>	<b>Dimensions (Width*Thickness) mm</b>
1-	12.03*1.94
2-	12.15*2.19
3-	12.25*2.37
<b>Samples for 90° degree</b>	<b>Dimensions (Width*Thickness) mm</b>
1-	12.20*2.22
2-	12.13*2.37
3-	11.75*1.99

*Table 2: Dimensions of bending specimens*

### 2.3.2: Tensile test specimens

Tensile test samples were cut from composite laminate manufactured using non-woven carbon fiber according to **ASTM standard D3039/3039M**. In total, 12 specimens were tested for four different angles (0°, 30°, 60°, 90°) angles—three specimens for one angle. Table 3 consists of data regarding the dimensions of all 12 samples.

<b>Samples for 0° degree</b>	<b>Dimensions (Width*Thickness) mm</b>
1-	24.23*2.31
2-	24.38*2.22
3-	24.34*2.38
<b>Samples for 30° degree</b>	<b>Dimensions (Width*Thickness) mm</b>
1-	24.40*2.28
2-	24.50*2.33
3-	24.57*2.26
<b>Samples for 60° degree</b>	<b>Dimensions (Width*Thickness) mm</b>
1-	24.58*2.18
2-	24.56*2.36
3-	24.52*2.47
<b>Samples for 90° degree</b>	<b>Dimensions (Width*Thickness) mm</b>
1-	23.03*2.12
2-	24.26*2.35
3-	24.48*2.08

*Table 3: Dimensions of tensile specimens*

### 2.3.3: Compression test specimens

Compression test samples were cut from composite laminate manufactured using non-woven carbon fiber according to **ASTM standard D695**. In total, 12 specimens were tested for four different angles (0°, 30°, 60°, 90°) angles—three specimens for one angle. Table 4 consists of data regarding the dimensions of all 12 samples.

<b>Samples for 0° degree</b>	<b>Dimensions (Width*Thickness) mm</b>
1-	9.53*2.32
2-	9.52*2.34
3-	9.49*2.40
<b>Samples for 30° degree</b>	<b>Dimensions (Width*Thickness) mm</b>
1-	9.42*2.24
2-	9.57*2.29
3-	9.44*2.22
<b>Samples for 60° degree</b>	<b>Dimensions (Width*Thickness) mm</b>
1-	9.42*2.04
2-	9.50*2.42
3-	9.46*2.46
<b>Samples for 90° degree</b>	<b>Dimensions (Width*Thickness) mm</b>
1-	9.30*1.96
2-	9.45*2.14
3-	9.47*2.15

*Table 4: Dimensions of compression specimens*

Compression tests were done after putting the strain gauges (HBM 1-LY48-3/350) on the specimens. Strain gauges were placed in the center of the compression specimens as shown. Figure 17 shows the pattern in which the strain gauges were glued to the compression specimens.



*Figure 17: Strain gauges bonded to compression specimens.*

Strain gauges are used to measure mechanical deformation. Strain gauges are bonded with the structure, and they can also be embedded in the structure to measure deformation[40] By using strain gauges (HBM 1-LY48-3/350) on the specimens and placing them on Instron 8801, National Instrument NI 9237 system was used to amplify strain signals.

Table 5 below shows the specifications of strain gauges that were used on compression specimens to measure the strain used:

<b>Name</b>	<b>Specifications</b>
<b>Resistance</b>	$350\Omega \pm 0.30\%$
<b>K-Factor</b>	$2.10 \pm 1.0\%$
<b>Transverse sensitivity</b>	0.1%
<b>Temperature compensation: with plastics</b>	$65[10^{-6}/K]$
<b>Order number</b>	1-LY48-3/350
<b>Type</b>	3/350 LY48
<b>Temperature coefficient of gage factor</b>	$101 \pm 10[10^{-6}/K]$ (-10 °C ... +45 °C)

*Table 5: Specifications of strain gauges used for compression tests.*

### 2.3.4: Shear test specimens

Shear test samples were cut from composite laminate that was manufactured consisting of non-woven carbon fiber according to **ASTM standard D5379**. In total, 12 specimens were tested for four different angles (0°, 30°, 60°, 90°) angles—three specimens for one angle. Table 6 consists of data regarding the dimensions of all 12 samples.

<b>Samples for 0° degree</b>	<b>Dimensions (Width*Thickness) mm</b>
1-	12.19*2.56
2-	11.68*2.30
3-	11.82*2.20
<b>Samples for 30° degree</b>	<b>Dimensions (Width*Thickness) mm</b>
1-	11.70*2.20
2-	11.84*2.25
3-	12.10*2.35
<b>Samples for 60° degree</b>	<b>Dimensions (Width*Thickness) mm</b>
1-	11.65*2.27
2-	11.68*2.27
3-	11.83*2.38
<b>Samples for 90° degree</b>	<b>Dimensions (Width*Thickness) mm</b>
1-	11.63*2.18
2-	11.52*2.17
3-	11.75*2.05

*Table 6: Dimensions of shear specimens*

The DIC system was used, along with Instron 8801, to test shear specimens, and the whole procedure was repeated as it was done during the tensile testing of the samples.

## 2.4: Mechanical tests

### 2.4.1: Three-point bending test

Figure 18 illustrates the specifications of three-point bending test setup during the experiments. Three-point bending test was applied on each specimen one by one according to standard conditions. Force and displacement data were then acquired from the data acquisition system, and then, finally, analysis was carried out to measure stress and strain on the composite specimens. Testing speed was 0.8mm/min.



*Figure 18: Specimen undergoing bending during three-point bending test.*

To find the stress using the force and displacement data the following equation was used:

$$\sigma_f = 3PL/2bd^2 \quad [41]$$

Where:

$\sigma_f$  = Stress in outer fibers at midpoint (MPa)

P = Load at a given point (N)

L = Support span (mm)

d = Depth of beam tested (mm)

b = Width of beam tested (mm)

To find the strain, the following equation was used:

$$\varepsilon_f = 6Dd/L^2 \quad [41]$$

Where:

$\varepsilon_f$  = Strain in the outer surface (mm/mm)

D = Maximum deflection in the center of beam (mm)

L = Support span (mm)

d = Depth of beam tested (mm)

Both equations are taken from **standard D790**, according to which all the testing conditions were respected. To calculate the modulus, we used the stress strain curve that was made using force and displacement data. Using the trendline feature an equation can be developed in the form:

$$Y = mx + c$$

Where:

Y = represents stress ( $\sigma$ )

x = represents strain ( $\varepsilon$ )

m = represents slope of the stress-strain curve which is actually the 'Modulus'

c = represents constant

Finally, stress, strain, and modulus were found in the end.

## 2.4.2: Tensile test



*Figure 19: Tensile test configuration*

Figure 19 above shows the DIC image of the tensile specimen during the tensile testing. When the experiments are done, data is acquired from the acquisition system. After that, data is post-processed, analyzed, and converted into (.mat) and (.csv) files. A MATLAB script is then used to find the specimens' stress, strain, and modulus using (.mat) and (.csv) data acquired from the acquisition system. Testing speed was 2mm/min.

In the script, stress was calculated using the equation:

$$F^{tu} = P^{max} / A \quad [42]$$

Where:

$F^{tu}$  = Ultimate tensile strength (MPa)

$P^{max}$  = Maximum force before failure (N)

A = Average cross-sectional area of specimen (mm<sup>2</sup>)

In order to calculate the modulus using stress-strain data 'polyfit' feature was used. Using a polyfit feature a linear polynomial can be fit to the stress-strain curve and slope can be found, that will eventually represent the modulus. Therefore, modulus can be calculated.

### 2.4.3: Compression test

Figure 20 below shows the testing configuration of compression test. UTM usually gives force data, while strain or displacement data is generally captured by strain gauges to measure strain in the specimens. The speed of testing was  $1.3 \pm 0.3$ mm/min.

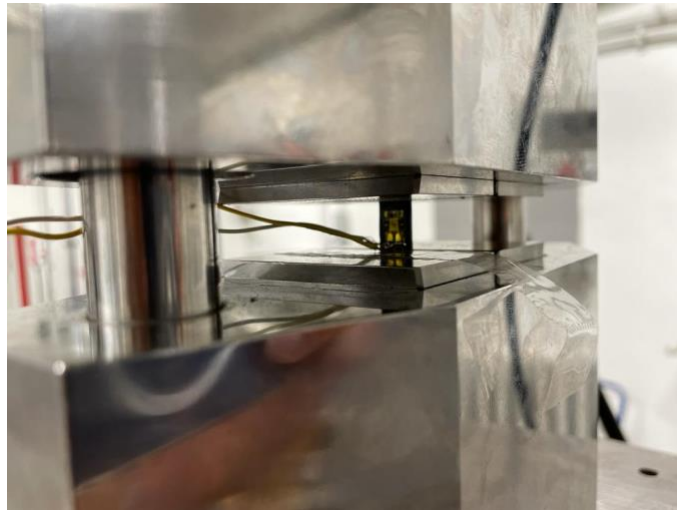


*Figure 20: Compression test configuration*

After the tests, load and strain data is acquired from the acquisition system. Stress can be calculated using equation:

$$\sigma_{\text{compression}} = F/A \quad [43]$$

Where:

$\sigma_{\text{compression}}$  = Compressive strength (Mpa)

F = Maximum compressive load (N)

A = Minimum cross-sectional area of specimen (mm)

Using slope of the stress-strain curve from stress-strain graph, modulus is calculated.

#### 2.4.4: Shear test

Figure 21 below shows the shear testing at Instron 8801 along with DIC system. DIC helped gather strain/displacement data and then used for analysis. The speed of testing was 2mm/min.

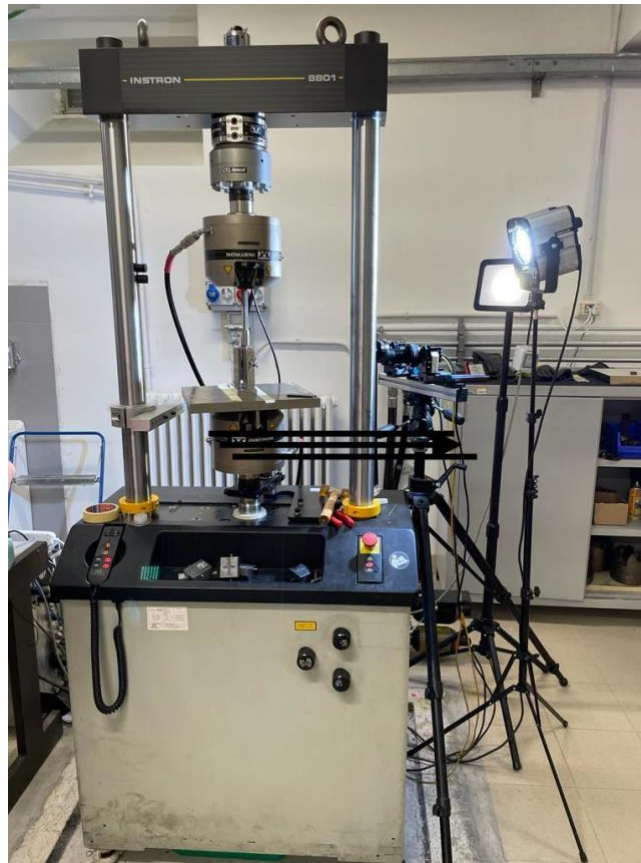


*Figure 21: Instron 8801 along with DIC system during shear testing*



*Figure 22: Shear testing configuration*

Figure 22 above shows the shear specimen as it is fixed between the jaws of testing machine. After completing the experiments, data is collected from the acquisition system. Data is post-processed, analyzed, and converted into (.mat) and (.csv) files. A MATLAB script is then used to find the specimens' stress, strain, and modulus using (.mat) and (.csv) data from the acquisition system.

In the script, stress was calculated using the equation:

$$F^u = P^u / A \quad [44]$$

Where:

$F^u$  = Ultimate strength (MPa)

$P^u$  = Load at 5% engineering shear strain (N)

$A$  = Cross-sectional area of specimen (mm<sup>2</sup>)

The area is calculated using the equation:

$$A = w \times h$$

Where:

$w$  = width across the notch of the specimen (mm)

$h$  = thickness at the notch (mm)

The 'poly fit' feature was used to calculate the modulus using stress-strain data. Using a poly fit feature, a linear polynomial can be fit to the stress-strain curve, and a slope can be found that will eventually represent the modulus. Therefore, modulus can be calculated.

# Chapter 3: Results and discussion

Results obtained from the analysis of data from experimentation are discussed below:

## 3.1: Bending test

### 3.1.1: 0° degree

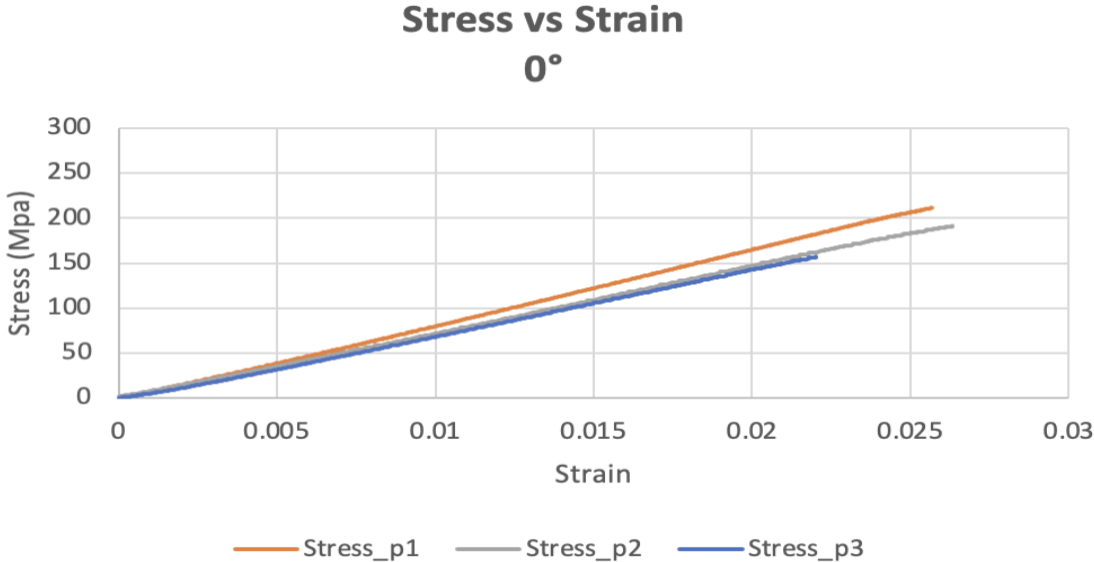


Figure 23: Stress-strain curves for 0° specimens

Figure 23 shows that when the bending tests were applied on specimens where epoxy flows in 0° direction, composite specimens showed around 187 MPa of mean stress. One of the specimens also showed the highest stress, around 211 MPa. Curves of 2<sup>nd</sup> specimen and 3<sup>rd</sup> specimen are superimposed. Both curves follow the same path. However, the strength in the 2<sup>nd</sup> specimen is more than the 3<sup>rd</sup> specimen. The mean modulus was almost 7040 MPa. By analyzing the stress at each specimen, one can see that there is not a significant difference in values of stresses among the three specimens. Therefore, a mean stress of around 187 MPa is obtained at the end of the analysis for specimens in which the flow direction of epoxy was 0°.

### 3.1.2: 30° degree

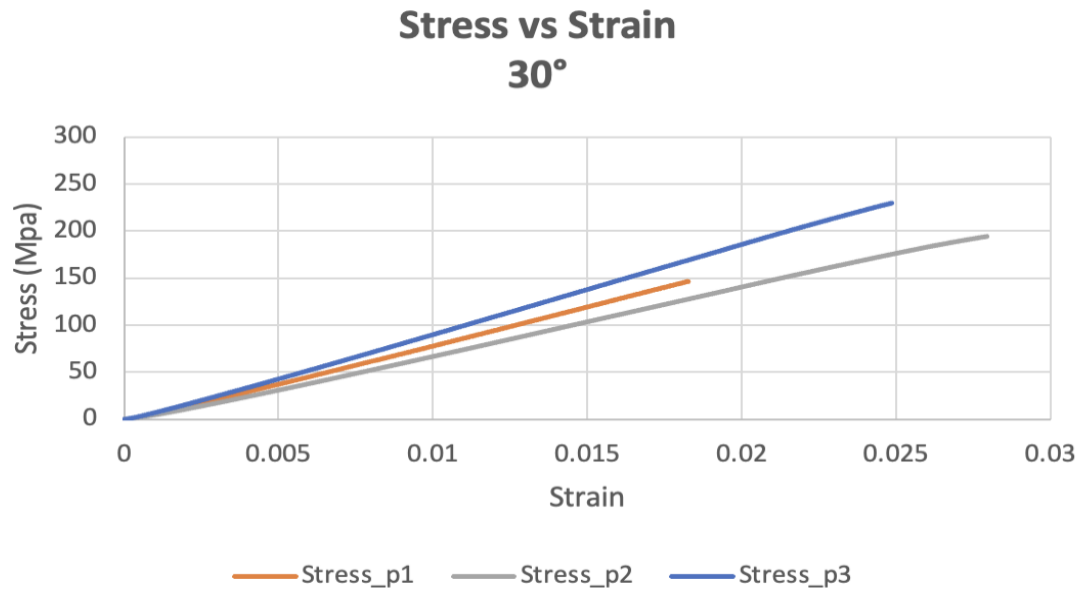


Figure 24: Stress-strain curves for 30° specimens

Figure 24 shows that when the bending tests were applied on specimens where the epoxy flow was at 30° with respect to the referenced 0° direction, composite specimens showed around 190 MPa of mean stress. One of the specimens also showed the highest stress, around 211 MPa. The mean modulus was almost 7610 MPa. It is worth noting that stress increases in a 30° direction and is more significant than in 0° direction. In most of the cases, it can be concluded that the fiber-epoxy matrix is more potent in these specimens as compared to the samples of 0°. When the fibers align themselves in the direction of the flow of epoxy, the strength of the composite increases even more because the bonding is more robust. All three curves show different strengths and unique mechanical properties. Therefore, a mean stress of around 190 MPa is obtained at the end of the analysis.

### 3.1.3: 60° degree

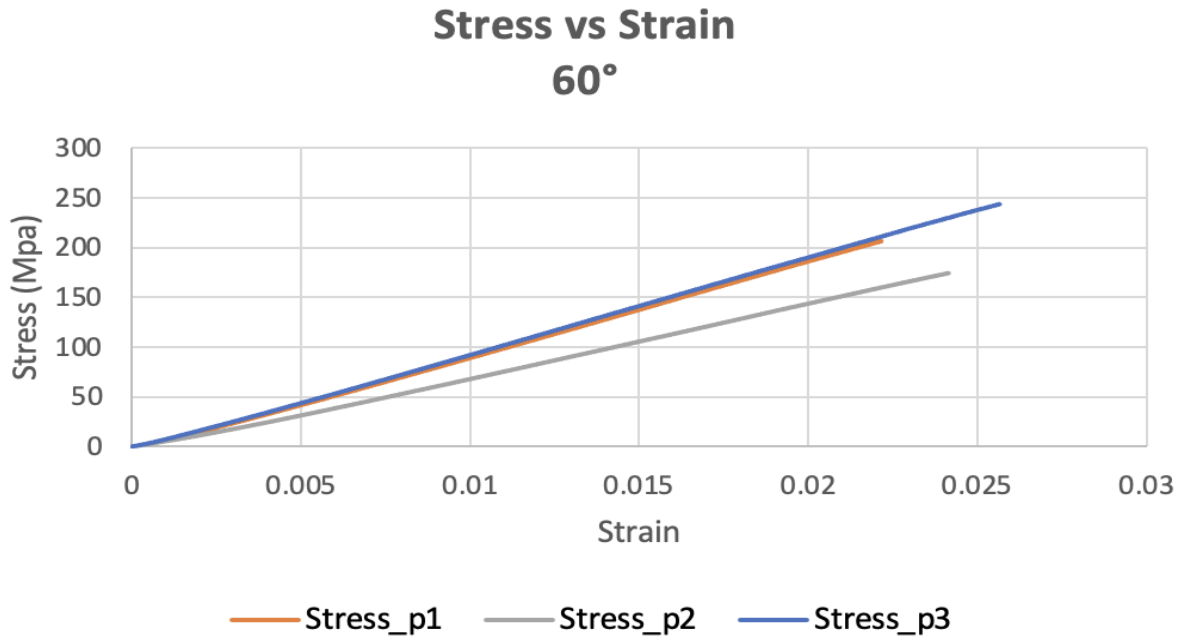


Figure 25: Stress-strain curves for 60° specimens

Figure 25 shows that when the bending tests were applied on specimens where the epoxy flow was at 60° concerning the referenced 0° direction, composite specimens showed around 208 MPa of mean stress. One of the specimens also showed the highest stress, around 243 MPa. The mean modulus was almost 7920 MPa. It is worth noting that stress increases in a 60° direction and is more significant compared 0° and 30° directions. Moreover, a mean stress of around 208 MPa is obtained at the end of the analysis for specimens where the epoxy flow was at 60° concerning the referenced 0° direction. Curves of 1<sup>st</sup> and 3<sup>rd</sup> specimen are super imposed. They have almost similar linear elastic behavior. However, the strength of 3<sup>rd</sup> specimen is 15% more than the 1<sup>st</sup> specimen. From the results, it can be concluded that stress depends on several factors and not solely on the flow direction of epoxy. The orientation of fibers and the population of fibers in the specific region plays a vital role in the values of stresses.

### 3.1.4: 90° degree

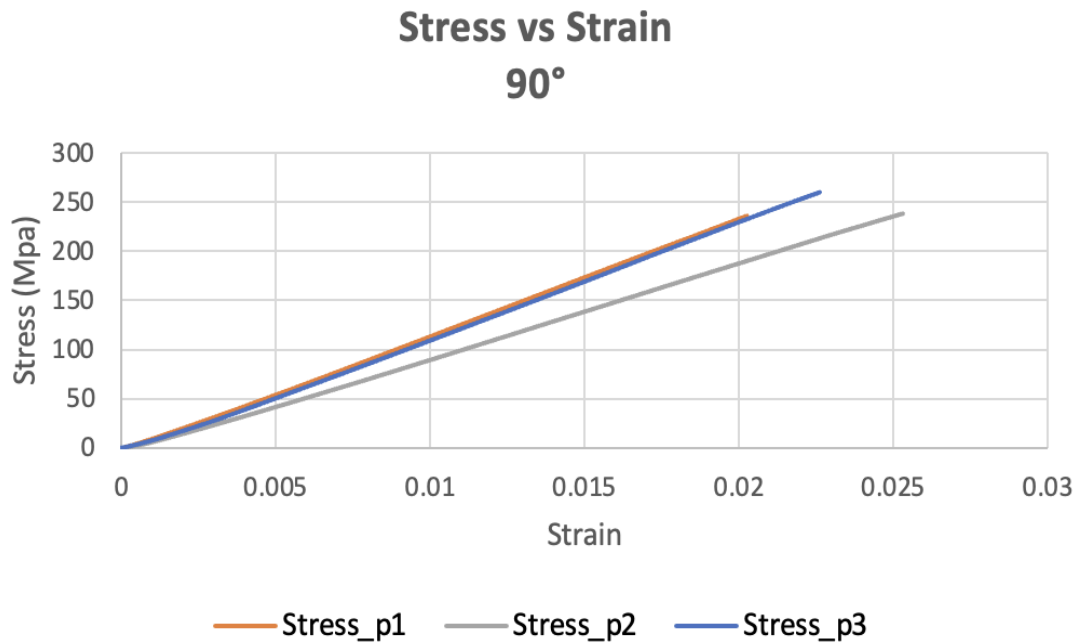
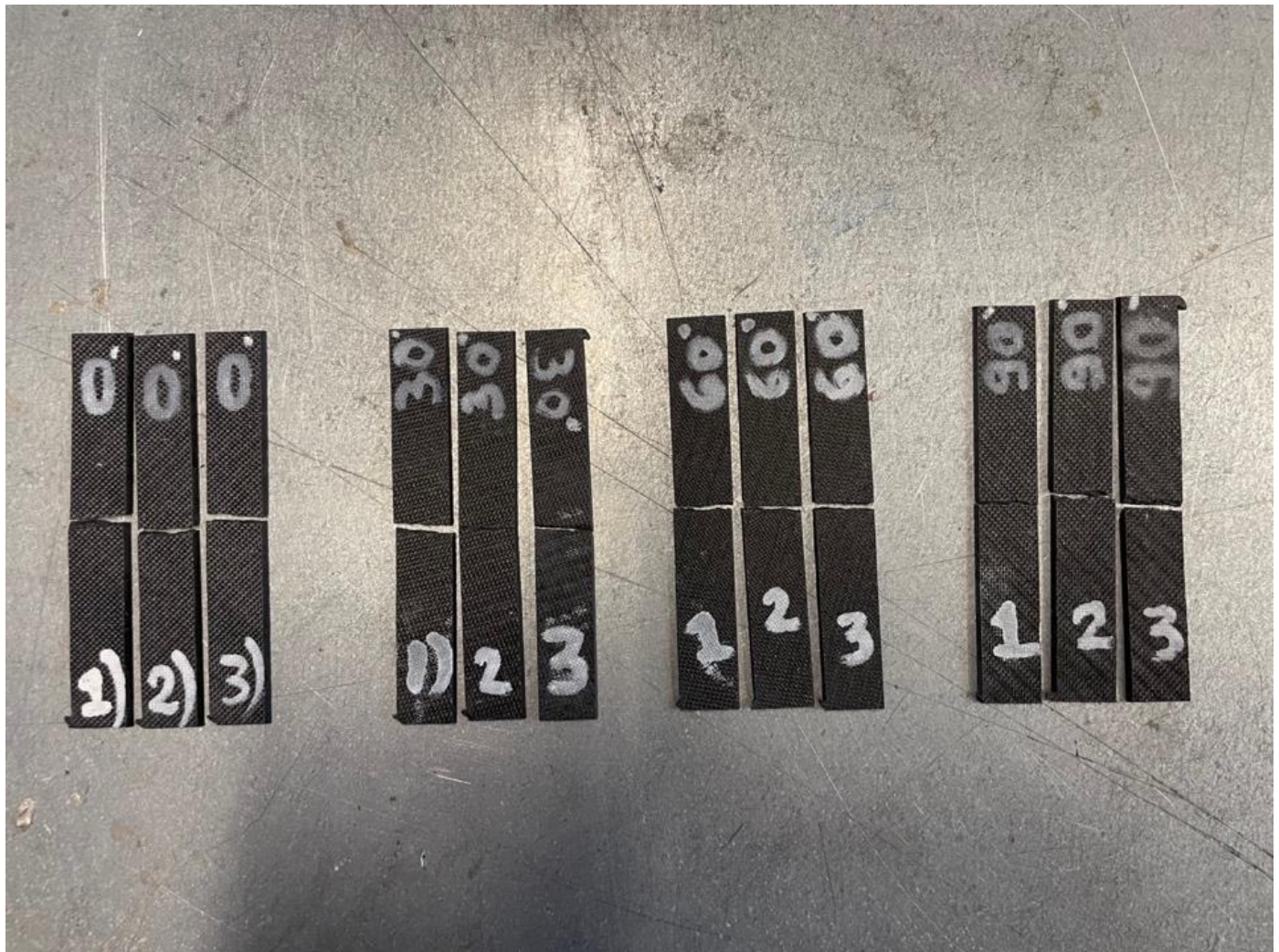


Figure 26: Stress-strain curves for 90° specimens

Figure 26 shows that when the bending tests were applied on specimens where the epoxy flow was at 90° concerning the referenced 0° direction, composite specimens showed around 245 MPa of mean stress. One of the specimens also showed the highest stress, around 260 MPa. The mean modulus was almost 9800 MPa. It is worth noting that stress increases in 90° direction and is much larger than what the results show in 0°, 30°, and 60° direction. Therefore, a mean stress of around 245 MPa is obtained at the end of analysis for specimens in which flow of epoxy was in 90° concerning referenced 0° direction. So, out of all the directions, at 90°, maximum stress is obtained, which is somehow a strange behavior of non-woven carbon composites. Since the flow of epoxy was in 0° direction, one can imagine that maximum stress will be obtained in the direction of the flow of epoxy. In 90° orientation stress was 24% more than in 0° orientation. Maximum stress in 90° direction maybe because some specific configuration of fibers enhances the composite's overall strength in this orientation. Moreover, it can also be said that the specimens of 90° orientation have perfect fiber matrix composition, which enhances the

mechanical properties of these specimens, which resulted in high stress compared to other orientation.

Figure 27 Illustrates the breaking pattern of bending test specimens. It can be seen that single fracture occurred in all orientations.



*Figure 27: Specimens after bending test*

### 3.1.5: Comparison of bending stress at different orientations

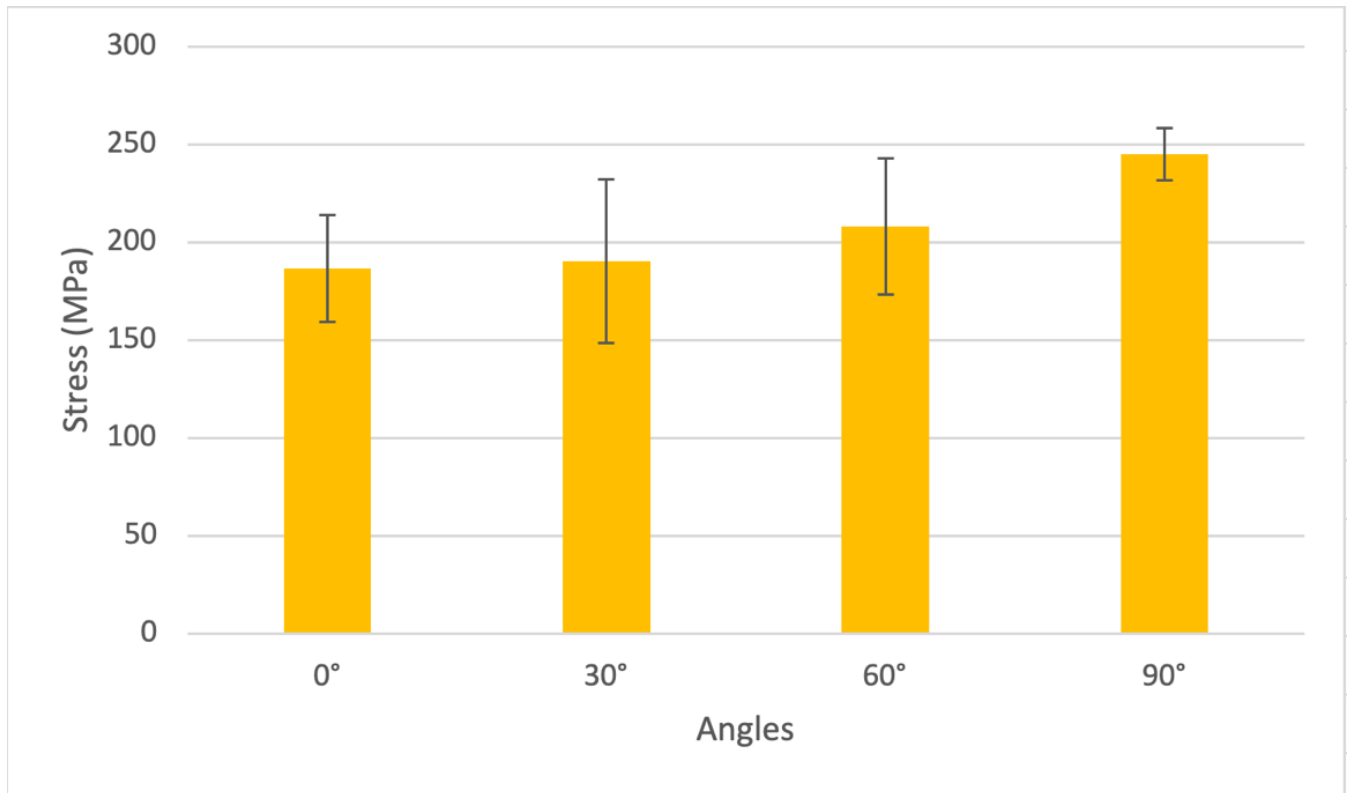


Figure 28: Bar chart showing bending stress at different orientations.

The bar chart in the Figure 28 shows that maximum stress is found to be in 90° orientation. There is no surprise in it because maximum force was required to rupture the specimens with 90° orientation, so it can be concluded that these specimens will exhibit high mechanical strength. Minimum stress was found in 0° direction while maximum stress was found in 90° direction. In 90° direction there is 24% more stress than in 0° direction. Although in the chart above, it is seen that there is a difference in the values of stresses at different orientations, they are not too big. In short, it cannot be concluded that solid or weak stresses exist in any specific direction. Overall, the whole composite represents a balanced distribution of stresses. The stochastic nature of fiber distribution, composition, and population of carbon fibers at specific locations and, of course, the orientation considering the flow of epoxy play their role in determining the final mechanical properties of these composites. To sum up, it cannot be concluded that there is only one factor,

such as the orientation of fibers with respect to the flow of epoxy, but combined, many factors contribute to the final strength of these composites. These mechanical properties vary from composites to composites.

### 3.1.6: Comparison of bending modulus at different orientations

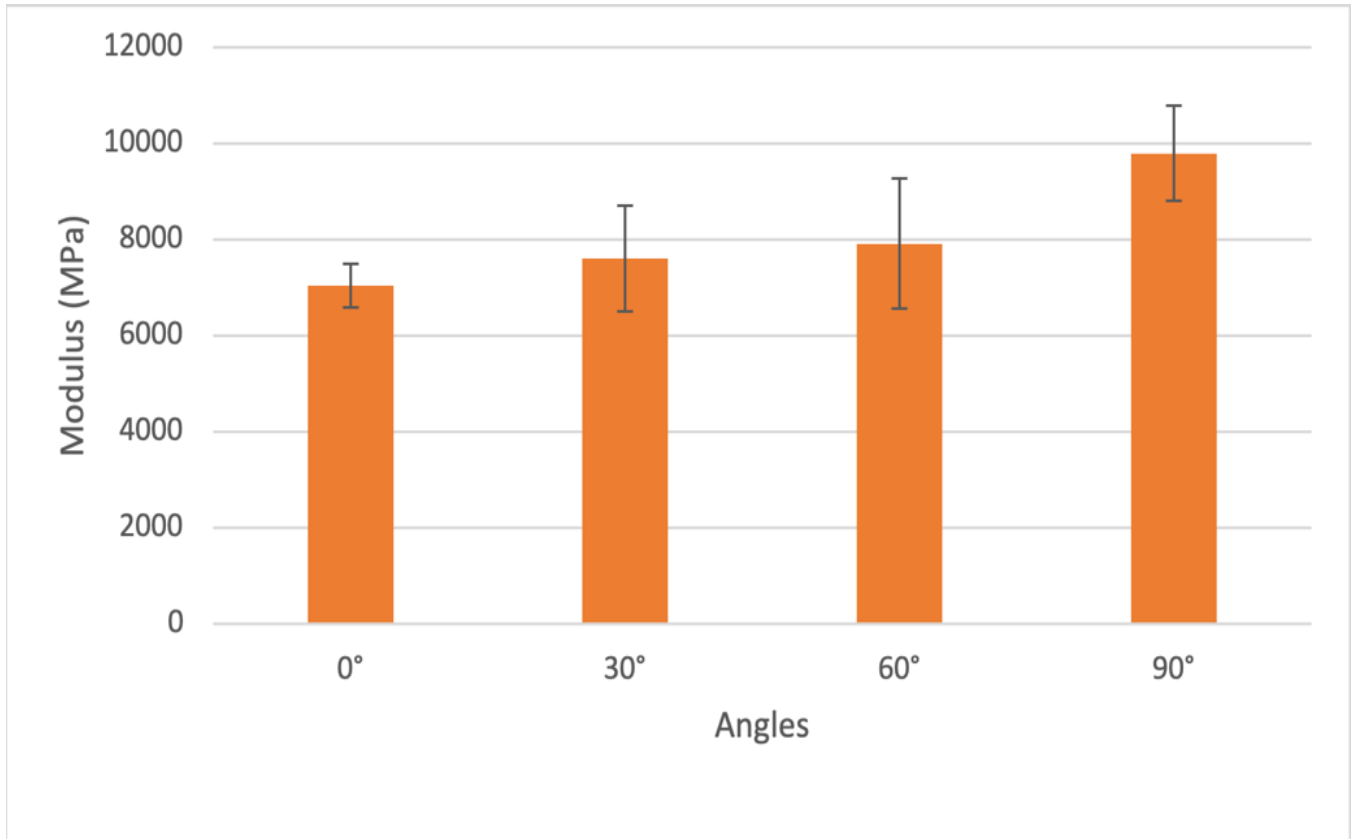


Figure 29: Bar chart showing bending modulus at different orientations.

The bar chart in Figure 29 shows that the highest modulus was found in 90° orientation with 9800 MPa, while the lowest was in 0° orientation with 7040 MPa, which was 28% lower than in 90° direction. The bar chart of modulus looks the same as that of stress. It represents the isotropic nature of non-woven composites where the mechanical properties are almost identical in all directions without any significant difference. Therefore, the modulus in these composites usually represents the average stiffness of the material. As the strength was higher in the 90°

direction, the modulus was also higher because the strength usually influences the composite's modulus.

### 3.1.7: Comparison of bending strain at different orientations

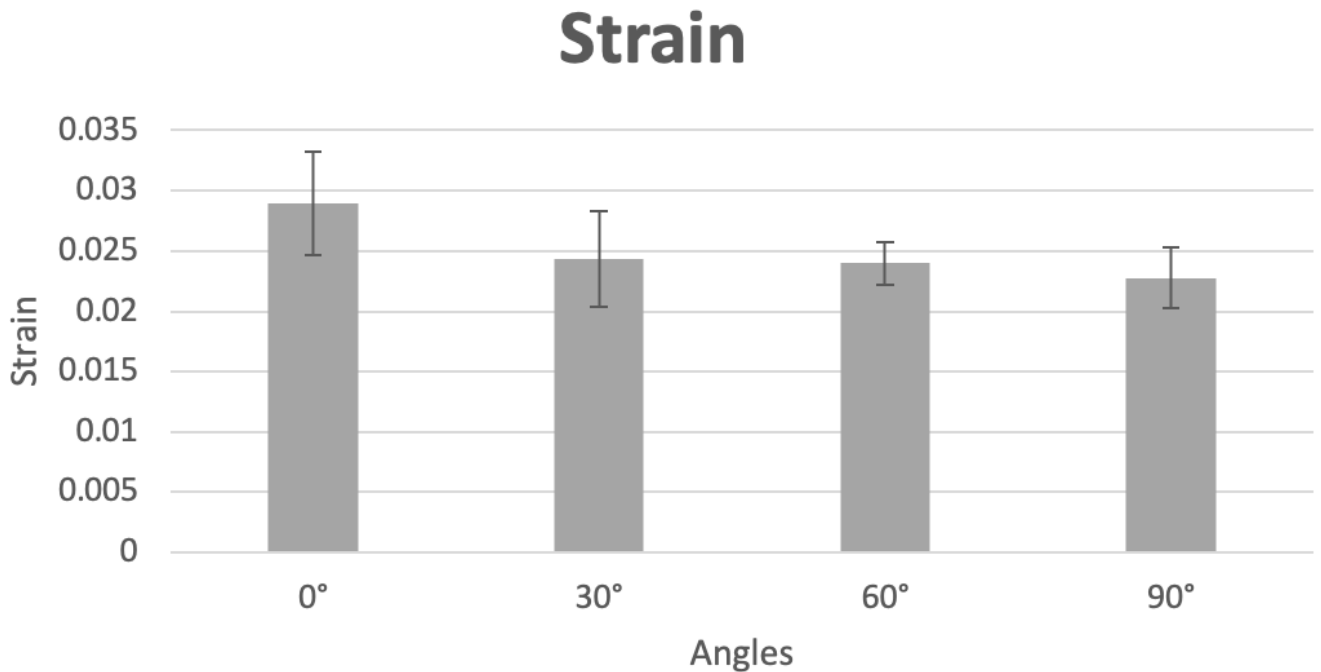


Figure 30: Bar chart showing bending strain at different orientations.

The bar chart in Figure 30 represents the values of strains at four different orientations. The maximum strain was found in 0° specimens, while the minimum strain was found in 90° specimens. Since minimum stress was found in 0° orientation, which represents that fiber matrix composition was not so strong in that orientation to resist the applied load, maximum strain is found in 0° direction as is indicated in the bar chart above. Sometimes, it also happens that localized high strain can be obtained due to stress concentration regions, although stress in that region is minimal. From the chart, it is also seen that 30° and 60° orientations have almost

similar strains, thus indicating that the deformation of the material in these orientations is the same.

Table 7 shows the mean force, mean stress, mean strain, and mean modulus in all four directions, along with their standard deviations. Maximum bending force, maximum bending stress, and maximum bending modulus were found to be in 90° orientation, while maximum bending strain was found to be in 0° direction.

<b>Stress</b>				
<b>Angles</b>	<b>0°</b>	<b>30°</b>	<b>60°</b>	<b>90°</b>
<b>Mean stress (MPa)</b>	186.6	190.3	208.1	245
<b>STDEV</b>	27.4	41.8	34.7	13.4
<b>Modulus</b>				
<b>Angles</b>	<b>0°</b>	<b>30°</b>	<b>60°</b>	<b>90°</b>
<b>Mean modulus (MPa)</b>	7039.6	7610	7920	9800
<b>STDEV</b>	450.4	1095.1	1358	990.3
<b>Strain</b>				
<b>Angles</b>	<b>0°</b>	<b>30°</b>	<b>60°</b>	<b>90°</b>
<b>Mean strain</b>	0.0289527	0.024344	0.0240067	0.022739
<b>STDEV</b>	0.0042574	0.003929	0.001768	0.002521

*Table 7: Mean force, mean stress, mean strain, and mean modulus at different orientations*

## 3.2: Tensile tests

### 3.2.1: 0° degree

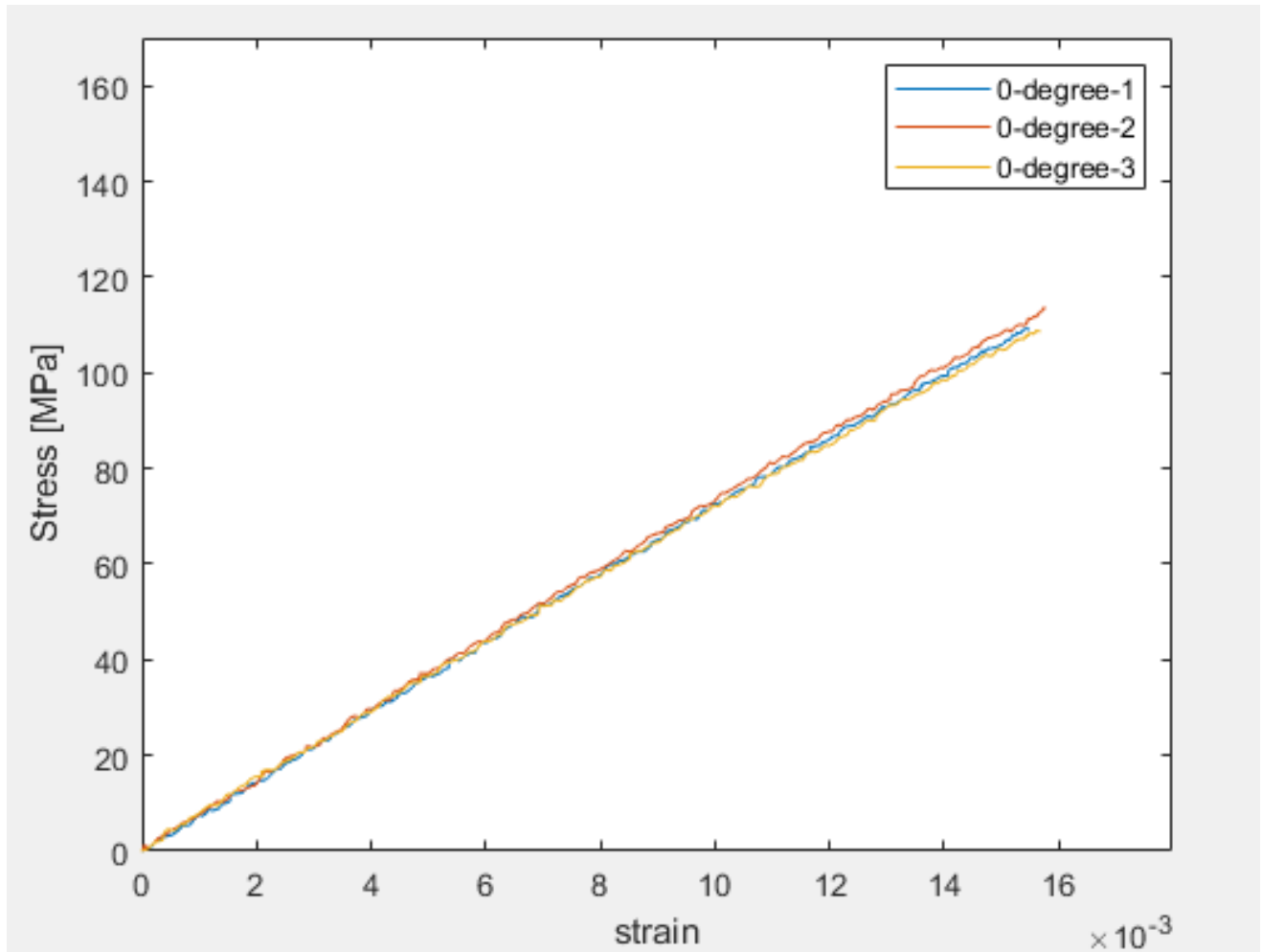


Figure 31: Stress vs strain at 0° degree

Figure 31 shows that when the bending tests were applied on specimens where epoxy flows in 0° direction, the mean stress composite specimens showed around 112 MPa. One of the specimens also showed the highest stress, around 115 MPa. The mean modulus was almost 7288 MPa. By analyzing the stress at each specimen, one can see that there is not a significant difference in values of stresses. All three curves show similar linear elastic behavior, while the curves of 1<sup>st</sup>

and 3<sup>rd</sup> specimens are superimposed on each other. A mean stress of around 112 MPa is obtained at the end of the analysis for specimens in which the flow direction of epoxy was 0°.

Consequently, there is a uniform distribution of stresses in all three specimens, which is also evident from the above curves. In the initial part, curves also overlap, indicating the level of similarity among the mechanical properties of these specimens.

### 3.2.2: 30° degree

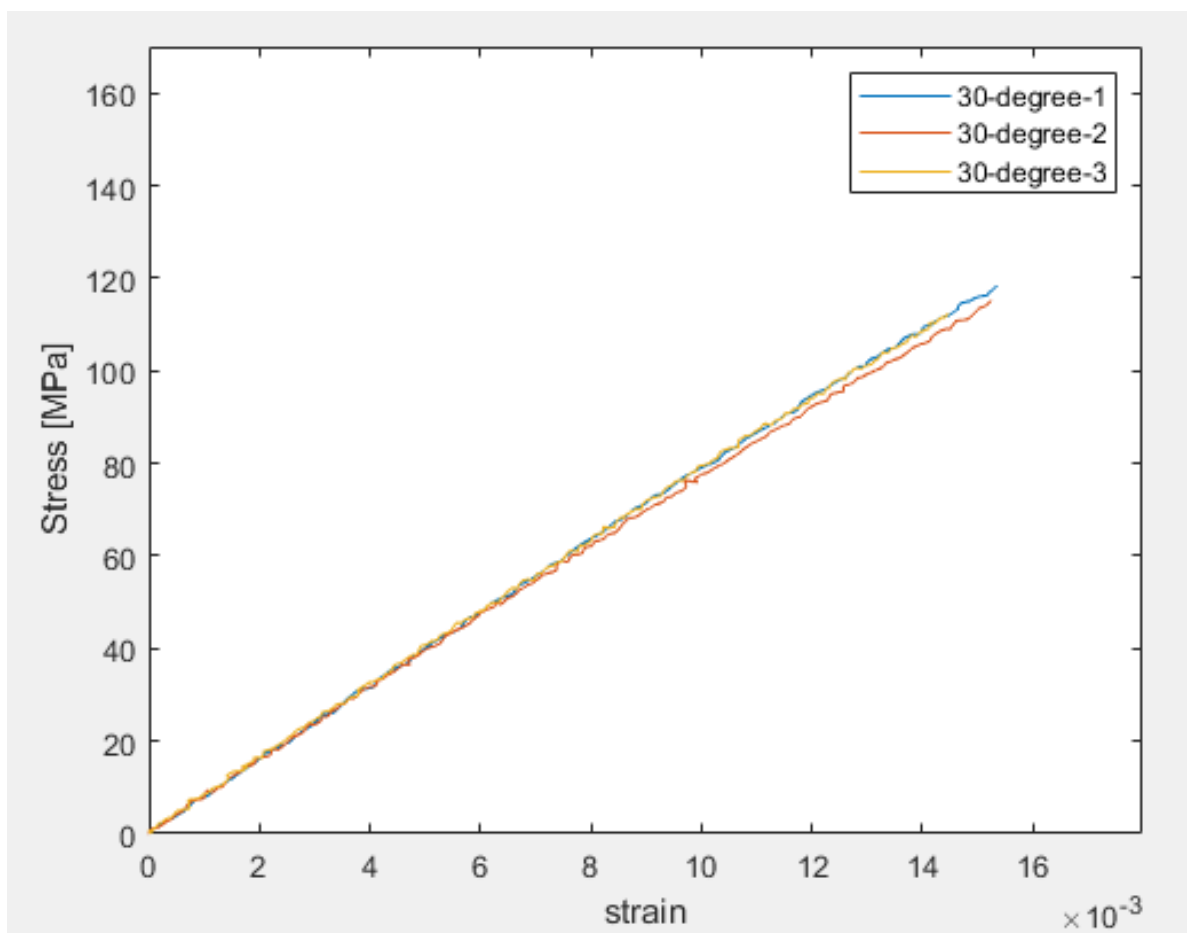


Figure 32: Stress vs strain at 30° degree

Figure 32 shows that when the bending tests were applied on specimens where the epoxy flow was at 30° concerning the referenced 0° direction, the mean stress composite specimens showed was around 116 MPa. One of the specimens also showed the highest stress, around 119 MPa. The

mean modulus was almost 7962 MPa. It is worth noting that stress increases in a 30° direction and is more significant than the results in a 0° direction. Linear elastic curves of 1<sup>st</sup> specimen and 3<sup>rd</sup> specimen overlap each other. The difference in the mechanical strength of these three specimens is less than 5%, which represents a high level of uniformity. A mean stress of around 116 MPa is obtained at the end of the analysis for specimens where the epoxy flow was at 30° concerning the referenced 0° direction. Sometimes, the composites' manufacturing process also determines the composites' final mechanical properties. These composites were manufactured with a vacuum infusion process, so maybe there is more resin infusion in specific locations, so the mechanical properties are enhanced, thus resulting in good mechanical strength.

### 3.2.3: 60° degree

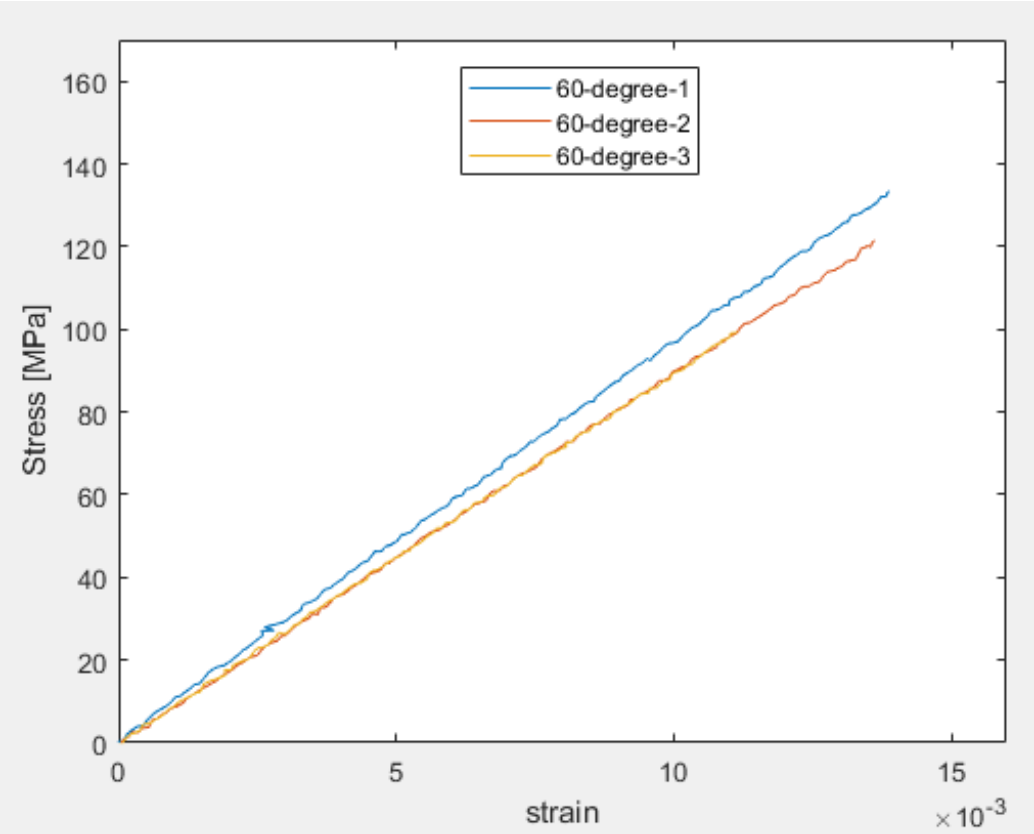


Figure 33: Stress vs strain at 60° degree

Figure 33 shows that when the bending tests were applied on specimens where the epoxy flow was at 60° with respect to the referenced 0° direction, the mean stress composite specimens showed was around 119 MPa. One of the specimens also showed the highest stress, around 135 MPa. The mean modulus was almost 9250 MPa. It is worth noting that stress increases in a 60° direction and is larger than the results in 0° and 30° directions. Therefore, a mean stress of around 119 MPa is obtained at the end of the analysis for specimens where the epoxy flow was at 60° concerning the referenced 0° direction. Among the three samples, linear elastic behavior of two of them are very similar to each other, indicating almost the same values of the stresses.

### 3.2.4: 90° degree

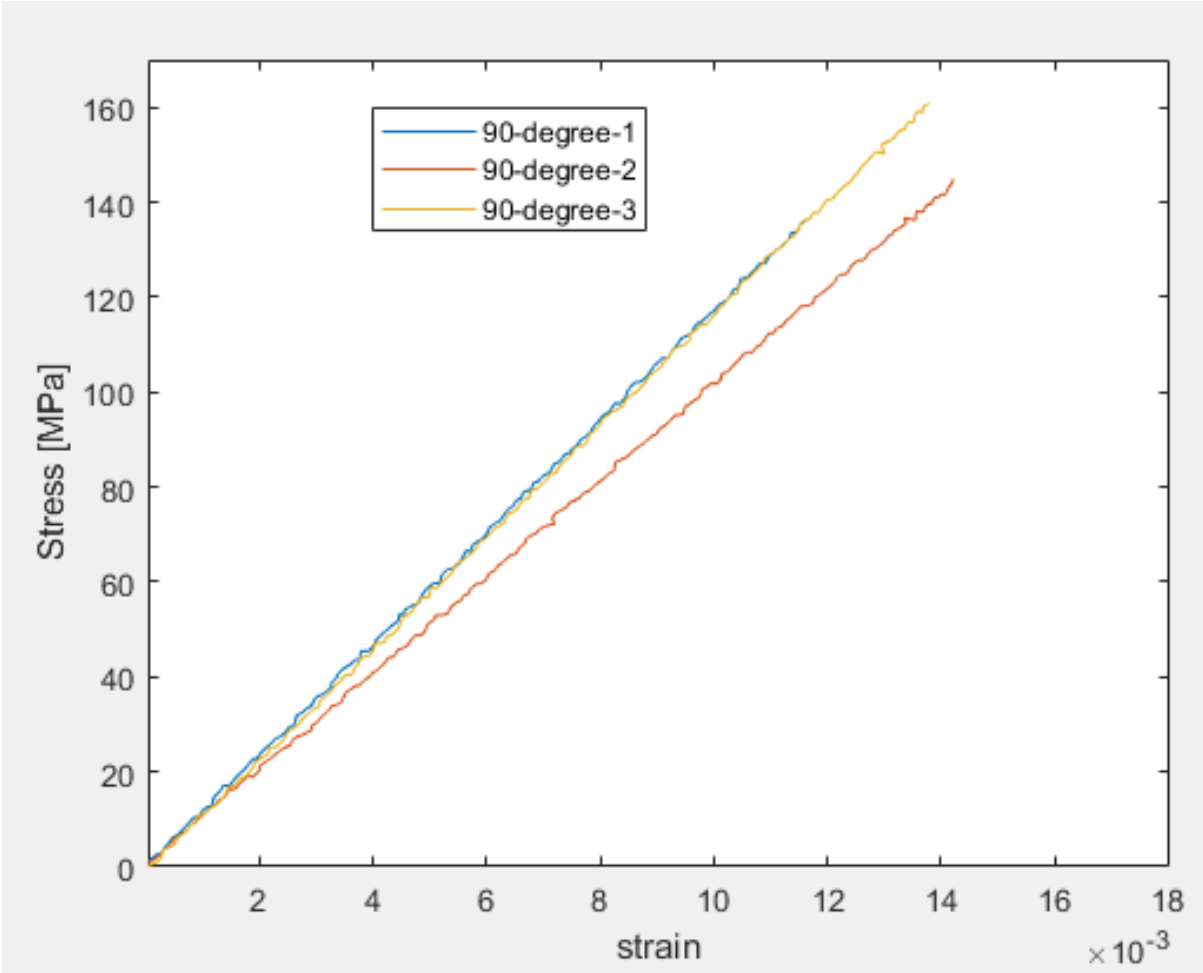
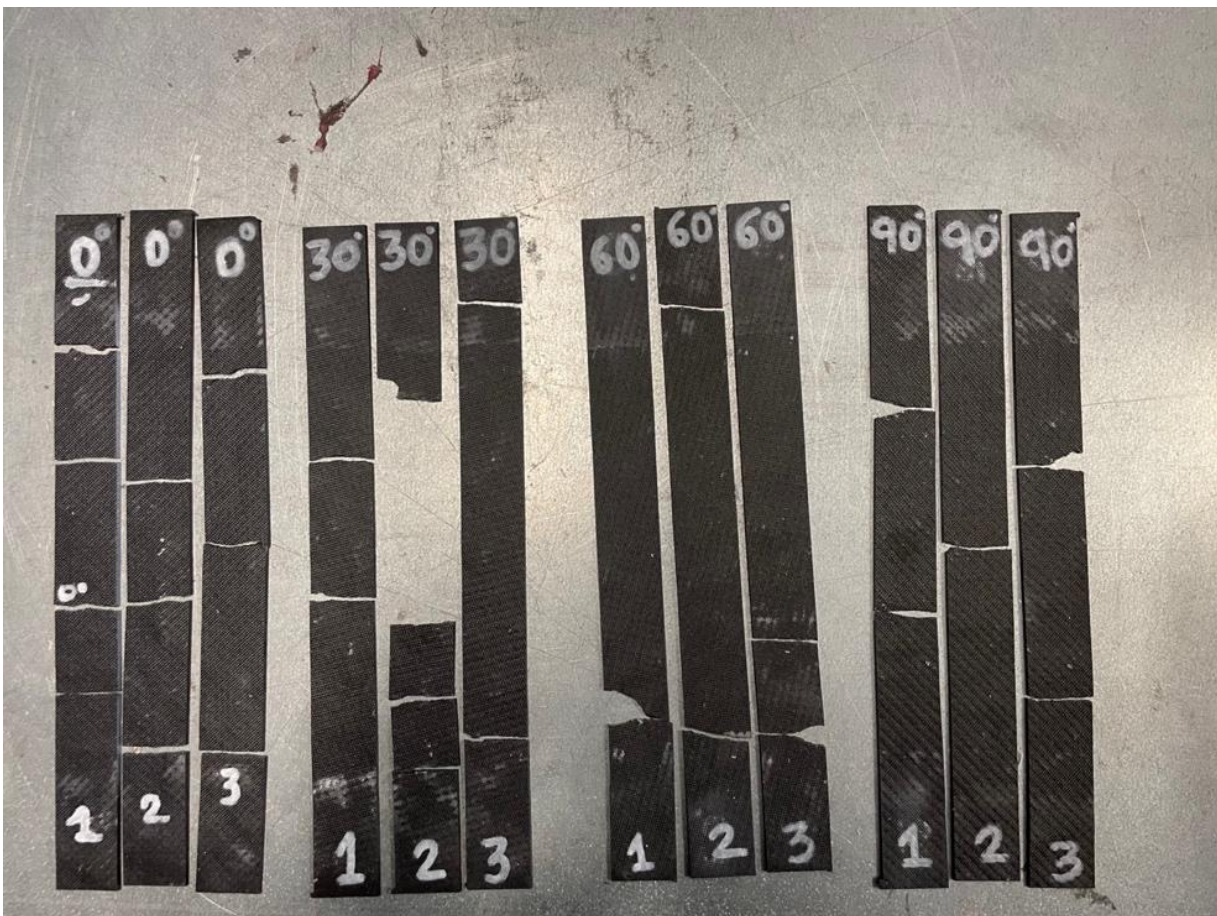


Figure 34: Stress vs strain at 90° degree

Figure 34 shows that when the bending tests were applied on specimens where the epoxy flow was at 90° concerning the referenced 0° direction, composite specimens showed around 148 MPa of mean stress. One of the specimens also showed the highest stress, around 162 MPa. The curves of 1<sup>st</sup> and 3<sup>rd</sup> specimen exhibit a high degree of overlap, which is evident of similar linear elastic behavior. The mean modulus was almost 11093 MPa. It is worth noting that stress increases in 90° direction and is much larger than what the results show in 0°, 30°, and 60° direction. Therefore, a mean stress of around 148 MPa is obtained at the end of analysis for specimens in which flow of epoxy was in 90° concerning referenced 0° direction. So, out of all the directions, at 90°, maximum stress is obtained. Figure 35 shows the specimens fractured by tensile testing. Multiple fractures occurred in all orientations.



*Figure 35: Specimens after tensile test*

### 3.2.5: Comparison of tensile stress at different orientations

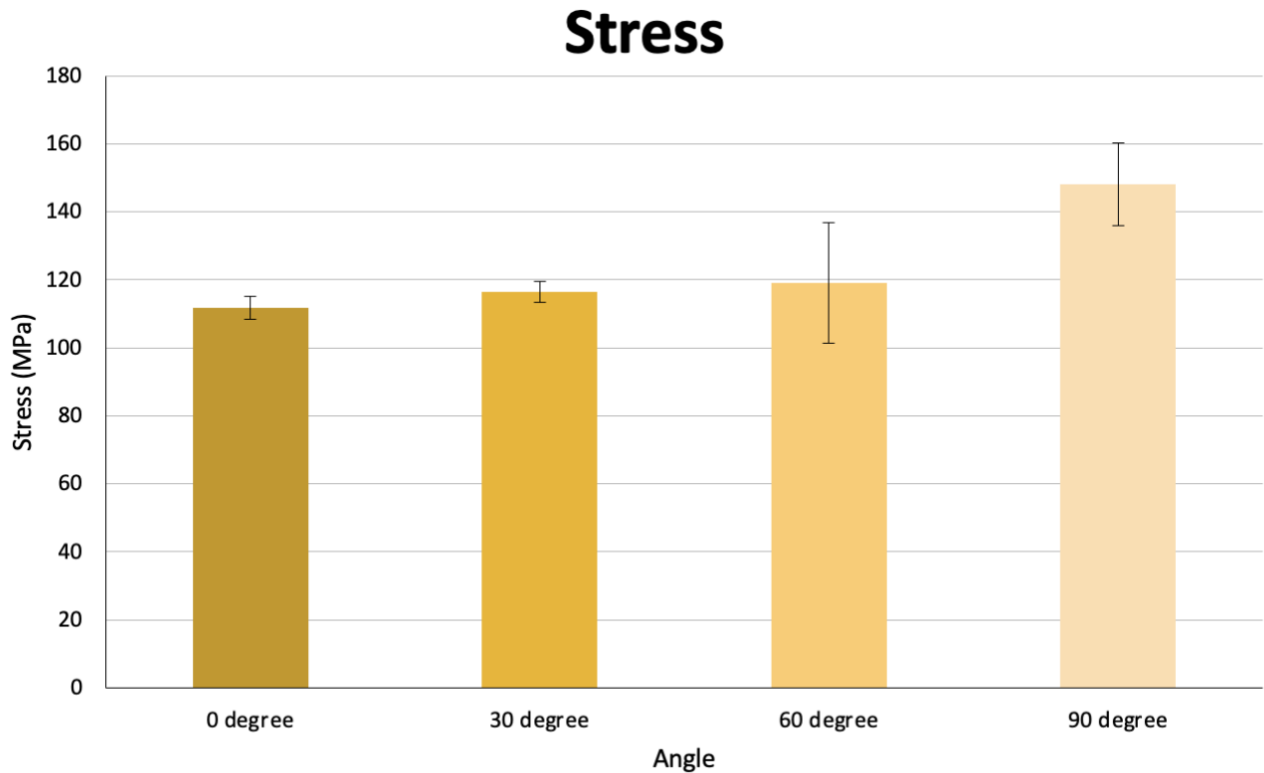
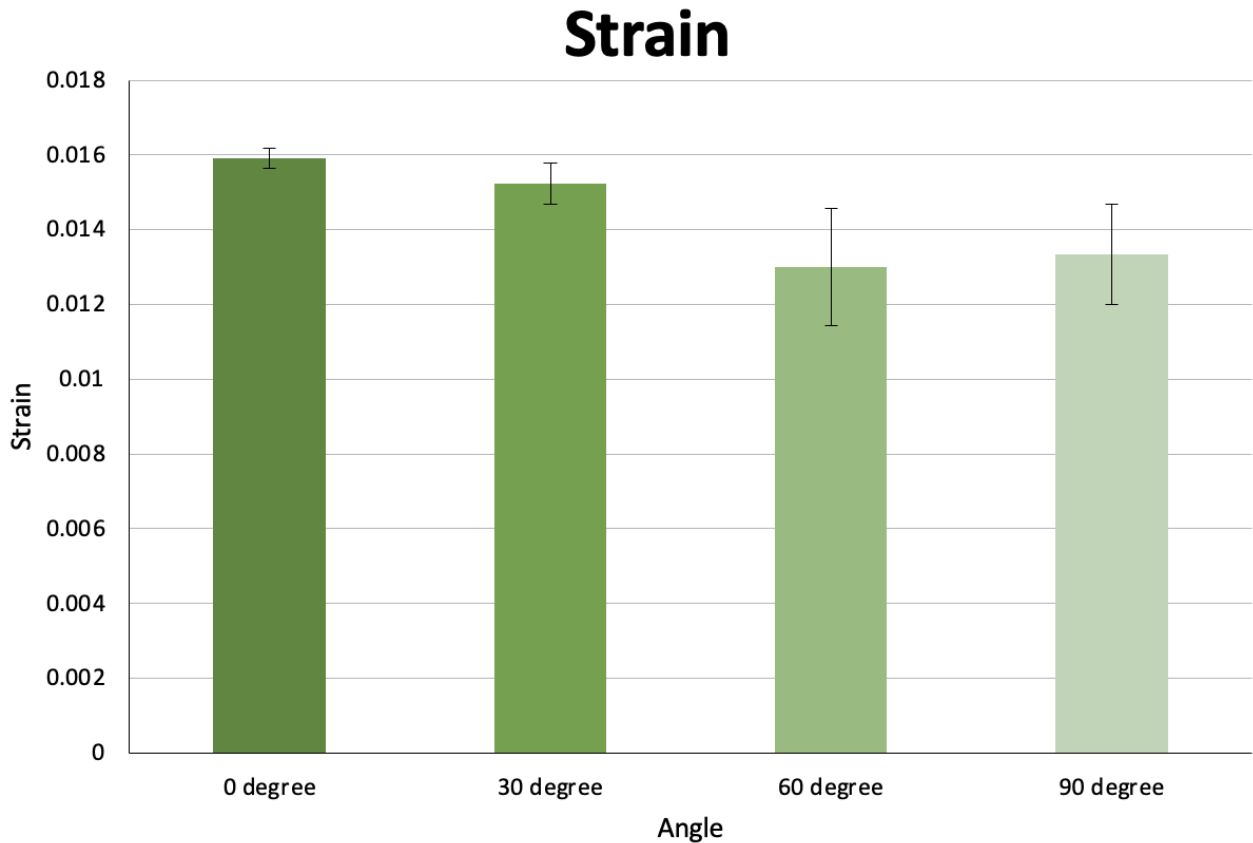


Figure 36: Bar chart showing tensile stress at different orientations.

The bar chart in Figure 36 shows the average mean stress at four different orientations. 90° orientation exhibits the maximum amount of stress. Also, it is shown that 30° and 60° exhibit the same value stresses, and the difference in the strength of these orientations is just 4%. 0° orientation shows 24% less stress than 90° orientation. Moreover, it is pretty interesting that the trend in the values of stresses in this bar chart that belongs to tensile is very similar to the one of bending stresses. The results also indicate the isotropic behavior of the non-woven carbon composites. As in non-woven composites, fibers are randomly oriented, so there could be regions with high-stress levels and low-stress levels within the composite.

### 3.2.6: Comparison of tensile strain at different orientations



*Figure 37: Bar chart showing tensile strain at different orientations.*

The bar chart in Figure 37 shows the trend in strain is also like the one in the bending tests. At 0° orientation, there is maximum strain experienced by the specimens, while at 90°, there is minimum strain. In non-woven composites where the fibers are randomly oriented, isotropic behavior is widespread, so whenever the strain is applied, there is almost similar deformation experienced by the composite and, therefore, similar strain in nearly all directions. Maximum strain at 0° shows that the fiber-matrix composition in that orientation was weaker, and it could not resist the deformation well. One interesting outcome is the similarity in the strain values of 60° and 90° directions that are almost like each other. However, one can expect this behavior while working with non-woven composites.

### 3.2.7: Comparison of tensile modulus at different orientations

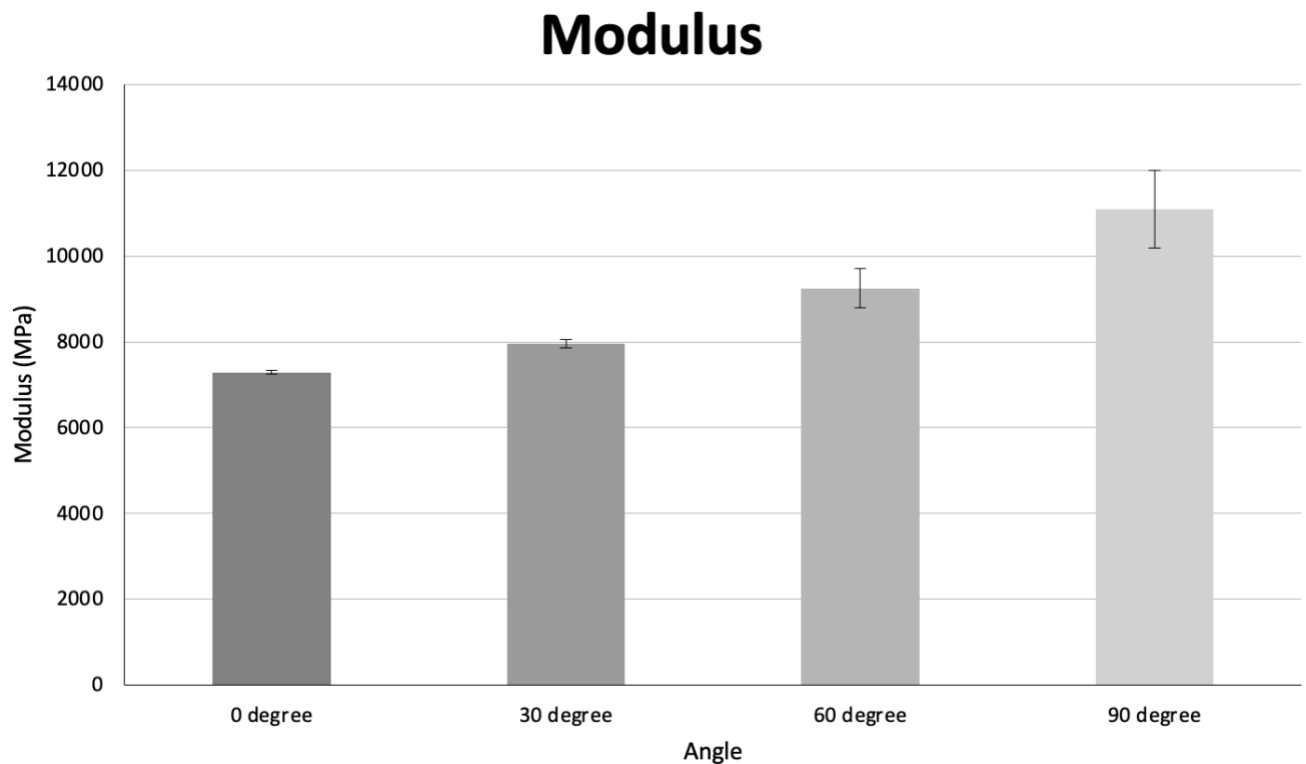


Figure 38: Bar chart showing tensile modulus at different orientations.

The bar chart in Figure 38 shows that the highest modulus was found in 90° orientation with 11093 MPa, while it was 34% in 0° orientation with 7288 MPa. The trend is the same when compared to the bending tests. However, in the case of tensile specimens with 90° orientation, the modulus is relatively high compared to that in specimens with 90° orientation in bending tests. In bending tests, the highest modulus achieved was around 9800MPa; in tensile tests, the highest modulus achieved was around 11000MPa. So, tensile specimens show 11.6% more stiffness than bending specimens. Therefore, in 90° orientation, the stress is also highest among all directions, and modulus is also highest among all orientations.

Table 8 shows the mean stress, mean strain, and mean modulus in all four directions, along with their standard deviations. Maximum tensile stress and maximum tensile modulus were found to be in 90° orientation, while maximum tensile strain was in 0° direction.

**Error! Reference source not found.** shows the specimens fractured by tensile testing.

<b>Stress</b>				
<b>Angles</b>	<b>0°</b>	<b>30°</b>	<b>60°</b>	<b>90°</b>
<b>Mean stress (MPa)</b>	111.8	116.5	119	148
<b>STDEV</b>	3.4	3	17.7	12.2
<b>Modulus</b>				
<b>Angles</b>	<b>0°</b>	<b>30°</b>	<b>60°</b>	<b>90°</b>
<b>Mean modulus (MPa)</b>	7288	7962	9250	11093
<b>STDEV</b>	42.2	97.4	457.8	909.2
<b>Strain</b>				
<b>Angles</b>	<b>0°</b>	<b>30°</b>	<b>60°</b>	<b>90°</b>
<b>Mean strain</b>	0.0159	0.0152	0.013	0.0133
<b>STDEV</b>	0.0002645	0.00055075	0.001562	0.0013428

*Table 8: Mean stress, mean strain, and mean modulus at different orientations.*

## 3.3- Compression tests

### 3.3.1: 0° degree

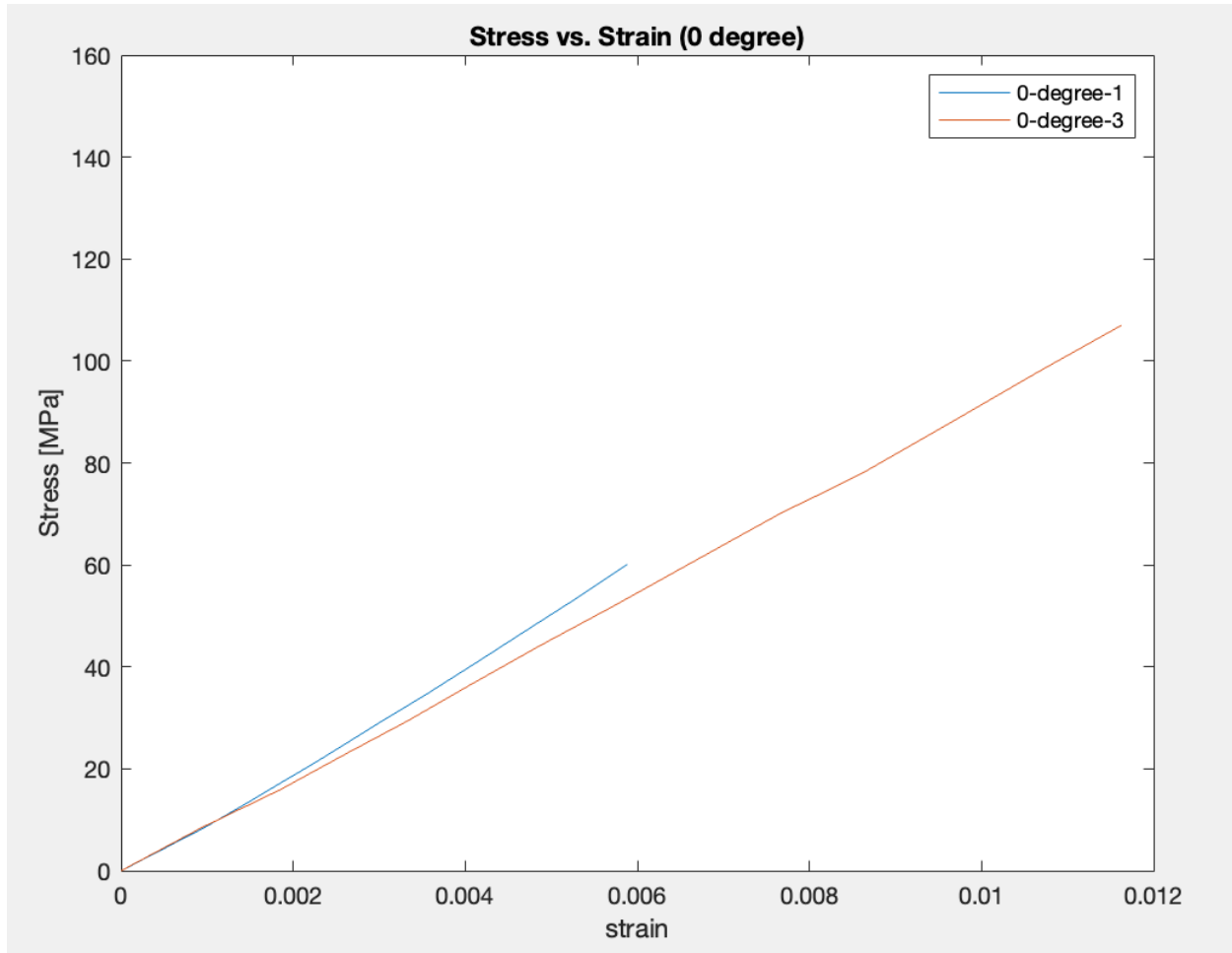


Figure 39: Stress vs strain at 0° degree

Figure 39 shows the compression test result applied on specimens with 0° orientation. Two specimens were tested, and stress-strain curves were obtained. The first specimen shows a maximum stress of around 88 MPa, while the second specimen shows a maximum strength of approximately 131 MPa. One can expect such behavior in nonwoven composites where there is significant variation in the level of stresses in different locations. This trend is usually due to the non-random fiber orientation in the laminates. However, considering these two specimens, the difference in the stress value in the two specimens is enormous. Therefore, it is tough to predict

what possible strength can be achieved with this orientation. It can be expected that more or less around 100 MPa stress can be seen in this configuration. Substantial differences between these results also put a question mark on the inconsistency during the tests or in the material of the specimens. There could also be other variable factors that affected the results significantly.

### 3.3.2: 30° degree

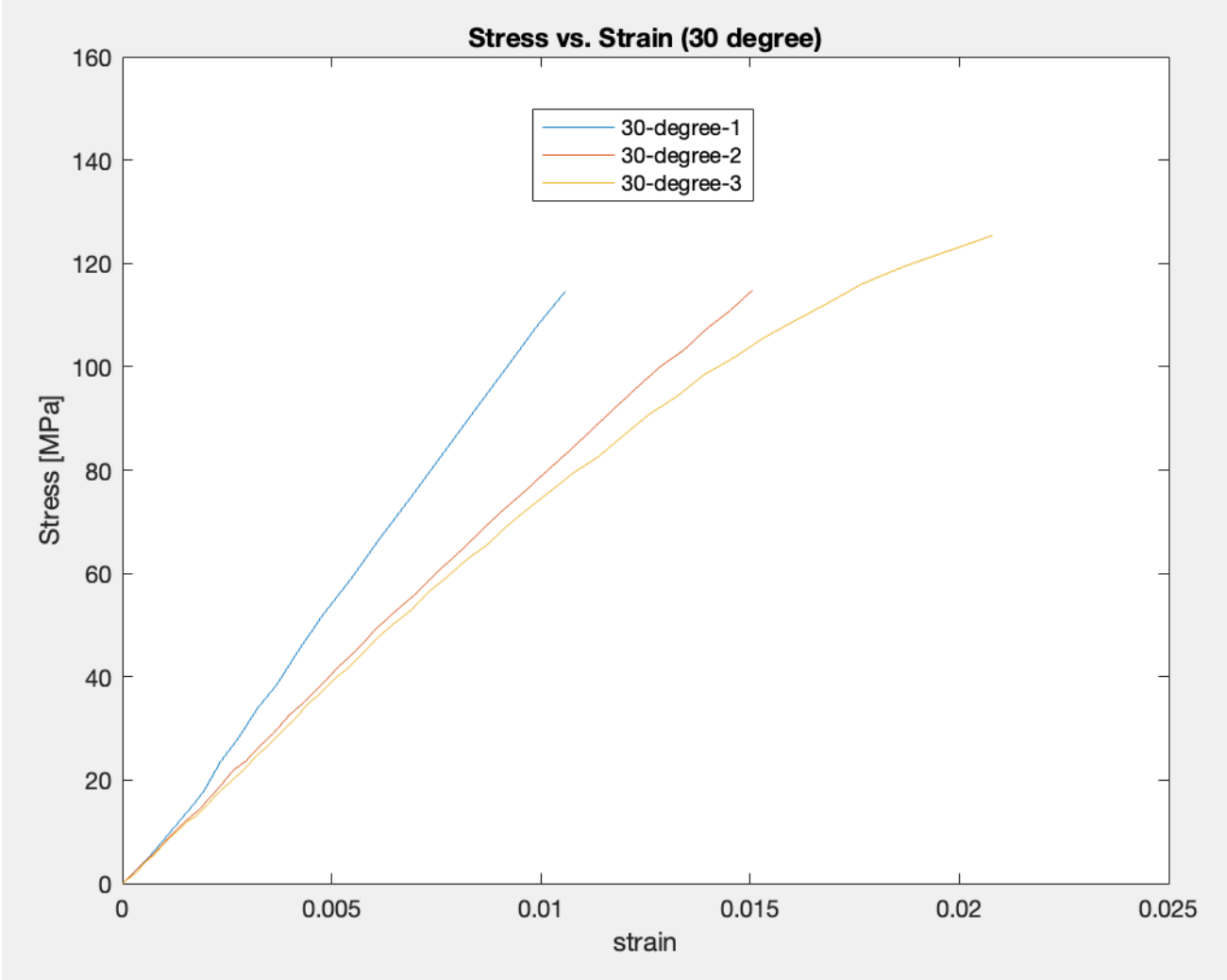


Figure 40: Stress vs strain at 30° degree

Figure 40 shows the results of the three specimens that belong to 30° orientation. 1<sup>st</sup>, 2<sup>nd</sup>, and 3<sup>rd</sup> specimens show around 115.5 MPa, 115.7 MPa, and 126.5 MPa stress, respectively. The overall

average stress of this orientation is around 119 MPa, which is considerable. The stress-strain curve for the 1st specimen does not relate to the other two samples, but it is linear. Curves of 2<sup>nd</sup> and 3<sup>rd</sup> specimens are superimposed on each other during the initial stage of the test, indicating that the samples' behavior to the compression load was the same. But they start to deviate as the test proceeds to end. The result shows the consistency in the mechanical properties of 2<sup>nd</sup> and 3<sup>rd</sup> specimens. Results also indicate the change in the homogeneity of the material. The distinct material response in the first specimen may be due to the non-uniform material properties. With the nonwoven carbon composite, the fibers' orientation also impacts the mechanical behavior of the specimens. Variations in the distribution and orientation of the fibers may lead to the difference in these stress-strain curves.

### 3.3.3: 60° degree

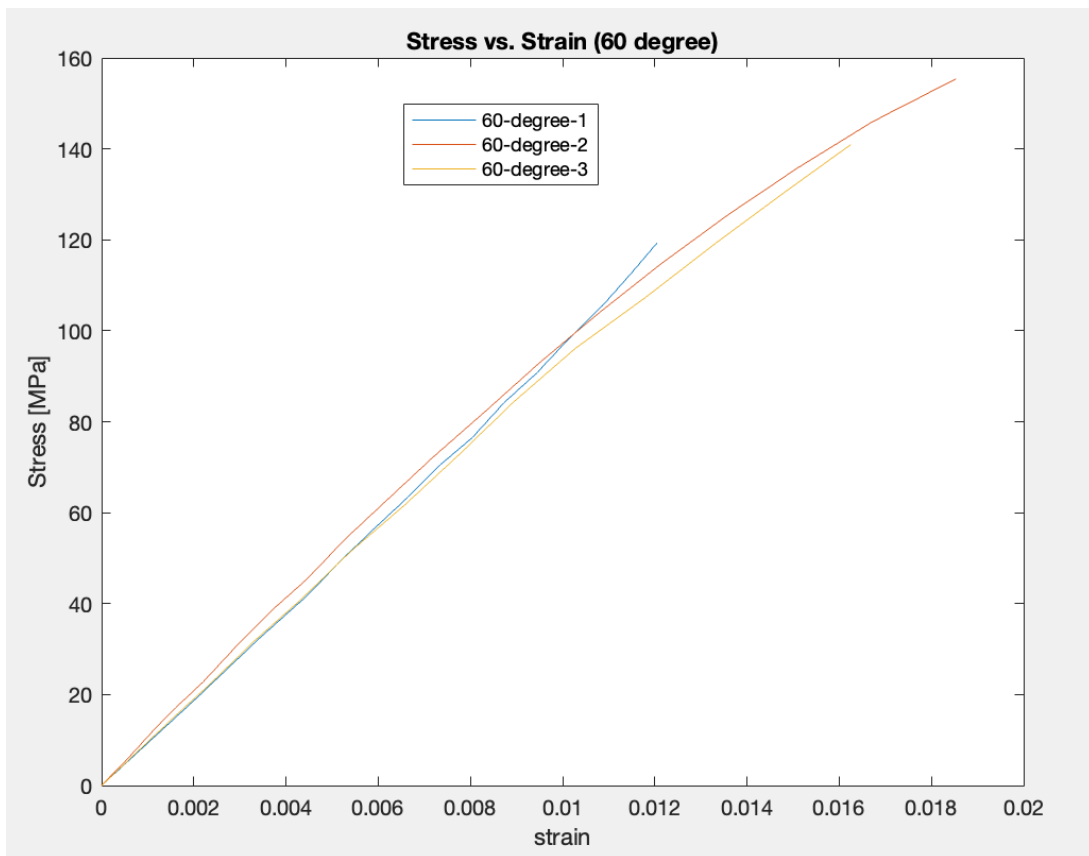


Figure 41: Stress vs strain at 60° degree

Figure 41 shows the results of compression test on three specimens that belong to 60° orientation. 1<sup>st</sup>, 2<sup>nd</sup>, and 3<sup>rd</sup> specimens show around 134 MPa, 144 MPa, and 158 MPa stress, respectively. Three curves shown on the graph have predictable material behavior. Three specimens have the same linear stress-strain curves, indicating a high level of consistency, which is a positive sign. Results show that three specimens lie in the linear elastic region, which means that they are elastically deformed, and when the load is removed, they will return to their original shape. Many materials show this type of behavior, and also composites show this behavior. Curves of 1<sup>st</sup> and 3<sup>rd</sup> specimen coincide perfectly during the initial stage of test, but they start to deviate as the test proceeds to end. However, one different thing is the level of strength shown by the specimens under a compression load, as one of the specimens shows higher stress of around 158 MPa, which could be due to many factors, such as differences in the mechanical properties of the composite at different locations, resin content and also the orientation of fibers at specific location considering that we are working with non-woven carbon composites.

### 3.3.4: 90° degree

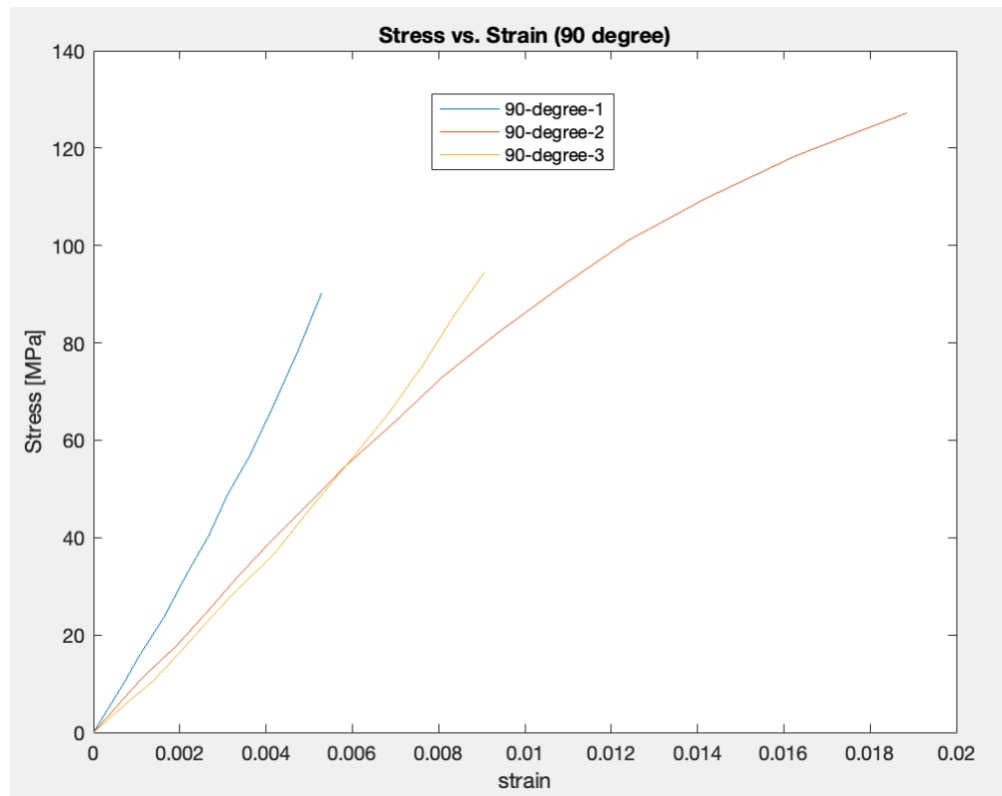
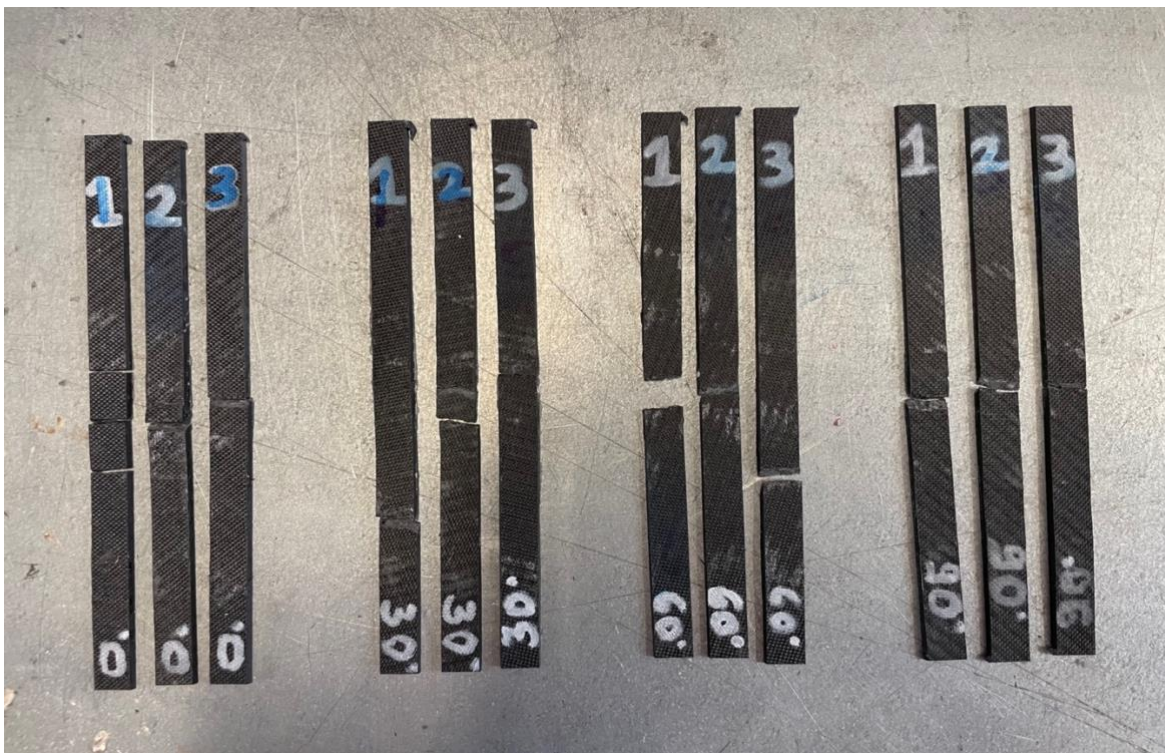


Figure 42: Stress vs strain at 90° degree

Figure 42 shows the results for specimens that belong to 90° orientation. 1<sup>st</sup>, 2<sup>nd</sup>, and 3<sup>rd</sup> specimens show around 116 MPa, 124 MPa, and 133 MPa stress, respectively. The mean stress of specimens oriented at 90° is less than that of specimens oriented at 60°. All three specimens show linear elastic behavior, but there is substantial variability in the mechanical properties of these specimens. Mechanical properties in these specimens are greatly influenced by fiber orientation, fiber density, and fiber-matrix composition. For the 2<sup>nd</sup> and the 3<sup>rd</sup> specimens, it can be seen that the curves almost extend in the same linear elastic region at the beginning of the test. Toward the end of the test, the curve for the second specimen bends, indicating a transition from linear elastic deformation to plastic deformation, or it also shows the onset of material yielding. At the yielding point, the material deviates from its elastic behavior and undergoes plastic deformation, meaning it will not return to its original shape. Figure 43 shows the specimens after compression tests. Most of the specimens undergo multiple fractures.



*Figure 43: Specimens after compression test*

### 3.3.5: Comparison of compression stress at different orientations

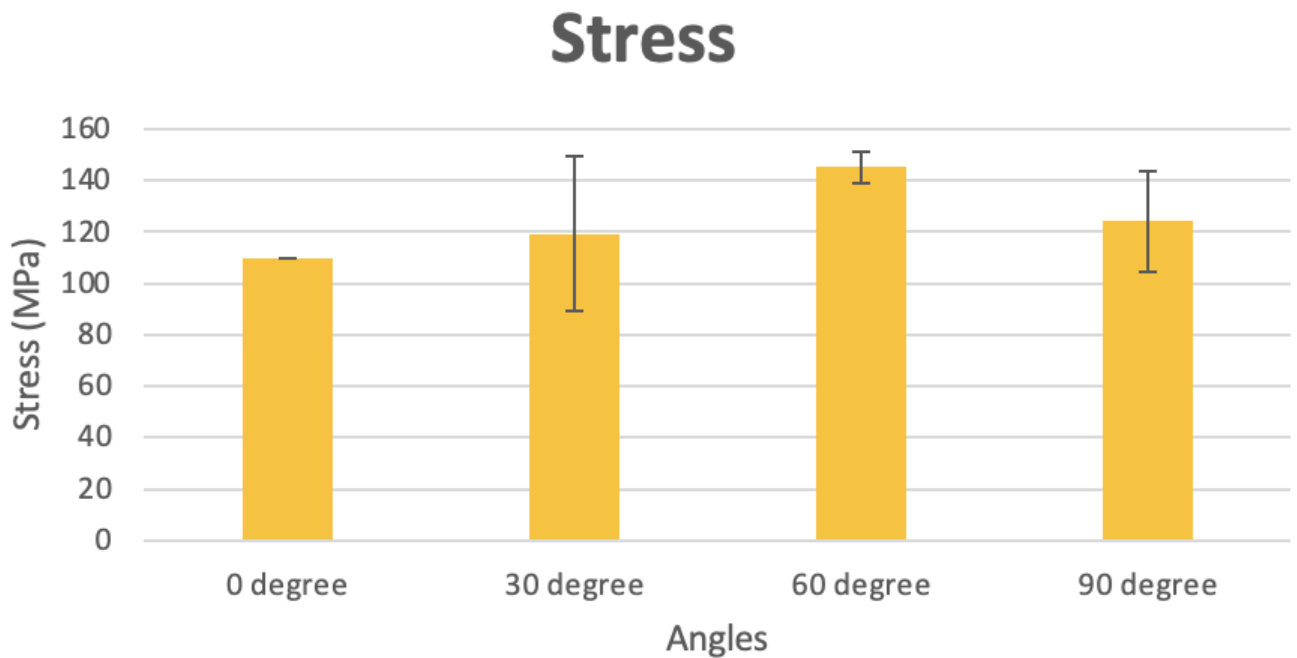


Figure 44: Bar chart showing compression stress at different orientations.

Figure 44 represents the average value of stress at four different orientations 0°, 30°, 60°, and 90°. Specimens oriented at 30°, 60°, and 90° show stress of about 119 MPa, 145 MPa, and 124 MPa, respectively. The minimum stress is shown by the specimens of 0° orientation with around 110 MPa, which is 24% less than the specimens in 60° orientation which exhibit the maximum stress, which is 145 MPa. In all four orientations, different stresses are obtained. At 0° direction, minimum stress is obtained, which indicates the lower load-bearing capability of the composite due to the alignment of fibers with respect to the compression load. Moreover, with a 60° orientation, it can be seen that it has high resistance to the compression load as it exhibits maximum stress. For 30° and 90° orientation, the strength is almost the same with only 4% difference in the values of stresses.

### 3.3.6: Comparison of compression strain at different orientations

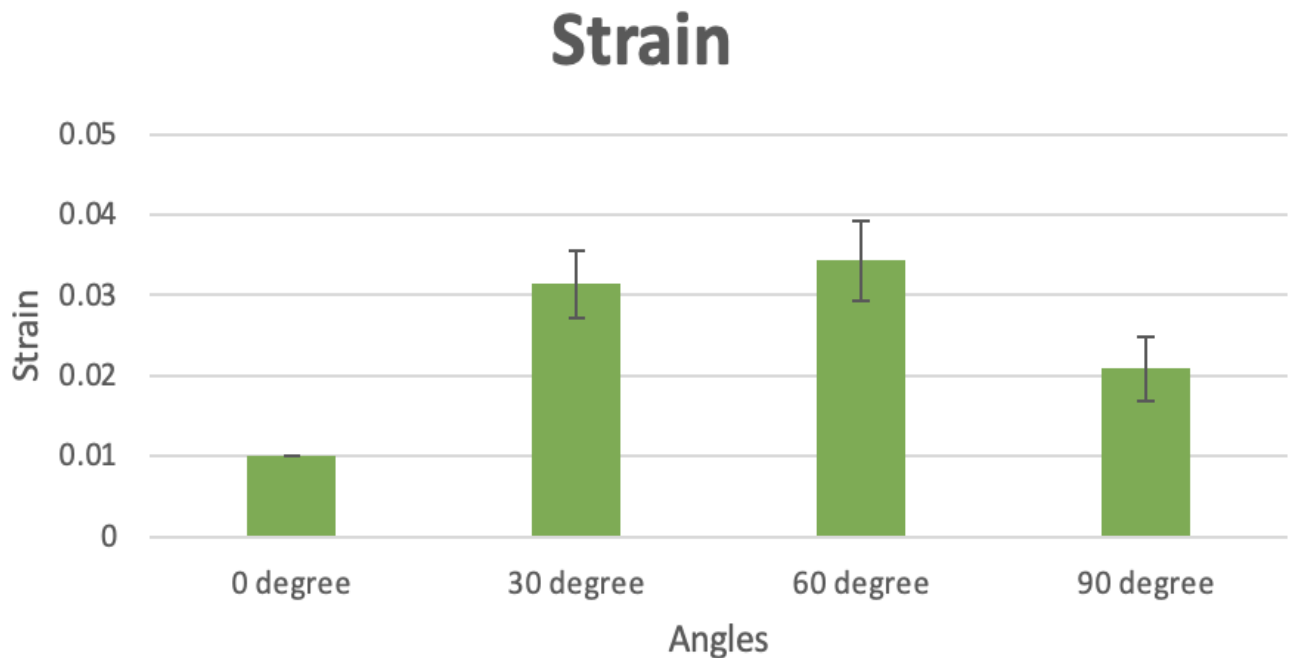


Figure 45: Bar chart showing compression strain at different orientations.

Figure 45 represents the average value of strain at four different orientations  $0^\circ$ ,  $30^\circ$ ,  $60^\circ$ , and  $90^\circ$ . The values of strain for  $0^\circ$ ,  $30^\circ$ ,  $60^\circ$  and  $90^\circ$  directions are 0.01005, 0.03136, 0.0343 and 0.02087 respectively. The lowest strain was experienced in  $0^\circ$  orientation, while the highest strain was experienced in  $60^\circ$  orientation. When comparing the strain results with that of stress, it is noticed that maximum strain is obtained in  $60^\circ$  orientation where there is also maximum stress, and minimum strain is obtained in  $0^\circ$  orientation where stress is also lowest. So, it can be said results follow Hook's law, according to which the stress and strain follow a linear relationship.

### 3.3.7: Comparison of compression modulus at different orientations

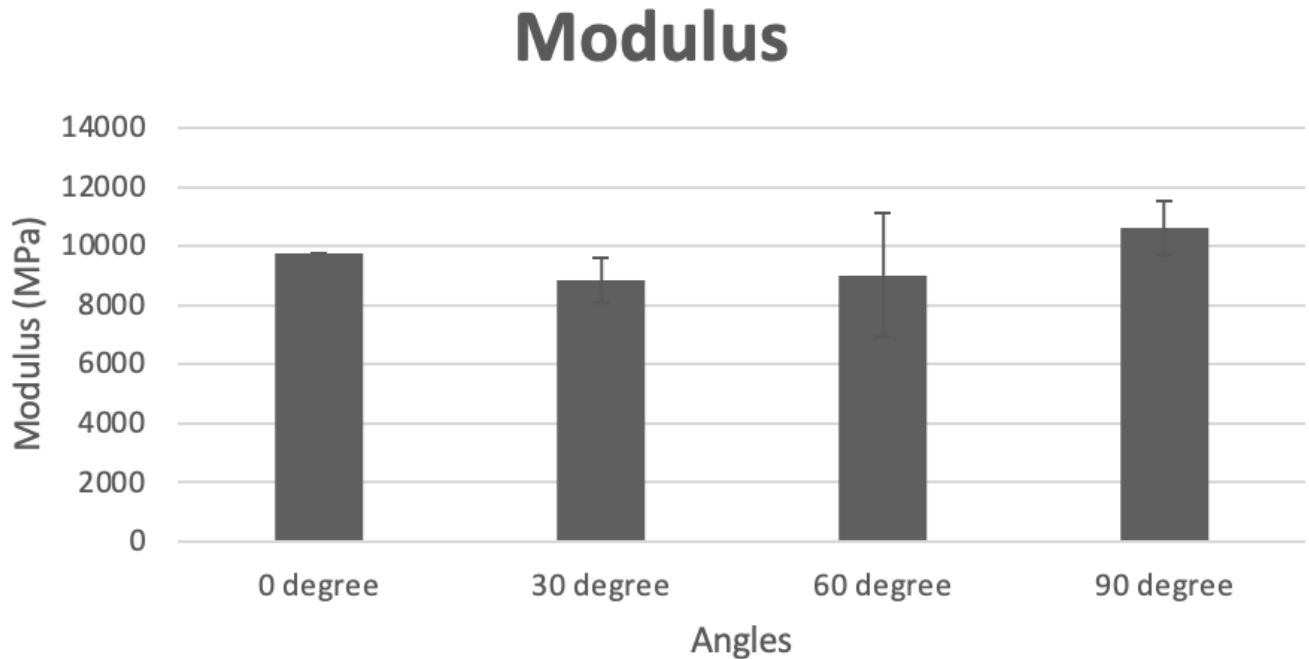


Figure 46: Bar chart showing compression modulus at different orientations.

In Figure 46, the bar graph represents the average value of modulus at four different orientations 0°, 30°, 60°, and 90°. The values of modulus for 0°, 30°, 60° and 90° orientations are 9734 MPa, 8852 MPa, 9000 MPa, and 10632 MPa respectively. Results indicate that the fiber orientation and the direction of the flow of resin greatly influence the stiffness and modulus of the specimens. Maximum modulus is shown by 90° orientation while minimum modulus is exhibited by 30° orientation. Therefore in 90° direction which exhibit highest modulus there is 16.7% more stiffness than in 30° orientation which exhibits lowest modulus. There are almost identical modulus values for the 30° and 60° directions, with only 1.6% difference in their values of stress.

Table 9 shows the mean stress, mean strain, and mean modulus in all four directions, along with their standard deviations. Maximum compression stress and maximum compression strain were found to be in a 60° orientation, while maximum compression modulus was in a 90° direction.

<b>Stress</b>				
<b>Angles</b>	<b>0°</b>	<b>30°</b>	<b>60°</b>	<b>90°</b>
<b>Mean stress (MPa)</b>	109.6	119.2	145.2	124.3
<b>STDEV</b>	30.24	6.3	12.1	8.6
<b>Modulus</b>				
<b>Angles</b>	<b>0°</b>	<b>30°</b>	<b>60°</b>	<b>90°</b>
<b>Mean modulus (MPa)</b>	9734	8852	9000.3	10631.7
<b>STDEV</b>	749.5	2095	902.5	5940.4
<b>Strain</b>				
<b>Angles</b>	<b>0°</b>	<b>30°</b>	<b>60°</b>	<b>90°</b>
<b>Mean strain</b>	0.01005	0.03136	0.0343	0.02087
<b>STDEV</b>	0.00417	0.00502	0.00396	0.00688

*Table 9: Mean stress, mean strain, and mean modulus at different orientations.*

## 3.4: Shear tests

### 3.4.1: 0° degree

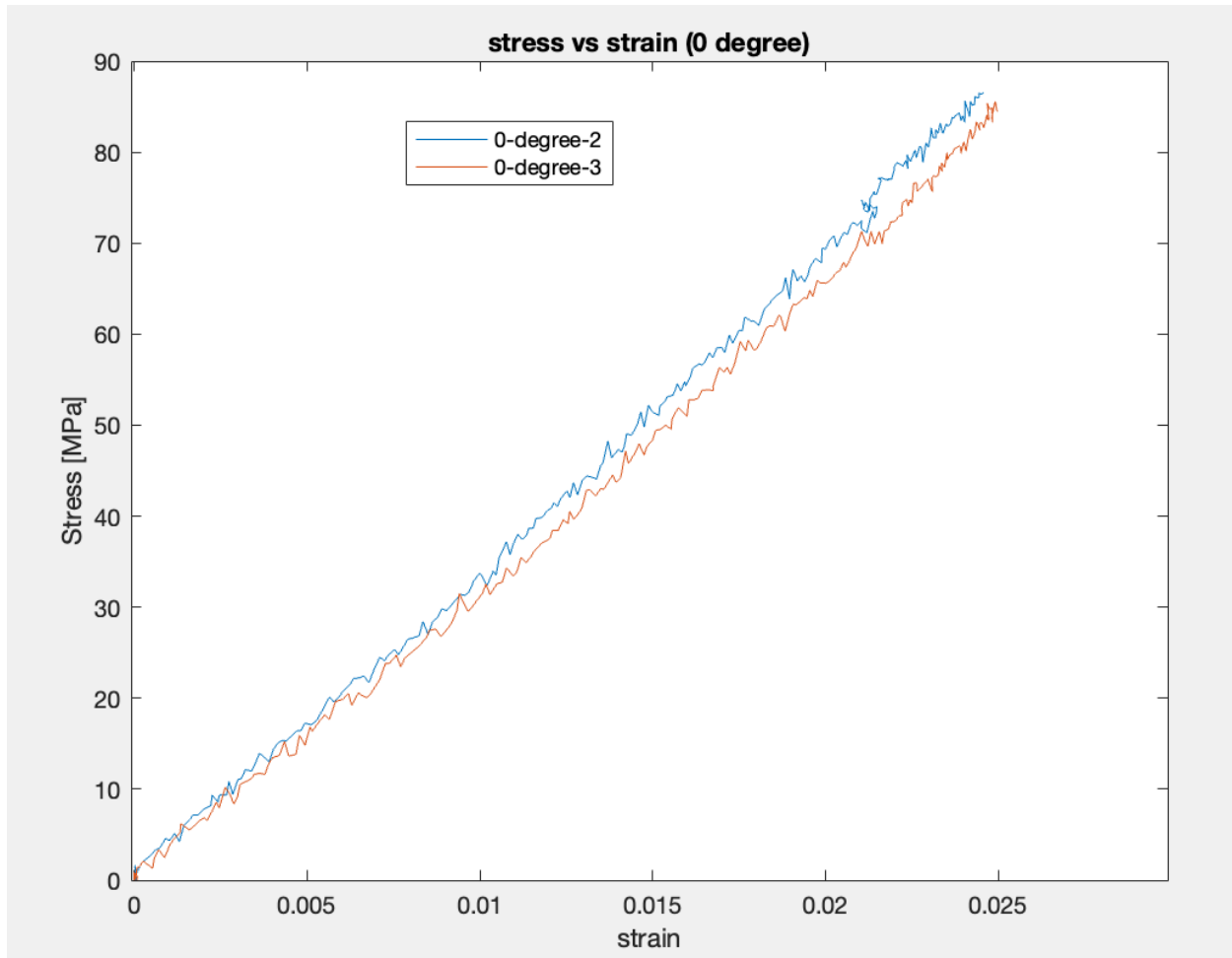


Figure 47: Stress vs strain at 0° degree

Figure 47 represents the stress-strain behavior of the specimens tested for shear load. The results show that both of the specimens show similar behavior. One of the specimens shows around 82.7 MPa of stress, while the other sample shows around 81.9 MPa, which is not a big difference. There is not only similarity in the values of strength but also in the shapes of the curves. Both curves show similar linear elastic behavior and are identical in form. This corresponds to homogeneity in the material's composition and indicates a high consistency in material properties and testing conditions. Results also suggest that the strength values in this case are free from

anomalies; they are reliable to use for specific applications. Also, one can predict that the fiber orientation in these specimens will be similar, corresponding to identical strength values.

### 3.4.2: 30° degree

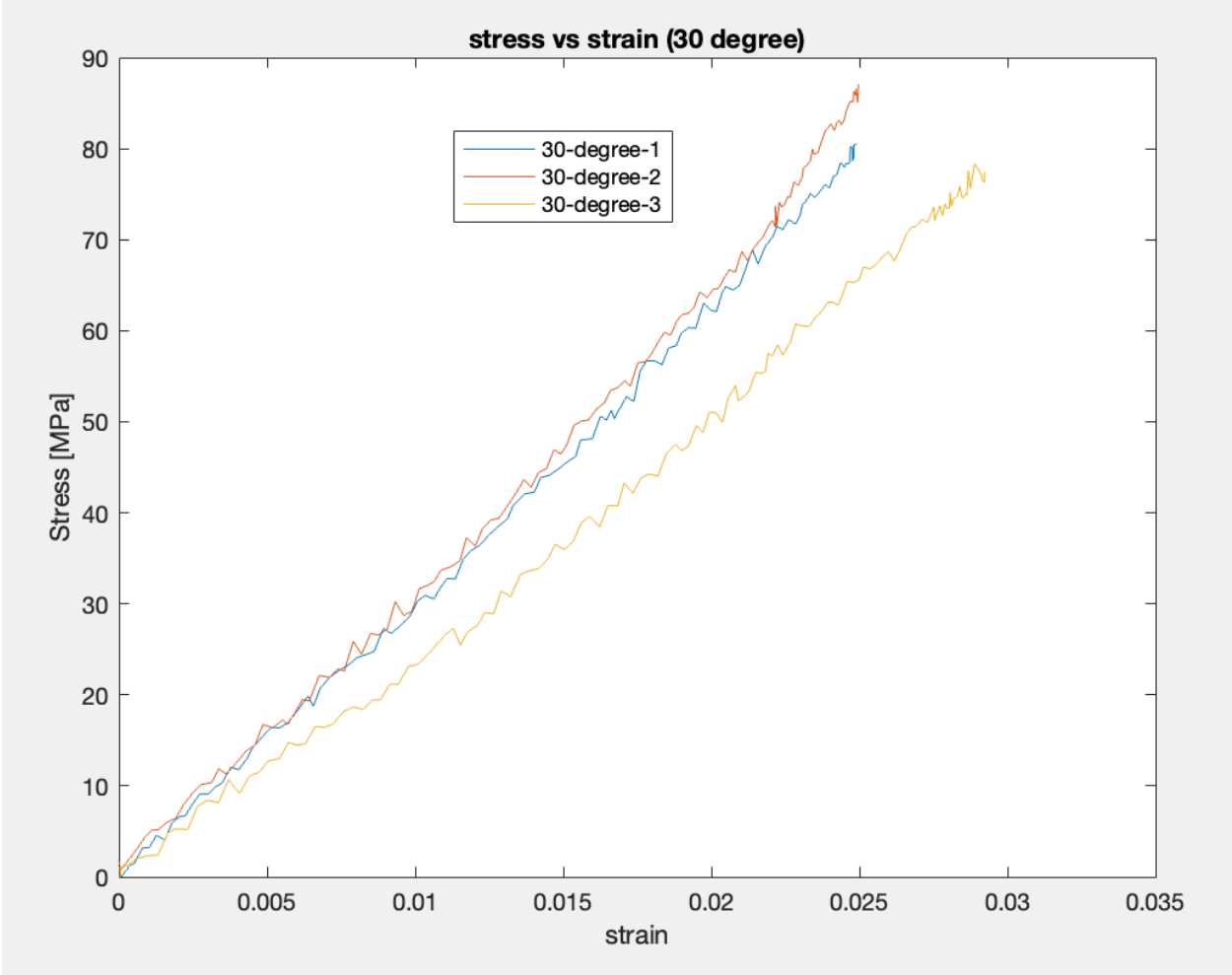


Figure 48: Stress vs strain at 30° degree

Figure 48 represents the stress-strain behavior of the specimens tested for the shear load. The stress values for the 1st, 2nd, and 3rd specimens are 77.3 MPa, 83.6 MPa, and 75.4 MPa, respectively. In general, all the three strength values are closely related. For the first and second specimens, linear elastic curves overlap. Both curves follow the same path from the beginning

until the end. They almost follow the same trend. However, the third specimen's strength value is similar to that of the first specimen, but their linear elastic behavior is different. For the first and the second specimens, the material homogeneity and fiber orientations of the specimens will likely be similar, which leads to constant stress-strain curves in the linear elastic region. The results indicate satisfactory behavior, with two samples having almost identical trends. In contrast, the third one has nearly the exact value of strength but with a different linear elastic behavior.

### 3.4.3: 60° degree

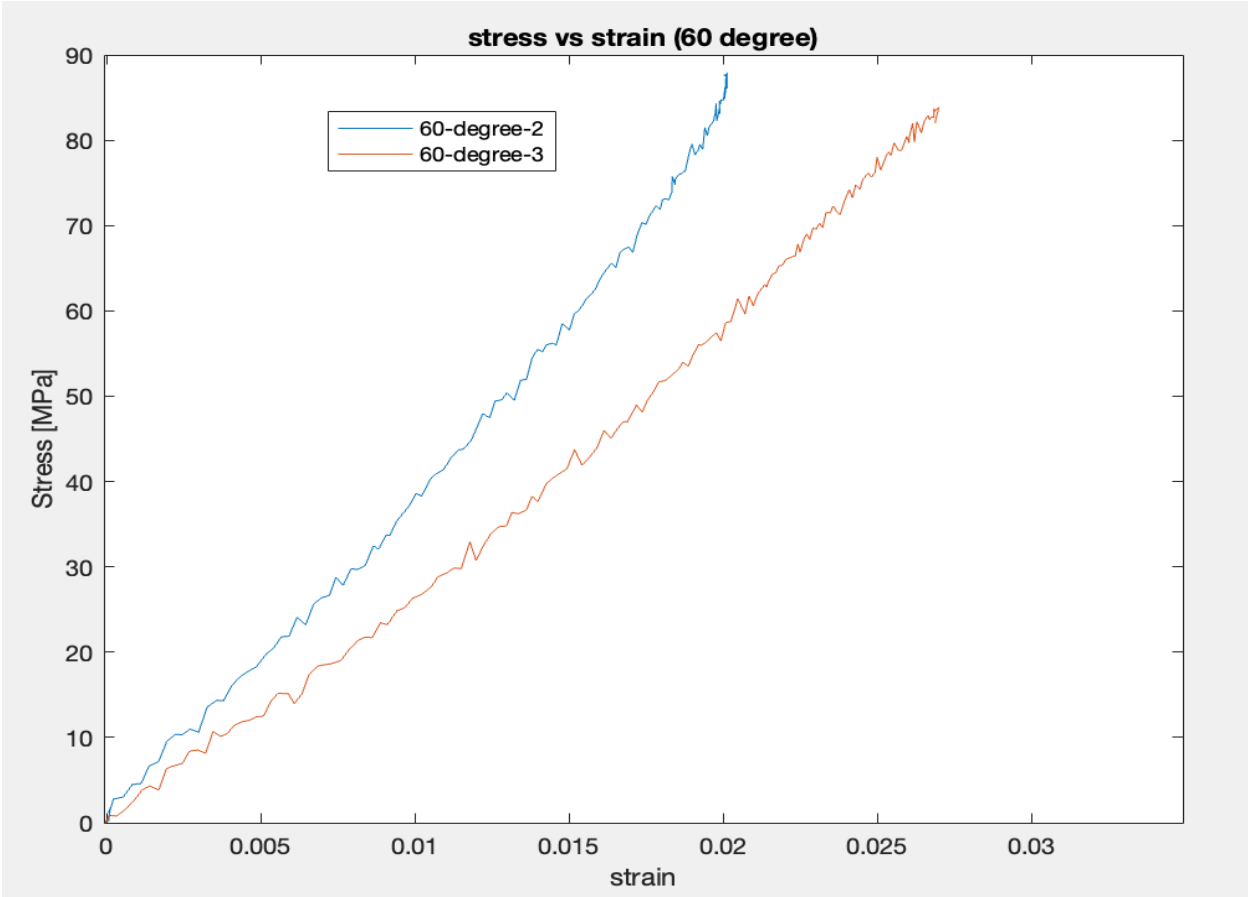


Figure 49: Stress vs strain at 60° degree

Figure 49 represent the stress-strain behavior of the specimens tested for shear load. The stress values for the 1st and 2nd specimens were 85MPa and 81.2MPa. There is no significant difference in the importance of the stresses, so strength is similar in both samples, but the linear elastic behavior of both specimens is different. It can be seen from the graph that both the curves have the same linear elastic behavior at the beginning of the test, but as the test proceeds, the change in linear elastic behavior is noticed. The strength of these two specimens is quite similar, which means that fiber orientation and fiber-resin matrix have not impacted the strength of these specimens. However, the difference may also be due to the manufacturing variabilities during the process.

### 3.4.4: 90° degree

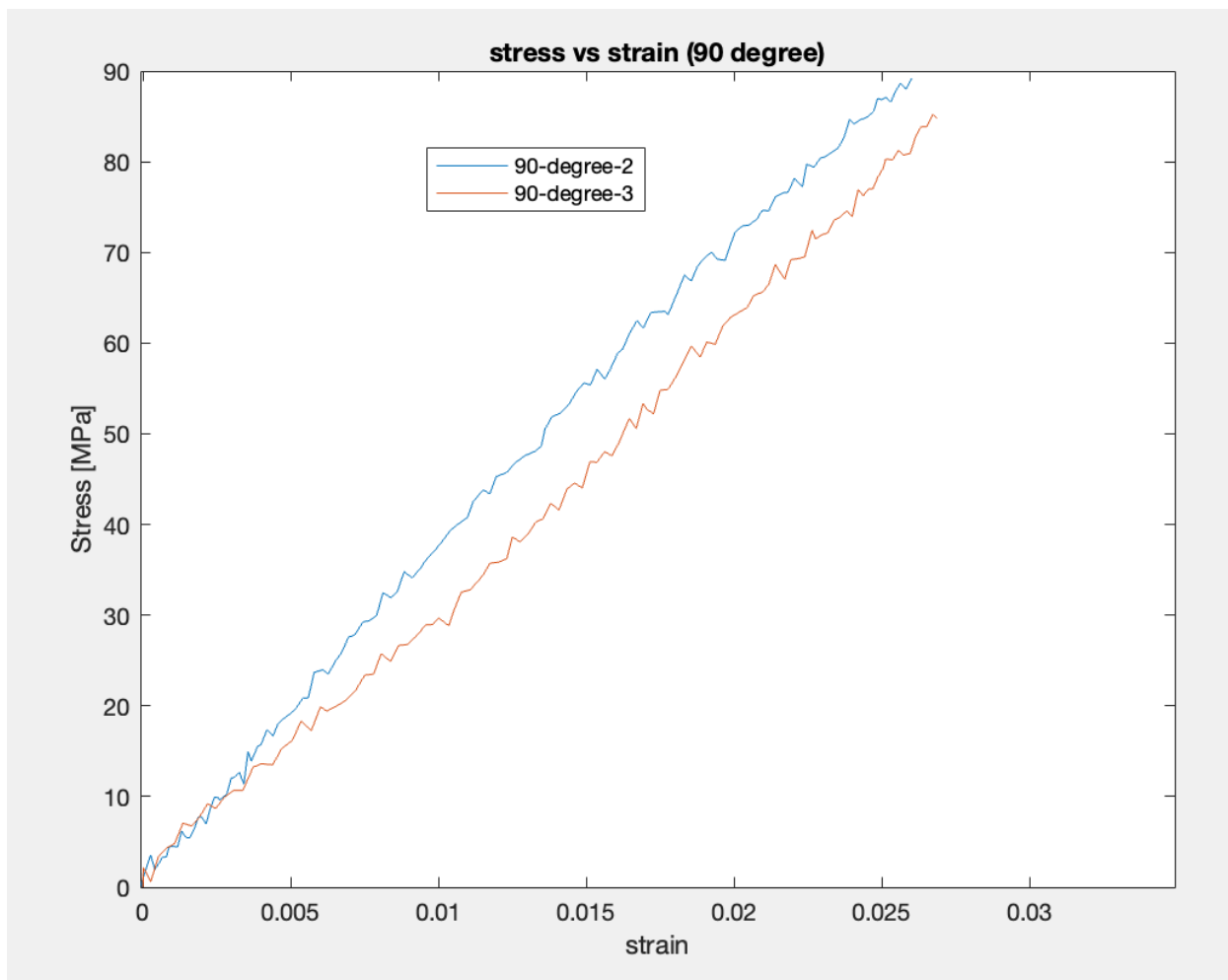


Figure 50: Stress vs strain at 90° degree

Figure 50 represents the stress-strain behavior of the specimens tested for the shear load. The stress values for the 1st and 2nd specimens were 84.3MPa and 80MPa. As discussed in the results of 60° orientation, the two samples have almost the same strength, but their linear elastic behavior is different. So, the reason for this behavior can be similar to the previous one.

Variabilities in the manufacturing processes and the material's response to the applied load led to such variations. This behavior is typical for nonwoven composites where fibers are randomly oriented without any specific orientation. It is seen that both specimens respond differently to the applied load. Results also indicate that although the two samples have the same strength, their deformation response differs in the elastic region. The slopes of the curves for each specimen are different, indicating each specimen's different elastic modulus. Figure 51 illustrates the specimens that undergo shear testing.



Figure 51: Specimens after shear test

### 3.4.5: Comparison of shear stress at different Orientations

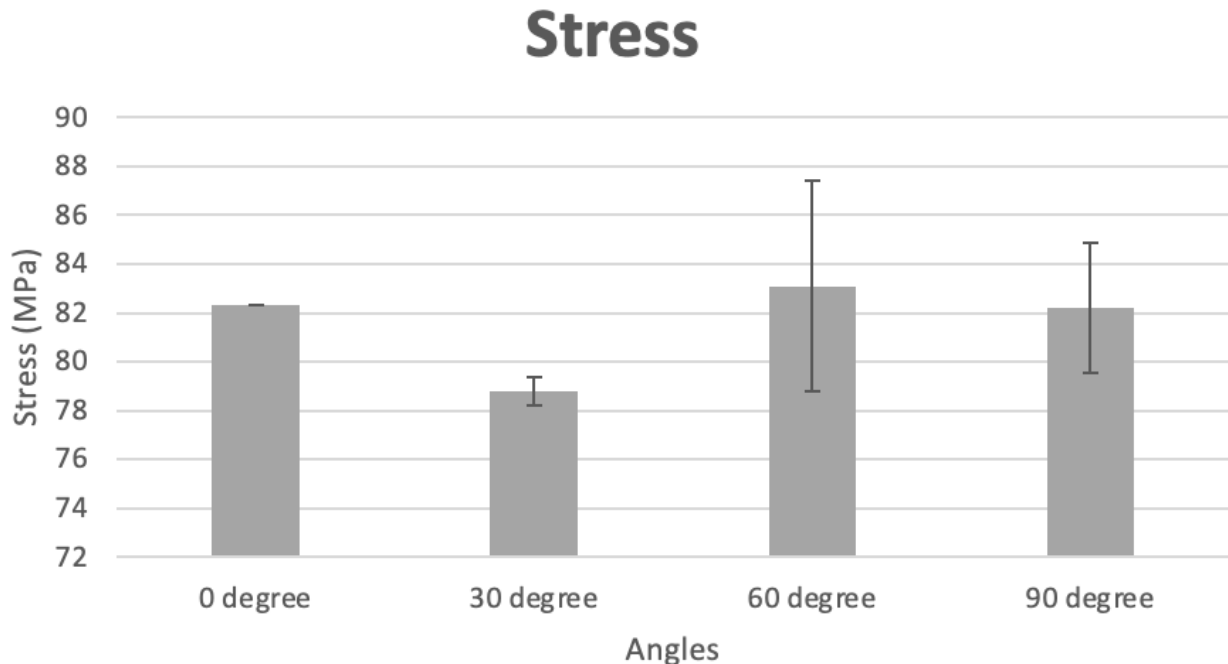
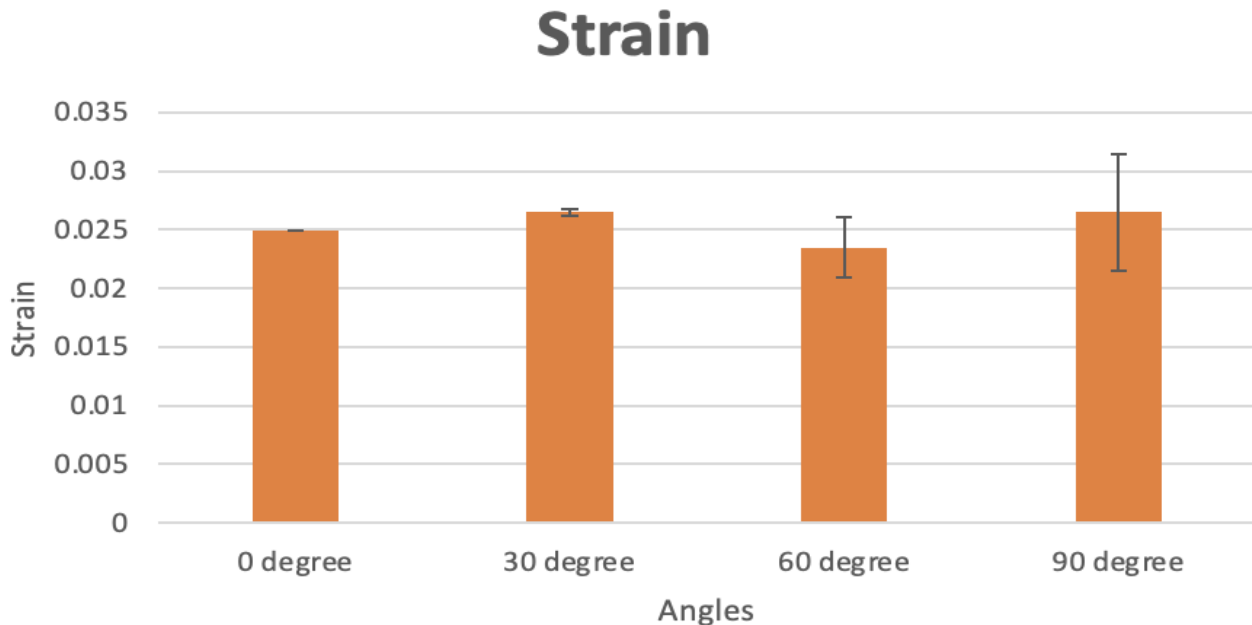


Figure 52: Bar chart showing shear stress at different orientations.

In Figure 52 the bar chart shows the average mean stress of specimens at different orientations. The specimens were tested for four different directions, 0°, 30°, 60° and 90° orientation with mean stress of 82.3 MPa, 78.8 MPa, 83.1 MPa and 82.2 MPa, respectively. Specimens with 60° orientation show the maximum strength value. The specimens for this orientation exhibited higher resistance to the applied shear load. At 30° orientation, there is a minimum strength value of 78.8 MPa which is only 4.2% less than the maximum stress value at 60°. The specimens at this orientation showed less resistance to an applied load compared to the specimens at 60°. For 0° and 30° orientations, the strength is the same, which indicates a high level of homogeneity and consistency in these two orientations. This high level of consistency in the results of these two orientations show that specimen that belongs to these orientations have less variability in manufacturing, and their fiber composition does not have any significant difference.

### 3.4.6: Comparison of shear strain at different Orientations



*Figure 53: Bar chart showing shear strain at different orientations.*

In Figure 53 the bar chart shows the average mean strain of specimens at different orientations. The samples were tested for four different directions, which were 0°, 30°, 60° and 90° orientation with mean strain of 0.0249, 0.0265, 0.0235, 0.0265 respectively. Maximum mean strain is exhibited by specimens at 30° and 90° orientations. At 60°, there is the total value of strength, while at that orientation, minimum deformation is witnessed, and a minimum value of strain is obtained.

### 3.4.7: Comparison of shear modulus at different Orientations

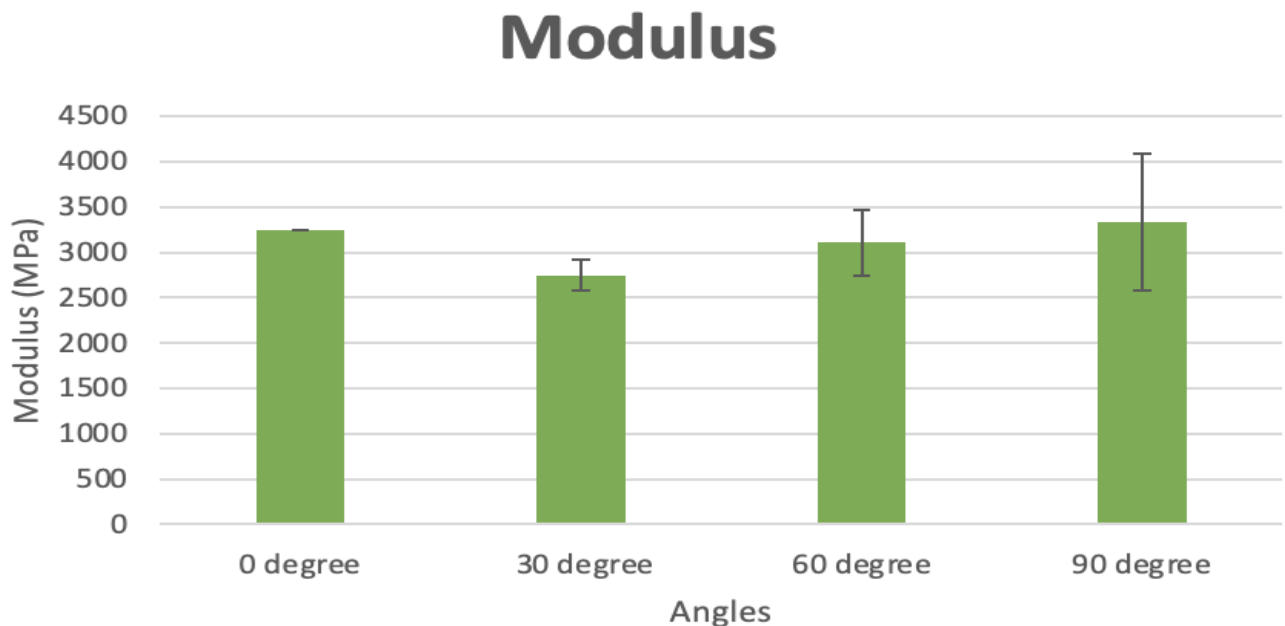


Figure 54: Bar chart showing shear modulus at different orientations.

In Figure 54 the bar chart shows the average mean modulus of specimens at different orientations. The specimens were tested for four different directions, which were 0°, 30°, 60°, and 90°, with a mean modulus of 3240 MPa, 2743 MPa, 3105 MPa, and 3335 MPa, respectively. Specimens exhibit the highest modulus at 90° orientation, while specimens with 30° orientation exhibit the lowest modulus. There is a slight difference of 2.8% in the strength values of 0° and 90° orientation, with 90° orientation showing higher strength than 0° orientation. This is common for non-woven composites, whose fiber orientation and composition often determine mechanical properties. High stiffness in 90° orientation indicates that fibers in these specimens have enhanced the stiffness.

Table 10 below shows the mean stress, mean strain, and mean modulus in all four directions, along with their standard deviations. Maximum shear stress is exhibited in 60° orientation.

Maximum shear strain is found in 30° and 90° orientation, while maximum modulus is in 90° direction.

<b>Stress</b>				
<b>Angles</b>	<b>0°</b>	<b>30°</b>	<b>60°</b>	<b>90°</b>
<b>Mean stress (MPa)</b>	82.3	78.8	83.1	82.2
<b>STDEV</b>	0.5656	4.29	2.7	3
<b>Modulus</b>				
<b>Angles</b>	<b>0°</b>	<b>30°</b>	<b>60°</b>	<b>90°</b>
<b>Mean modulus (MPa)</b>	3240	2743	3105	3335
<b>STDEV</b>	169.7	358.1	757	672
<b>Strain</b>				
<b>Angles</b>	<b>0°</b>	<b>30°</b>	<b>60°</b>	<b>90°</b>
<b>Mean strain</b>	0.0249	0.0265	0.0235	0.0265
<b>STDEV</b>	0.0002828	0.00257	0.00495	0.00071

*Table 10: Mean stress, mean strain, and mean modulus at different orientations*

## 3.5: Optical analysis

A microscopic study of the fractured specimens was conducted to understand the mechanical properties of the non-woven carbon composites by analyzing the fiber orientations and fracture. A representative sample from each orientation was chosen and examined under a microscope.

### 3.5.1: Microscopic study of bending specimens

- 0° degree

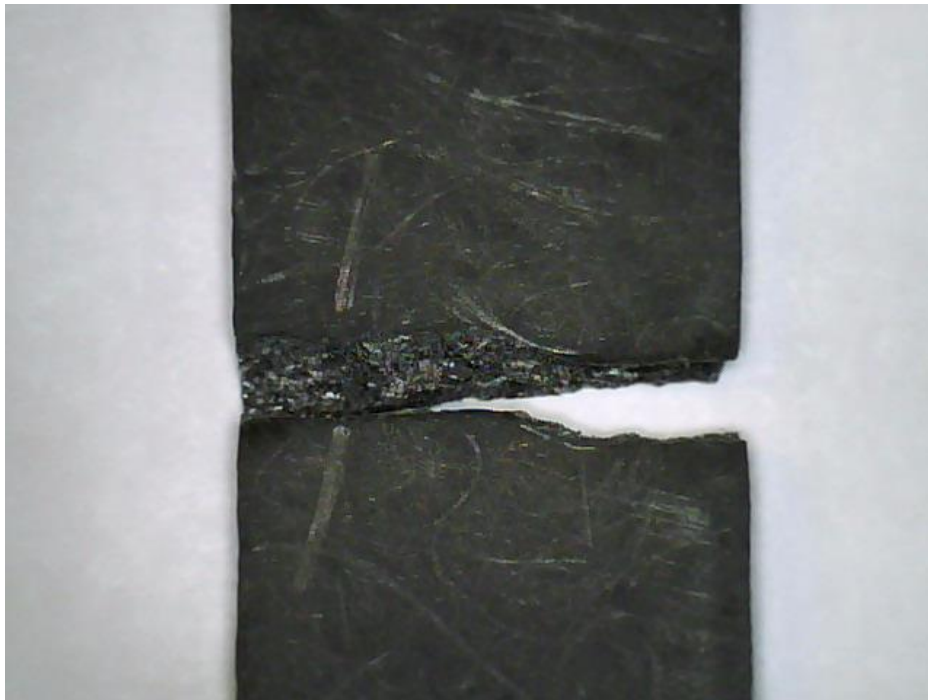


*Figure 55: Microscopic image of 0° fractured specimen*

In Figure 55 the representative specimen belongs to 0° orientation that was tested for bending test. It can be seen that fibers inside the composite are randomly oriented without any particular sequence. There is no specific direction in which fibers are organized. Also, the fiber density and composition are different in different locations. Looking at this specimen, it is clear that there is no void formation on the surface, and no other cracks appeared other than the one in the middle

that leads to the fracture of the specimen into two halves. Moreover, the fracture was brittle, and there was no fiber pullout at the fracture site. This is also indicative that fiber matrix bonding was good, and there was no lack of adhesion.

- **30° degree**



*Figure 56: Microscopic image of 30° fractured specimen*

In Figure 56 representative specimen belongs to 30° orientation tested for bending test. As is the case of non-woven carbon composites, in this specimen, it can be seen how the fibers are randomly oriented. These fibers are not arranged in random or quasi-random manner intentionally, but they are naturally arranged in this manner within the composite. Sometimes, local alignment may occur at specific locations, but it is scarce in the case of non-woven composites. There is a dense population of the fibers in the region of fracture. Some fibers have

different thickness and different lengths. This specimen undergoes brittle fracture, and there is no evidence of fiber pullout in this specimen.

- **60° degree**

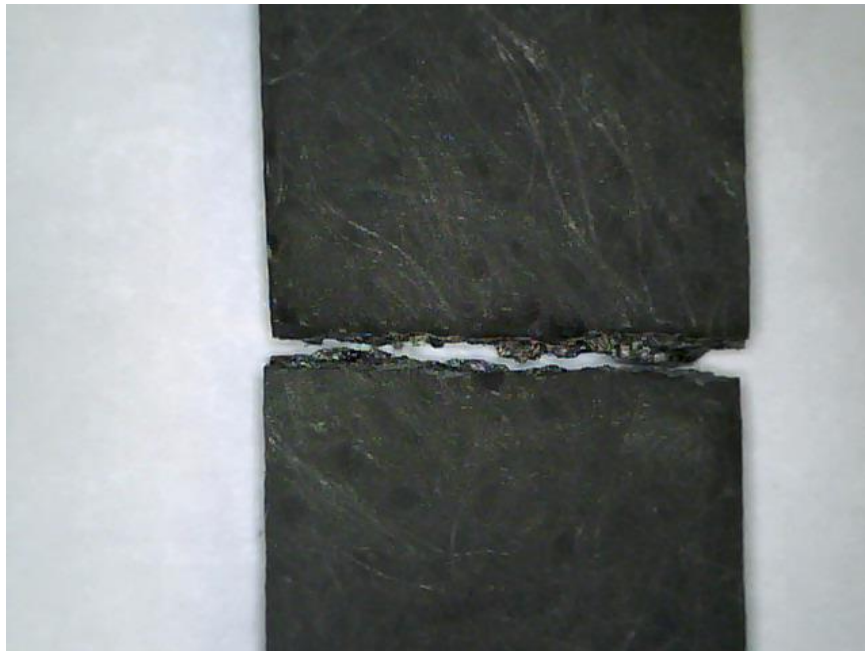


*Figure 57: Microscopic image of 60° fractured specimen*

In Figure 57 specimen belongs to 60° orientation tested for bending test. Looking at the specimen, it can be analyzed that the specimen exhibits non-random orientation of fibers as it was depicted in 0° and 30° orientation. Fibers are seen to be aligned randomly without any specific pattern. There is no evidence of voids on the surface, and there is no crack other than the one in the middle that leads to the specimen rupture. Also, there is no evidence of delamination in the fractured sample, so it can be said that there is no evidence of interfacial debonding. As with the other two samples, this specimen also undergoes brittle fracture.

- 90° degree



*Figure 58: Microscopic image of 90° fractured specimen*

In Figure 58 the representative specimen belongs to 90° orientation tested for bending test. A web of nonwoven fibers can be seen in the image. All the randomly oriented fibers are intermingled into each other. This is the property of nonwoven random composites where the fibers are randomly arranged. An epoxy matrix is visible in this image, as one can see a shiny part at the fracture site. This is evident that the epoxy matrix has maintained its support and cohesion in the composite. We can also say that the matrix has not deboned, which is a positive sign for composite structure. Such composite structures have good strength between matrix and reinforcement fibers. From the fracture, it can be analyzed that it was a brittle fracture. There was no fiber pullout. The structure deformed plastically and leads to the fracture in the composite specimen.

### 3.5.2: Microscopic study of tensile specimens

- 0° degree

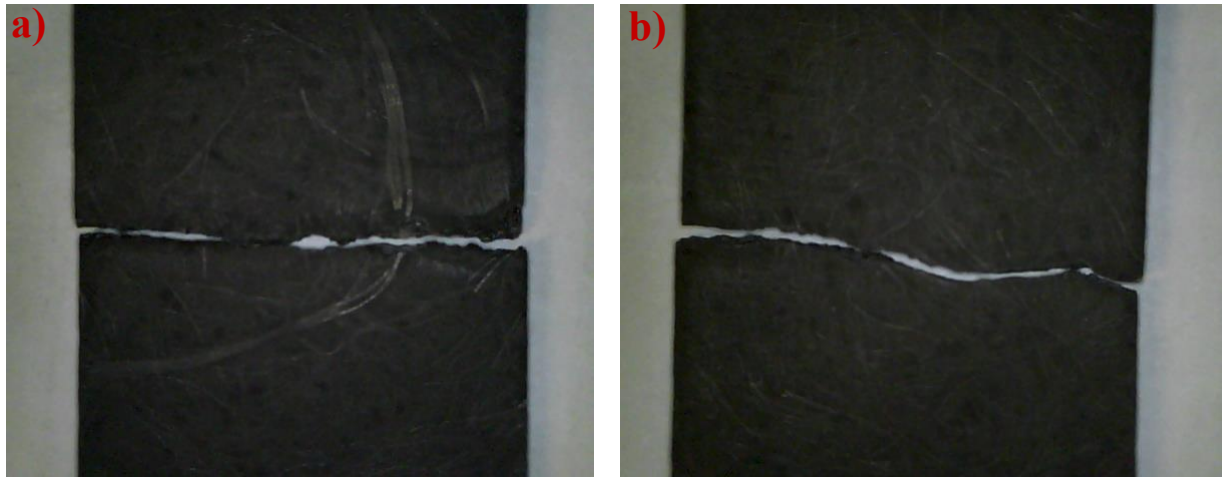


*Figure 59: Microscopic image of 0° fractured specimen*

Figure 59 shows the specimen that belongs to 0° orientation that are tested for tensile test. When tested for tensile test, the specimen was fractured at three locations. In the image (a), non-woven random fibers, which are randomly arranged, can be seen. A thick bundle of fibers also stretches through the fracture in the image (a). Similarly, in the image (c), another cluster of fibers can be seen. This clustering of fibers affects the mechanical properties of the composite, and in non-woven composites, they can be visible in different locations. This may occur during the fabrication process of non-woven fibers or sometimes during the manufacturing of non-woven composites. These clusters of fibers arranged themselves in a non-random pattern to give the composite unique mechanical properties.

Moreover, in this case, areas with high fiber content and regions with lower fiber content affect the mechanical properties of the composites. This accumulation of fibers may increase the strength of the composite at a certain level, but they also act as weak points due to the variation

in fiber orientation. All three fractures in this specimen were brittle without any evidence of fiber pull-out.



*Figure 60: Microscopic image of 0° fractured specimen near the grip*

Figure 60 shows the fracture that occurs near the grip of the 0° specimen; such fractures usually occur due to localized stress concentrations. This could be due to surface irregularities, sharp corners, and non-uniform clamping of the specimen.

- 30° degree

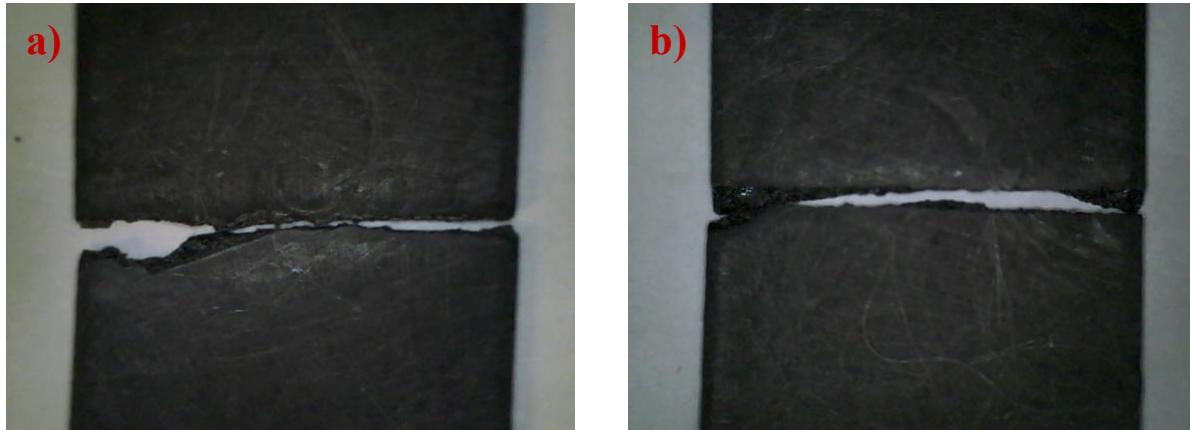


*Figure 61: Microscopic image of 30° fractured specimens*

Figure 61 shows the specimen that belongs to 30° orientation tested for tensile test. When tested for tensile tests, this specimen was fractured from 2 locations. It is hard to recognize fibers in these images because they are very thin and short. In both cases, it can be seen that there is fiber clustering near the site of fracture. In the image (b), some fibers can be seen oriented in different directions. Irregular brittle fracture took place at two locations, and as in the previous cases, there was no evidence of fiber pullout or delamination due to debonding.

- 60° degree

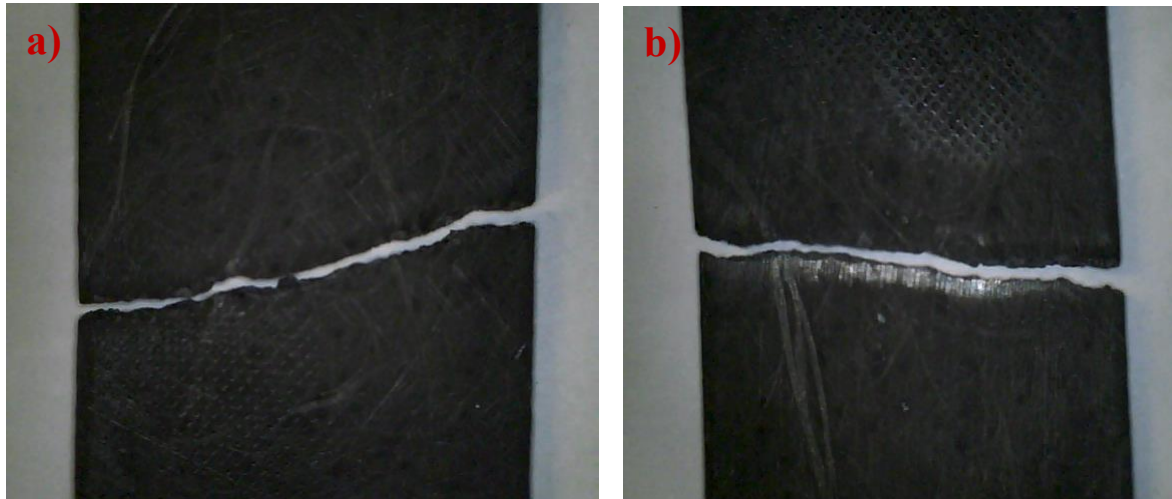


*Figure 62: Microscopic image of 60° fractured specimens*

Figure 62 represents a specimen of 60° orientation tested for tensile test. When tested for tensile test, this specimen was fractured from 2 locations. The difference between this specimen and those of 0° and 30° orientation is that it was fractured near the grips. Both fractures took place near the grips, and there was no fracture in the middle of the sample within the gauge length. It could be because of the non-uniform loading condition, particularly in this specimen. It could also be due to the misalignment of the grips that resulted in uneven stress distribution, which leads to material rupture at the ends.

The reinforcement in this specimen is very randomly distributed, and there is no proper pattern in which they are arranged. In the image (b), it can be seen that there is a fiber cluster near the site of fracture. In the previous specimens, the fracture was in areas with a fiber cluster; in this specimen, it's the same. Similarly, in image (a), it can be seen that the fibers near the fracture site are very random, and they form small clusters in different orientations. Their size and shape also differ from the fibers at a distance from the fracture. These different orientations are also responsible for the type of failure usually occurring in the composites because they influence the fracture mode.

## 90° degree



*Figure 63: Microscopic image of 90° fractured specimen*



*Figure 64: Microscopic image of 90° fractured specimen*

Figure 63 and Figure 64 belong to  $90^\circ$  orientation tested for the tensile test. When tested for tensile tests, this specimen was fractured from 2 locations. The two figures are not very precise due to the rough surface of the specimen. Both of the fractures occurred within the gauge length. In Figure 63 all the fibers seem to be of the same shape and size without any significant difference, and their composition appears uniform. Moreover, in Figure 64 the fracture seems more rigorous and severe. A small part of the composite has been separated from the specimen. In Figure 64 a thin bundle of fibers can be seen near the fracture site. This trend is the same in all fractured samples. Near the site of the fracture, there are fiber clusters. It can also be said that these fiber clusters acted as weak points within the composite as the variation in their orientation and their adhesion may have led to the formation of voids and defects within the composite that may have led to fracture.

### 3.5.3: Microscopic study of compression specimens

- $0^\circ$  degree

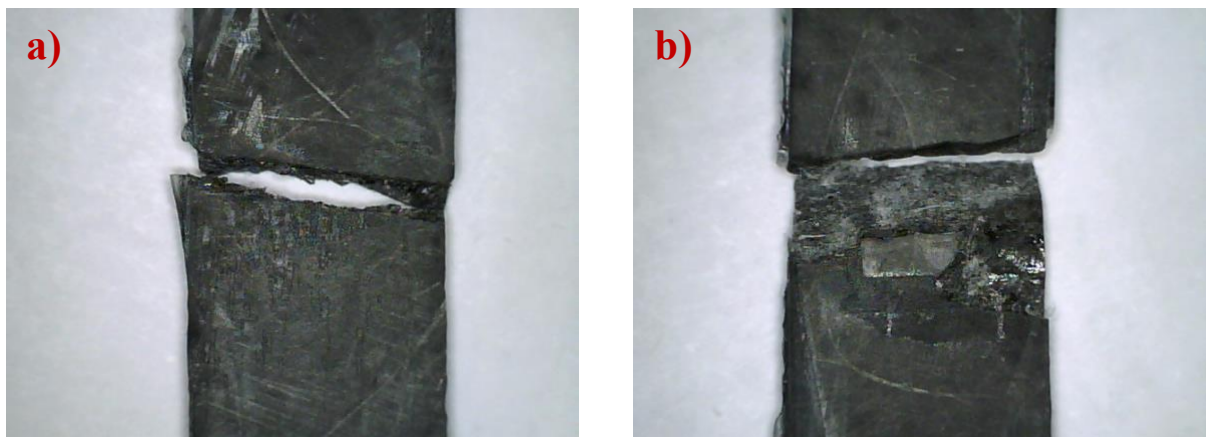


*Figure 65: Microscopic image of  $0^\circ$  fractured specimens*

The Figure 65 represents the fractured  $0^\circ$  specimen tested for compression. The specimen breaks at two locations near the middle of the gauge length. From the fracture, it can be determined that

fractured occurred due to buckling and crushing of the specimen, so most of the features appeared crushed. The fracture patterns also differ from those we saw in tensile fracture. In compression-loaded tests, the fractures are more inclined or oblique than straight fractures. In both images, fibers can be seen; these fibers are randomly arranged and oriented in different directions. The size of the fibers in this specimen seems to be the same, and there is no variation in their thickness. Usually, in compression tests, fibers inside composites are compressed at the fracture site. However, Due to the complicated fracture pattern, it is difficult to see whether the fibers are compressed at the fracture site. Other than the two primary fractures, there is no evidence of any other fracture or crack. There is no fiber pullout, and fractures are ductile.

- **30° degree**

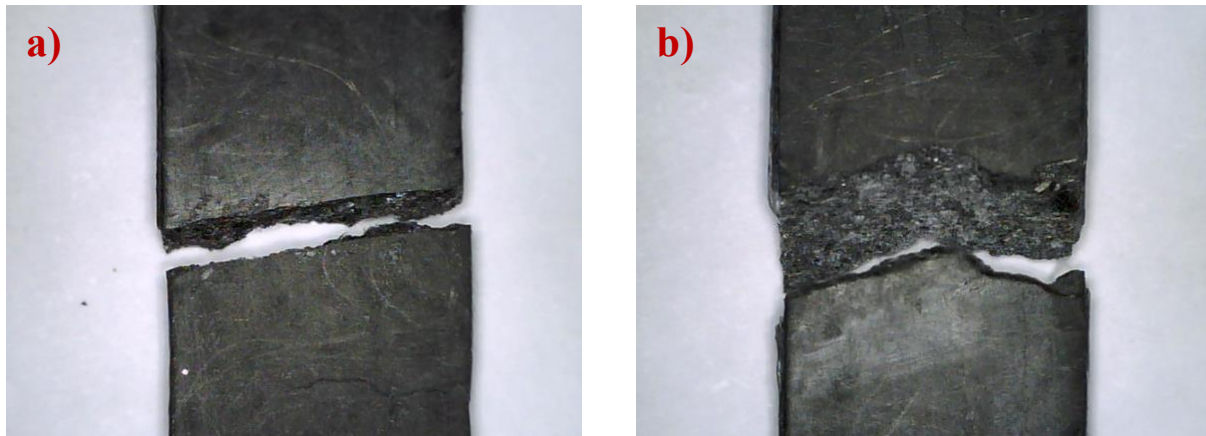


*Figure 66: Microscopic image of 30° fractured specimens*

Figure 66 shows the specimen that belongs 30° specimen. The sample breaks at two locations near the middle of the gauge length. Two fractures exactly occurred in the middle of the gauge length. The image (b) shows that the fracture was more rigorous and damaging than the one in the image (a). In the image (a), the fracture resembles a brittle fracture. However, in the image (b), the fracture is inclined and is a ductile fracture. So, at a distance of just a few centimeters, we can see the ductile and brittle behavior of the composite. As with the non-woven random

fiber composites, fibers in these specimens are also randomly organized. There is no clustering of fibers in the sites of the fracture. Thin fibers can be seen oriented in different directions.

- **60° degree**



*Figure 67: Microscopic image of 60° fractured specimen*

Figure 67 represents the fractured 60° specimen tested for compression. The specimen breaks at just one location within the gauge length. A web of fibers can be seen as randomly organized. The size and shape of the fibers seem to be similar, and they do not have any pattern. From the image, it can be seen that there is a massive population of fibers randomly arranged at the fracture site. The specimen experienced an inclined ductile fracture and no fiber pullout. At the fracture site, white powder-like fragments appear that are evident that the fracture has led to the breaking of the matrix. There was also no evidence of the other cracks or fiber pullout.

- 90° degree

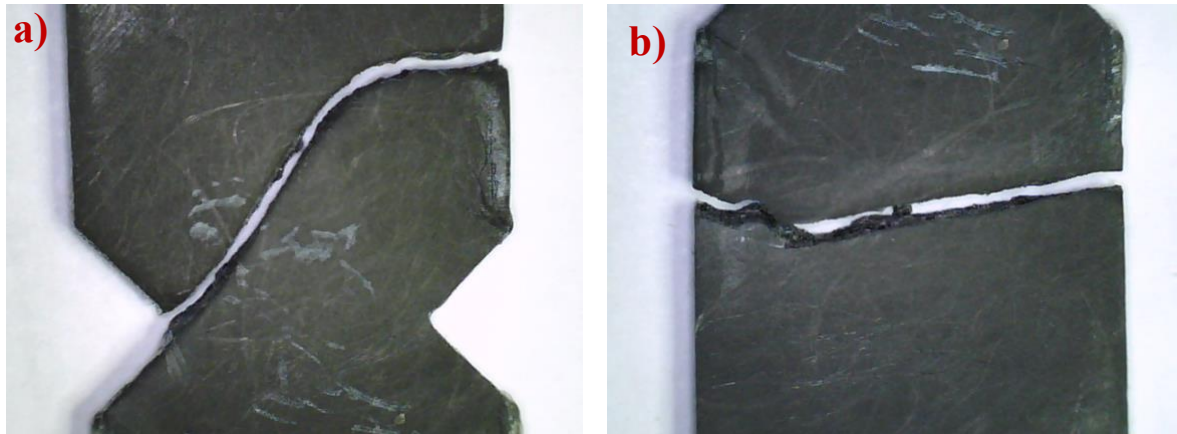


*Figure 68: Microscopic image of 90° fractured specimen*

Figure 68 represents the fractured 90° specimen tested for compression. The sample breaks at just one location within the gauge length. From the fracture, it can be determined that the fracture occurred due to buckling and crushing of the specimen. Many single fibers can be seen randomly arranged at the site of fracture. This inherently random orientation is characteristic of non-woven fiber composites, and they are oriented in unpredictable directions throughout the composite, as seen in the image. The size and shape of the fibers also seem to be similar to each other. The fracture was ductile without any fiber pullout.

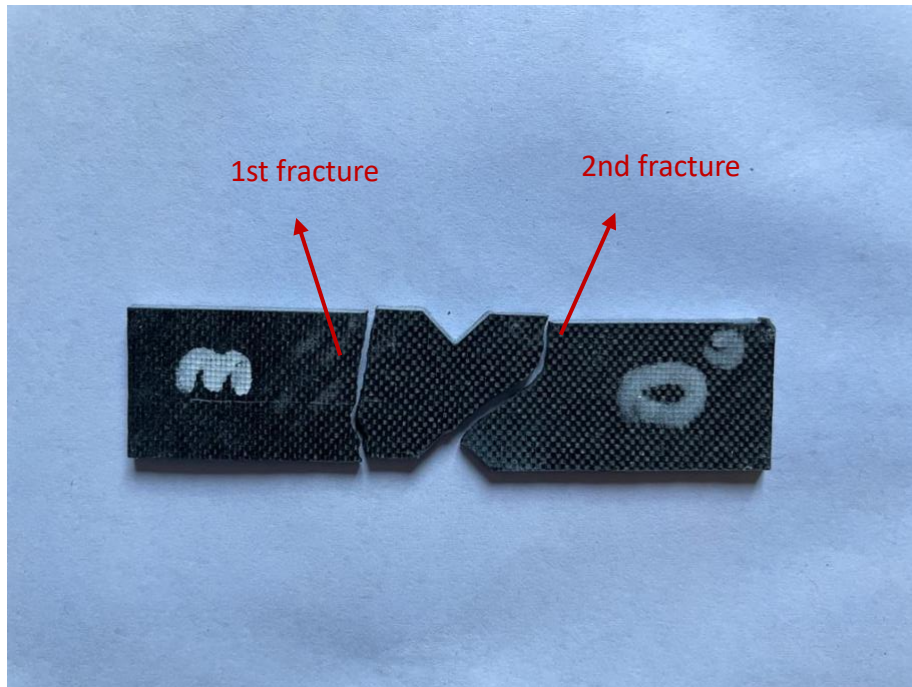
### 3.5.4: Microscopic study of shear specimens

- 0° degree



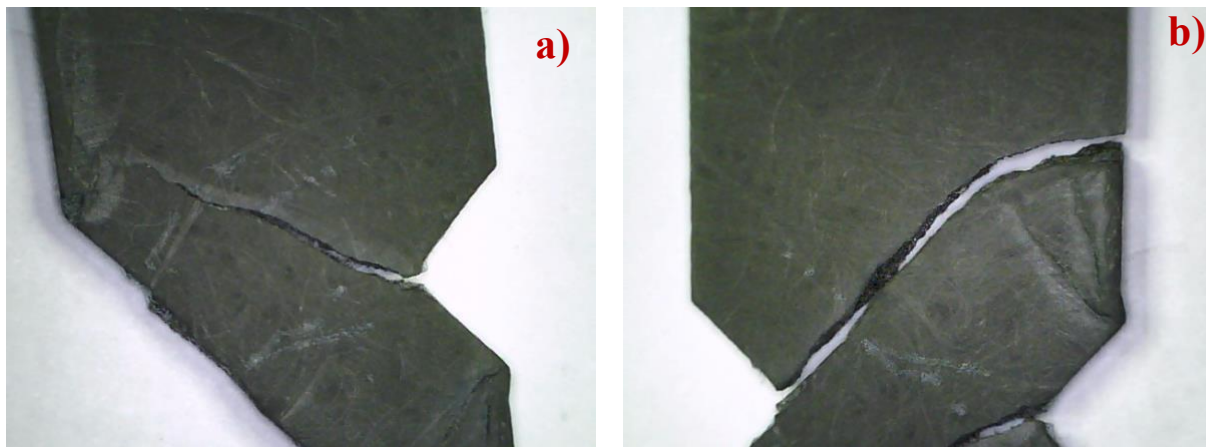
*Figure 69: Microscopic image of 0° fractured specimens*

Figure 69 represents the fractured 0° specimen tested for shear. The specimen breaks at two locations within the gauge length. Shear samples usually fail due to sliding or shearing of the layers. It is also evident in the image (a). In image (a), a brittle fracture occurred near the notch in the middle of the specimen due to the sliding, where the stress concentration was already high. In the image (b), the fracture occurred a few centimeters from the notch and was also brittle. Some of the random fibers are also visible in the figure. Although the density of fibers is not much, they can be seen stretching at different locations and are haphazardly oriented at different angles compared to the shear direction. There was no fiber pull-out evidence of solid bonding within the fiber matrix material. Figure 70 below shows two fractures that occurred in the specimen after the shear testing.



*Figure 70: 0° Specimen fractured by shear testing.*

- **30° degree**



*Figure 71: Microscopic image of 30° fractured specimens*

Figure 71 represents the fractured 30° specimen tested for shear. In the image (b), the specimen breaks near the notch, and this fracture continues till the other end. There was also a big crack

image (a), that the other side of the notch, but it did not result in a fracture. The fibers are randomly organized. There is no clustering of fibers visible in the specimen. Small and thin fibers can be seen at the site of fracture. Many other short fibers can be seen in the sample at different locations, which are organized haphazardly. Both fractures were ductile.

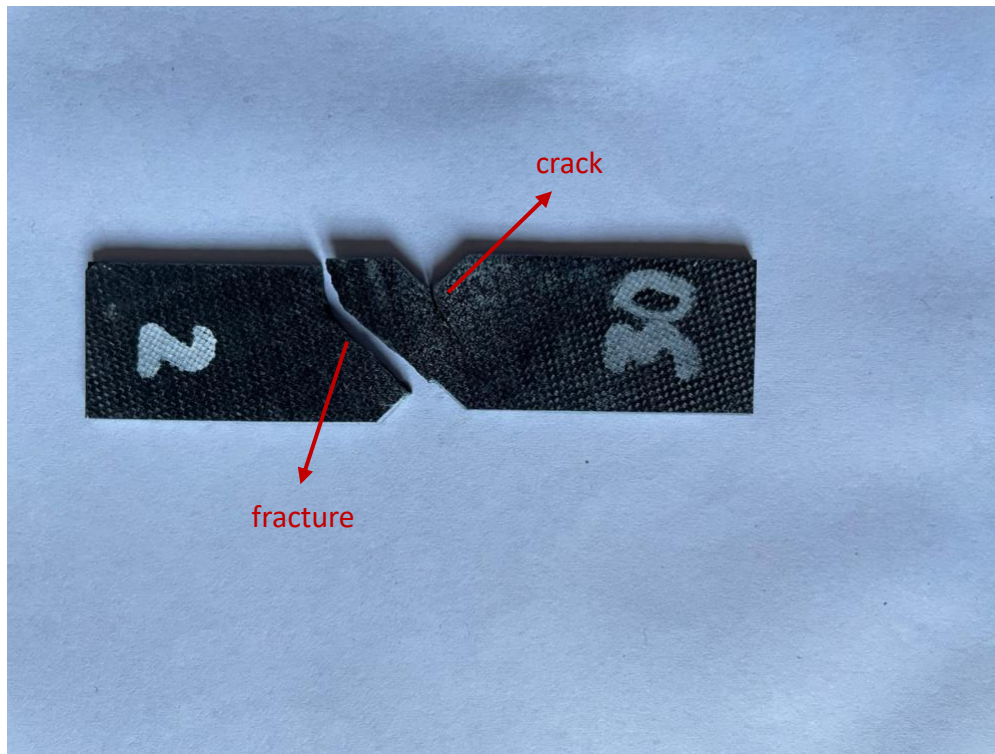


*Figure 72: 30° Specimen fractured by shear testing.*

Figure 72 shows the fracture and a crack that occurred in the specimen after the shear testing.

- 60° degree

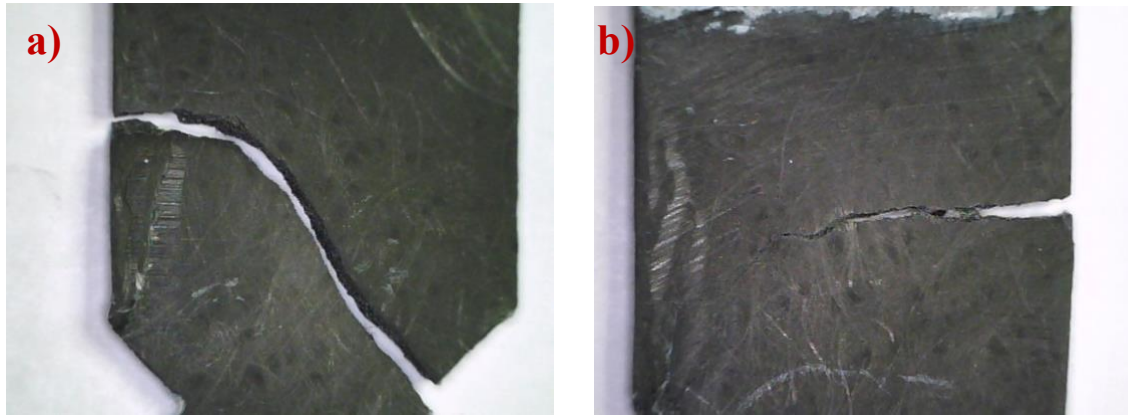


*Figure 73: Microscopic image of 60° fractured specimens*

Figure 73 represents the fractured 60° specimen tested for shear. The first fracture, image (a), occurred near the notch, and this fracture continued till the other end. There was another crack in the sample, but it did not result in a fracture. This crack was a few centimeters from the notch and can be seen in image (b). Like all other nonwoven composite specimens, this specimen has nonrandom fibers in different locations. In the image (a), near the fracture site, nonwoven random fibers stretch across the fracture. In the image (b), small and thin clusters of fibers can be seen across the crack, which is non-uniformly organized. The fracture was a ductile fracture. As with all other shear specimens, this specimen also experienced the fracture in an inclined direction, characteristic of shear fracture.

Figure 74 shows the fracture and a crack that occurred in the specimen after the shear testing.

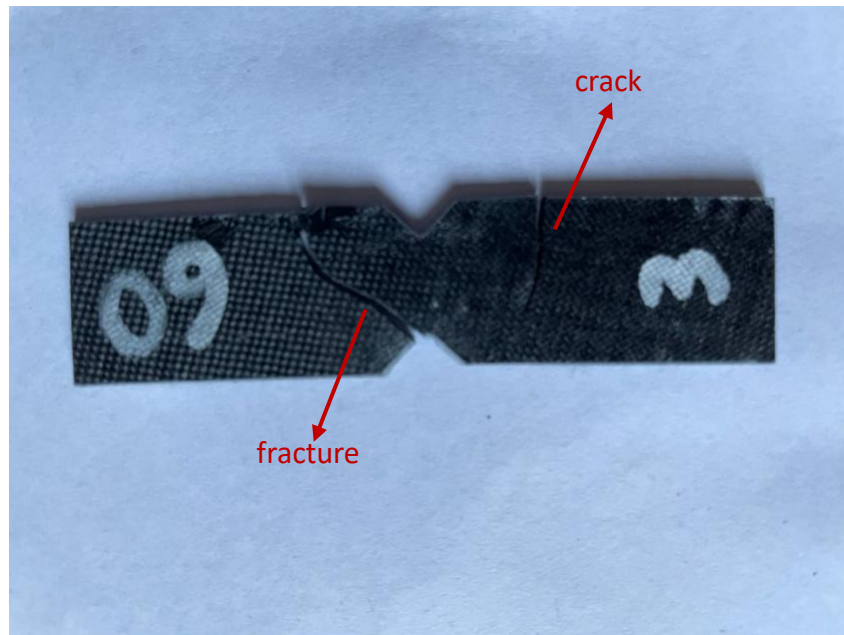


Figure 74: 60° Specimen fractured by shear testing.

- 90° degree

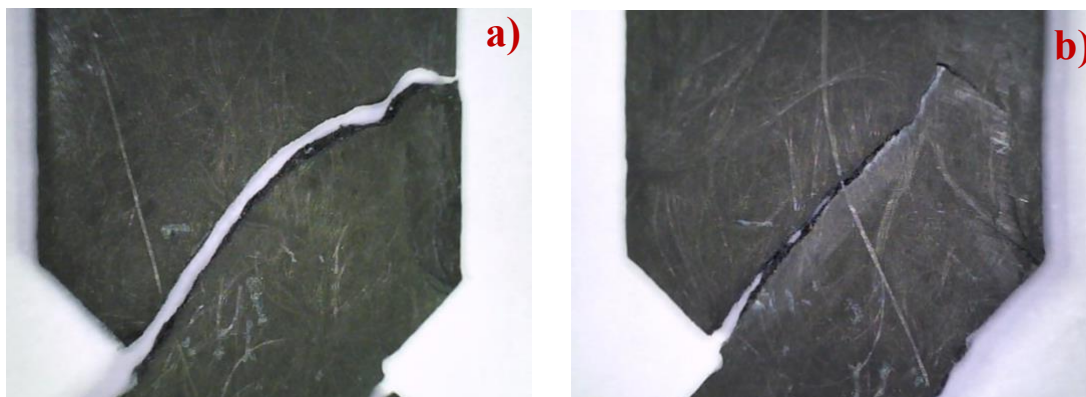
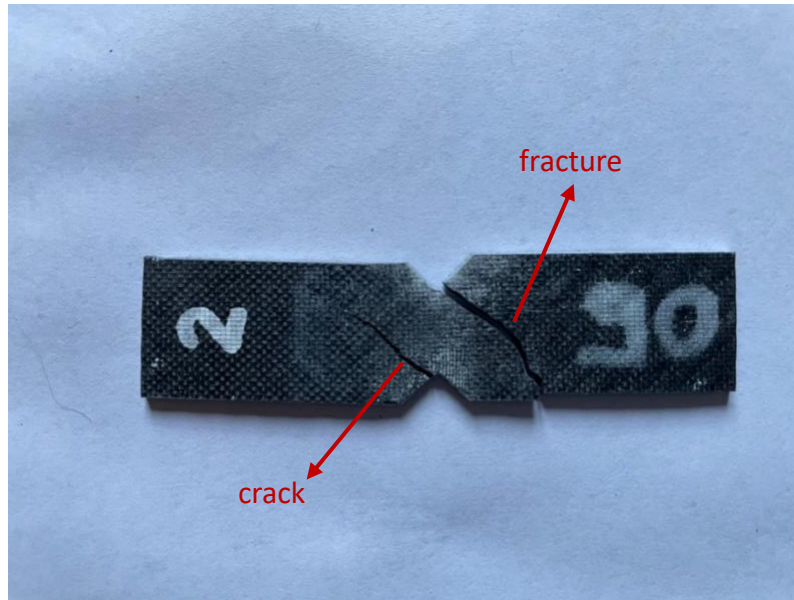


Figure 75: Microscopic image of 90° fractured specimens

Figure 75 represents the fractured 90° specimen tested for shear. The specimen image (a) breaks near the notch, and this fracture continues till the other end. There was also a big crack image

(b), on the other side of the notch, but it did not result in a fracture. In both images, thick and long fibers stretch through the fractures. Also, a web of tiny, dense fibers is randomly arranged in different orientations near the fractures. It can be seen that long and short fibers are intermingled into each other and placed in nonrandom patterns to form a web-like appearance within the composite. The fracture was ductile and inclined, as with all other shear specimens.



*Figure 76: 90° Specimen fractured by shear testing.*

Figure 76 above shows the fracture and a crack that occurred in the specimen after the shear testing.

## Chapter 4: Conclusion

This thesis aimed to understand the mechanical properties of non-woven carbon composites made with epoxy resin matrix. Composite laminates were manufactured using the vacuum infusion process. Specimens were cut using a water jet cutting system according to ASTM guidelines at four different angles ( $0^\circ$ ,  $30^\circ$ ,  $60^\circ$ ,  $90^\circ$ ) with respect to the resin flow direction. Four mechanical tests were performed: three-point bending, tensile, compression, and shear. For tensile and shear tests, a DIC system was used to map strain on the surface of the specimens.

The results showed that for the case of bending and tensile tests, maximum strength was obtained for specimens oriented at  $90^\circ$ . The bending test has shown at  $90^\circ$  a mean stress of 245MPa ( Figure 28 ) and a mean modulus of 9800MPa ( Figure 29 ). Moreover, in the case of the tensile test, specimens oriented at  $90^\circ$  have shown a mean stress of 148MPa ( Figure 36 ) and a mean modulus of 11093MPa ( Figure 38 ). In compression and shear tests, specimens oriented at  $60^\circ$  have shown maximum stress, while specimens oriented at  $90^\circ$  have shown maximum modulus. In compression and shear tests,  $60^\circ$  orientation resulted in maximum mean stress of 145MPa ( Figure 44 ) and 83MPa ( Figure 52 ), respectively. For compression and shear tests,  $90^\circ$  orientation yielded maximum mean moduli of 10632 MPa ( Figure 46 ) and 3335 MPa ( Figure 54 ), respectively. One remarkable result is that the maximum modulus is obtained for specimens oriented at  $90^\circ$  for all the mechanical tests.

For bending and tensile test results, the difference in the stress values, highlights the noteworthy variations in the strength at different orientations as seen in Table 7 and Table 8. In the case of shear tests, there is little difference in the stress values at four different orientations. Maximum strength in the case of shear tests was shown by specimens oriented at  $60^\circ$  which was around 83 MPa. All four orientations for shear tests have exhibited almost the same stress, so for what concerns random fibers composites, the effect of orientation can be negligible.

From the results obtained by the optical analysis on the fracture surfaces, it was possible to understand the orientation of fibers in the samples in proximity of fracture. One representative specimen for each orientation and for each mechanical test was analyzed. Optical analysis shows

that fibers in specimens are randomly oriented. This randomness in the fibers' orientation affects the composites' mechanical properties. It can either lead to isotropic or anisotropic properties, which depend on the distribution of the fibers. Noteworthy is that, in the case of tensile tests, fiber clustering was observed at the fracture site. Overall, it cannot be said that there is any specific arrangement of fibers because fibers are non-uniformly distributed in the specimens. However, a deep analysis with a more sophisticated microscope could yield more accurate results.

In conclusion, future studies are oriented towards a simulation analysis of the mechanical behavior of these materials so that the results can be compared to experimental values.

# Acknowledgment

I want to express my sincere gratitude to Professor Raffaele Ciardiello, Professor Davide Salvatore Paolino, and Engineer Andrea Iadarola for their invaluable guidance and unwavering support throughout the course of this thesis.

In particular, I extend my heartfelt appreciation to Professor Raffaele Ciardiello for entrusting me with this opportunity and for demonstrating unwavering confidence in my abilities. Your patience and support throughout this journey have been truly commendable.

I am deeply thankful to Andrea Iadarola, who has been a pillar of support from day one. Your dedication to assisting me, even from a distance, leaves me at a loss for words to adequately convey my gratitude.

I also wish to acknowledge my parents and other family members for their steadfast belief in me. Your unwavering faith has been a constant source of motivation and strength.

## References

- [1] H. Ahmad, A. A. Markina, M. V Porotnikov, and F. Ahmad, "A review of carbon fiber materials in automotive industry," *IOP Conf Ser Mater Sci Eng*, vol. 971, no. 3, p. 032011, Nov. 2020, doi: 10.1088/1757-899X/971/3/032011.
- [2] V. M. Raja and S. S. Kumar, "Determination of Static and Fatigue Characteristics of Carbon Fiber Reinforced Polyester Composites for Automobile Applications," *Materials Research*, vol. 22, no. 6, 2019, doi: 10.1590/1980-5373-mr-2019-0458.
- [3] Z. C. He, X. Shi, E. Li, and X. K. Li, "Elastic properties and multi-scale design of long carbon fiber nonwoven reinforced plane-based isotropic composite," *Compos Struct*, vol. 251, p. 112657, Nov. 2020, doi: 10.1016/j.compstruct.2020.112657.
- [4] T. Windhorst and G. Blount, "Carbon-carbon composites: a summary of recent developments and applications," *Mater Des*, vol. 18, no. 1, pp. 11–15, Feb. 1997, doi: 10.1016/S0261-3069(97)00024-1.
- [5] Y. Liu, B. Zwingmann, and M. Schlaich, "Carbon Fiber Reinforced Polymer for Cable Structures—A Review," *Polymers (Basel)*, vol. 7, no. 10, pp. 2078–2099, Oct. 2015, doi: 10.3390/polym7101501.
- [6] T. RAJMOHAN, K. PALANIKUMAR, and S. RANGANATHAN, "Evaluation of mechanical and wear properties of hybrid aluminium matrix composites," *Transactions of Nonferrous Metals Society of China*, vol. 23, no. 9, pp. 2509–2517, Sep. 2013, doi: 10.1016/S1003-6326(13)62762-4.
- [7] N. A. de Bruyne, "The adhesive properties of epoxy resins," *Journal of Applied Chemistry*, vol. 6, no. 7, pp. 303–310, May 2007, doi: 10.1002/jctb.5010060708.
- [8] B. Yuan, M. Ye, Y. Hu, F. Cheng, and X. Hu, "Flexure and flexure-after-impact properties of carbon fibre composites interleaved with ultra-thin non-woven aramid fibre veils," *Compos Part A Appl Sci Manuf*, vol. 131, p. 105813, Apr. 2020, doi: 10.1016/j.compositesa.2020.105813.
- [9] E. Ozeren Ozgul and M. H. Ozkul, "Effects of epoxy, hardener, and diluent types on the workability of epoxy mixtures," *Constr Build Mater*, vol. 158, pp. 369–377, Jan. 2018, doi: 10.1016/j.conbuildmat.2017.10.008.
- [10] A. C. Meeks, "Fracture and mechanical properties of epoxy resins and rubber-modified epoxy resins," *Polymer (Guildf)*, vol. 15, no. 10, pp. 675–681, Oct. 1974, doi: 10.1016/0032-3861(74)90060-3.
- [11] A. Ozturk, C. Kaynak, and T. Tincer, "Effects of liquid rubber modification on the behaviour of epoxy resin," *Eur Polym J*, vol. 37, no. 12, pp. 2353–2363, Dec. 2001, doi: 10.1016/S0014-3057(01)00158-6.
- [12] S. Liu, H. Zhang, Z. Zhang, T. Zhang, and S. Sprenger, "Tailoring the Mechanical Performance of Epoxy Resin by Various Nanoparticles," *Polymers and Polymer Composites*, vol. 16, no. 8, pp. 527–533, Oct. 2008, doi: 10.1177/096739110801600806.
- [13] P. Lv, Y. Feng, P. Zhang, H. Chen, N. Zhao, and W. Feng, "Increasing the interfacial strength in carbon fiber/epoxy composites by controlling the orientation and length of carbon

- nanotubes grown on the fibers,” *Carbon N Y*, vol. 49, no. 14, pp. 4665–4673, Nov. 2011, doi: 10.1016/j.carbon.2011.06.064.
- [14] Z. C. He, S. L. Huo, Eric. Li, H. T. Cheng, and L. M. Zhang, “Data-driven approach to characterize and optimize properties of carbon fiber non-woven composite materials,” *Compos Struct*, vol. 297, p. 115961, Oct. 2022, doi: 10.1016/j.compstruct.2022.115961.
- [15] J. Ivars, A. R. Labanieh, and D. Soulat, “Effect of the Fibre Orientation Distribution on the Mechanical and Preforming Behaviour of Nonwoven Preform Made of Recycled Carbon Fibres,” *Fibers*, vol. 9, no. 12, p. 82, Dec. 2021, doi: 10.3390/fib9120082.
- [16] M. Shibata, K.-I. Takachiyo, K. Ozawa, R. Yosomiya, and H. Takeishi, “Biodegradable polyester composites reinforced with short abaca fiber,” *J Appl Polym Sci*, vol. 85, no. 1, pp. 129–138, Jul. 2002, doi: 10.1002/app.10665.
- [17] S. Nikafshar *et al.*, “A renewable bio-based epoxy resin with improved mechanical performance that can compete with DGEBA,” *RSC Adv*, vol. 7, no. 14, pp. 8694–8701, 2017, doi: 10.1039/C6RA27283E.
- [18] “<https://www.tenowo.com/en/markets/composites/carbonfiber-nonwovens/>.”
- [19] S. Maiti, M. R. Islam, M. A. Uddin, S. Afroj, S. J. Eichhorn, and N. Karim, “Sustainable Fiber-Reinforced Composites: A Review,” *Adv Sustain Syst*, vol. 6, no. 11, p. 2200258, Nov. 2022, doi: 10.1002/adsu.202200258.
- [20] M. C. do Amaral, W. F. Zonatti, K. L. da Silva, D. Karam Junior, J. Amato Neto, and J. Baruque-Ramos, “Industrial textile recycling and reuse in Brazil: case study and considerations concerning the circular economy,” *Gestão & Produção*, vol. 25, no. 3, pp. 431–443, Apr. 2018, doi: 10.1590/0104-530x3305.
- [21] P. N. Britton, A. J. Sampson, C. F. Elliott, H. W. Graben, and W. E. Gettys, “Computer Simulation of the Mechanical Properties of Nonwoven Fabrics,” *Textile Research Journal*, vol. 53, no. 6, pp. 363–368, Jun. 1983, doi: 10.1177/004051758305300607.
- [22] R. A. Witik, R. Teuscher, V. Michaud, C. Ludwig, and J.-A. E. Månson, “Carbon fibre reinforced composite waste: An environmental assessment of recycling, energy recovery and landfilling,” *Compos Part A Appl Sci Manuf*, vol. 49, pp. 89–99, Jun. 2013, doi: 10.1016/j.compositesa.2013.02.009.
- [23] Y. S. Song, J. R. Youn, and T. G. Gutowski, “Life cycle energy analysis of fiber-reinforced composites,” *Compos Part A Appl Sci Manuf*, vol. 40, no. 8, pp. 1257–1265, Aug. 2009, doi: 10.1016/j.compositesa.2009.05.020.
- [24] S. V. Joshi, L. T. Drzal, A. K. Mohanty, and S. Arora, “Are natural fiber composites environmentally superior to glass fiber reinforced composites?,” *Compos Part A Appl Sci Manuf*, vol. 35, no. 3, pp. 371–376, Mar. 2004, doi: 10.1016/j.compositesa.2003.09.016.
- [25] “<https://link.springer.com/article/10.1007/s42824-020-00004-0>.”
- [26] “[https://ebrary.net/85855/engineering/structural\\_properties\\_weaveknit\\_design\\_porosity](https://ebrary.net/85855/engineering/structural_properties_weaveknit_design_porosity).”
- [27] J. Bachmann, M. Wiedemann, and P. Wierach, “Flexural Mechanical Properties of Hybrid Epoxy Composites Reinforced with Nonwoven Made of Flax Fibres and Recycled Carbon Fibres,” *Aerospace*, vol. 5, no. 4, p. 107, Oct. 2018, doi: 10.3390/aerospace5040107.
- [28] T. Dhilipkumar and M. Rajesh, “Effect of manufacturing processes and multi-walled carbon nanotube loading on mechanical and dynamic properties of glass fiber reinforced

- composites," *Polym Compos*, vol. 43, no. 3, pp. 1772–1786, Mar. 2022, doi: 10.1002/pc.26496.
- [29] E. J. Ekoi, A. N. Dickson, and D. P. Dowling, "Investigating the fatigue and mechanical behaviour of 3D printed woven and nonwoven continuous carbon fibre reinforced polymer (CFRP) composites," *Compos B Eng*, vol. 212, p. 108704, May 2021, doi: 10.1016/j.compositesb.2021.108704.
- [30] L. R. Meza, J. M. J. Schormans, J. J. C. Remmers, and V. S. Deshpande, "Shear response of 3D non-woven carbon fibre reinforced composites," *J Mech Phys Solids*, vol. 125, pp. 276–297, Apr. 2019, doi: 10.1016/j.jmps.2018.12.019.
- [31] B. Yuan, B. Tan, Y. Hu, J. Shaw, and X. Hu, "Improving impact resistance and residual compressive strength of carbon fibre composites using un-bonded non-woven short aramid fibre veil," *Compos Part A Appl Sci Manuf*, vol. 121, pp. 439–448, Jun. 2019, doi: 10.1016/j.compositesa.2019.04.006.
- [32] "<https://explorecomposites.com/articles/design-for-composites/basics-manufacturing-methods/>".
- [33] "[https://www.researchgate.net/figure/Normal-procedure-for-vacuum-infusion-process-9\\_fig1\\_325017393](https://www.researchgate.net/figure/Normal-procedure-for-vacuum-infusion-process-9_fig1_325017393)".
- [34] G. L. G. González, L. D. Rodrigues, M. A. Meggiolaro, and J. L. F. Freire, "Strains in Shallow and Deep Notches Using Two DIC Algorithms," 2016, pp. 281–294. doi: 10.1007/978-3-319-22446-6\_35.
- [35] "<https://www.easycomposites.co.uk/in2-epoxy-infusion-resin>".
- [36] "<https://www.easycomposites.co.uk/at30-epoxy-resin-hardener-fast-or-slow>".
- [37] "<https://www.easycomposites.co.uk/ov301-precision-curing-oven>".
- [38] "[https://www.iitk.ac.in/che/PG\\_research\\_lab/pdf/UTM\\_Web%20Info.pdf](https://www.iitk.ac.in/che/PG_research_lab/pdf/UTM_Web%20Info.pdf)".
- [39] "<https://www.correlatedsolutions.com/vic-2d/>".
- [40] A. Ajovalasit and G. Pitarresi, "Strain Measurement on Composites: Effects due to Strain Gauge Misalignment," *Strain*, vol. 47, pp. e84–e92, Jun. 2011, doi: 10.1111/j.1475-1305.2008.00546.x.
- [41] "<https://www.astm.org/d0790-17.html>".
- [42] "[https://www.astm.org/d3039\\_d3039m-17.html](https://www.astm.org/d3039_d3039m-17.html)".
- [43] "<https://www.astm.org/d0695-15.html>".
- [44] "[https://www.astm.org/d5379\\_d5379m-19e01.html](https://www.astm.org/d5379_d5379m-19e01.html)".